University of Liège

Faculty of Civil Engineering

Commonwealth Scientific and Industrial Research Organisation

Drilling Mechanics Group

Enhancement and parametric analysis of a model of a drilling assembly equipped with a rotary steerable system

Master memoir submitted by

Alexandre Huynen

For the graduation in Civil Engineering,
Civil Engineering Works

Academic Year 2009-2010

Jury:

Vincent Denoël	Professor	University of Liège	Supervisor
Hervé Degée	FNRS	University of Liège	Examiner
Robert Charlier	Professor	University of Liège	Examiner
Emmanuel Detournay	Professor	University of Minnesota	External examiner

Enhancement and parametric analysis of a model of a drilling assembly equipped with a rotary steerable system

Huynen Alexandre

University of Liège - Faculty of Civil Engineering
Academic Year 2009-2010

Abstract

Demand in products derived from crude oil and the decrease of the gas and petroleum reserves have been boosting the petroleum industry to always beat back the limit between reserves and resources, explaining why the interest for directional drilling has been growing up during the last several decades. Nowadays, rotary steerable systems are so efficient that they are becoming the benchmark for the industry. More than one million feet of well-bore are drilled every year using this technology.

The drilling industry handles dimensions and times that cover several order of magnitude. The time scale ranges from seconds for the bit revolution to days for the drilling of a well, while the length scale ranges from hundredth of millimetres for the penetration parameters of a bit in a rock formation to kilometres for the length of a drillstring. This makes the drilling industry such an unfamiliar field which confronts engineers to unconventional challenges.

This complexity may explain why, despite the substantial resources of the oil industry, directional drilling processes are still misapprehended. Indeed, the industry continues to rely on trial and error to control the direction of an oil well. Nevertheless, relatively recent theories try to comprehend the directional behaviour of a drilling assembly in order to predict, with relative success, the geometry of the borehole drilled. Mathematical models of the near-bit region of the drillstring already exist. However the literature covers especially drilling assembly equipped with a push-the-bit system. The main purpose of the second part of this work is to develop a **mathematical model of a drilling assembly** equipped with a point-the-bit system. This one is an enhancement of the *Mathematical Model of the Near-Bit Region of an Advancing Drilling System* developed by Detournay (2007). The model is composed of three interacting components: *(i)* the equations governing the geometrical evolution of the borehole, *(ii)* the laws that link the kinematical bit-rock penetration variables to the forces on the bit, and *(iii)* the relationships between the forces on the bit and the loads on the drillstring.

The third part of this work presents the results of a **parametric analysis** of this mathematical model. The parametric analysis, led in the framework of planar borehole trajectories and stationary solutions, focus on the the borehole curvature and distinguishes the two configurations of the *BHA*: with and without rotary steerable system.

Finally, a brief **case study** of a commercialised point-the-bit system is presented in the fourth part. The goal of this last section is to validate the mathematical model developed and highlight the limitations of this one. Some commonly accepted thoughts are also approached.

Amélioration et étude paramétrique d'un modèle d'assemblage de forage équipé d'un rotary steerable system

Huynen Alexandre

Université de Liège - Faculté des Sciences Appliquées
Année académique 2009-2010

Résumé

La demande croissante en produits dérivés du pétrole cumulée à l'épuisement des réserves ont contraint l'industrie pétrolière à toujours repousser les limites séparant réserve de ressource, expliquant pourquoi l'intérêt envers le forage directionnel n'a fait que croitre durant ces dernières décennies. Actuellement, les "rotary steerable systems" sont d'une efficacité telle qu'ils sont en passe de devenir la référence dans l'industrie. Plus de 300 kilomètres de puits sont forés chaque années au moyen de cette technologie.

L'industrie du forage pétrolier manipule des dimensions et des échelles de temps qui couvrent plusieurs ordres de grandeurs. Les temps mis en jeu varient de la seconde pour une révolution de la tête de forage aux jours pour le forage complet d'un puit. Les dimensions varient, quant à elles, du centième de millimètre pour la pénétration de l'outil dans la roche aux kilomètres pour la longueur du train de tige, faisant du forage pétrolier un domaine relativement inhabituel et qui confronte les ingénieurs à des défis peu conventionnels.

Cette complexité peut expliquer pourquoi, malgré les importantes ressources financières de l'industrie pétrolière, les processus intervenant dans le forage directionnel sont encore peu compris. Actuellement, l'industrie continue à baser le contrôle de la géométrie des puits sur une logique d'essais/erreurs. Néanmoins, certaines théories relativement récentes tentent de comprendre le comportement directionnel des assemblages de forage. Des modèles mathématiques de la garniture de forage existent, cependant la littérature couvre principalement les assemblages équipés de "push-the-bit system". Le but principal de la seconde partie de ce travail est de développer un **modèle mathématique d'un assemblage de forage** équipé d'un "point-the-bit system". Celui-ci est une amélioration du *Mathematical Model of the Near-Bit Region of an Advancing Drilling System* développé par Detournay (2007). Le modèle réside en trois composants couplés: *(i)* les équations régissant l'évolution géométrique du puit, *(ii)* les lois qui lient les grandeurs cinématiques de pénétration de l'outil dans la roche aux forces agissant sur l'outil, et *(iii)* les relations liant les forces appliquées à l'outil aux charges sur le train de tiges.

La troisième partie de ce travail présente les résultats d'une **analyse paramétrique** du modèle mathématique. Celle-ci, menée dans le contexte de trajectoires planes et de solutions stationnaires, se concentre sur la courbure du puit et distingue deux configurations pour la garniture de forage: avec et sans "rotary steerable system".

Pour finir, une **étude de cas** d'un "point-the-bit" commercial est présentée. Le but de cette dernière section est de valider le modèle mathématique développé et de mettre en évidence ses limitations. Certaines idées communément acceptées par l'industrie sont également abordées.

Acknowledgments

I would like to express my gratitude to my advisor, Dr. Vincent Denoël, and to Dr. Emmanuel Detournay for the confidence they grant me by giving me the opportunity to integrate a leading team and to live an experience of a lifetime.

I am also deeply indebted to Dr. Thomas Richard. The knowledge and experience he shared with me through many discussions have led to precious advices and suggestions. On top of that, his enthusiasm, friendship and encouragements have meant a lot to me.

Finally, I am beholden to the following people for various expressions of generosity, friendship and drink: Julien Marck and the joyful couple,Catalina Peña and Luc Perneder,my housemates and officemates; all the "Money Street crew" and especially Gary Gaspar with whom I had the chance to travel and discover this beautiful continent of Australia.

A particular thanks to my parents for their love and generous support throughout this amazing experience.

Contents

List of Figures

List of Tables

Used Symbols

Generally, capital letters (from Latin and Greek alphabet) are adopted to denote quantities referring to the borehole. Contrary, lower case letters denote quantities referring to the drillstring or the bit. Characters overhung by a hat apply to quantities evaluated at the bit, while characters overhung by a bar (two bars) apply to quantities evaluated at the first (second) stabilizer above the bit.

β	Inclination of the bit penetration on the bit axis	
δ	Dimensionless settlement under the first stabilizer	
δ_λ	The Dirac delta function in $x = \lambda$	
η	Lateral steering resistance	$\mathcal{O}(1 \sim 10^2)$
θ	Inclination of the *BHA* on the vertical	
θ_k	Kink angle between the two segment of the *BHA*	
θ_m	Average inclination of the *BHA* between the bit and the second stabilizer	
$\theta_{m,1}$	Average inclination of the *BHA* between the bit and the first stabilizer	
$\theta_{m,2}$	Average inclination of the *BHA* between the first and the second stabilizer	
κ	Dimensionless borehole curvature	$\mathcal{O}(10^{-4})$
$\varkappa_i$	Dimensionless length defined by $\varkappa_i = \lambda_i/\ell$	$\mathcal{O}(10^{-1})$
λ_i	Characteristic dimensions of the *BHA* (see Figure 16)	$\mathcal{O}(1 \sim 10$ m$)$
ν	Bit slenderness ($\nu = b/a$)	$\mathcal{O}(10^{-1} \sim 1)$
φ	Angular penetration per revolution	$\mathcal{O}(10^{-4}$ rad/rev$)$
χ	Angular steering resistance	$\mathcal{O}(10^{-6} \sim 1)$
ψ	Bit tilt	$\mathcal{O}(10^{-2} \sim 10^{-1}$ rad$)$
Γ_0	Dimensionless threshold contact moment	
Γ_1	Dimensionless threshold transverse contact force	
Γ_2	Dimensionless threshold axial contact force	
Δ	Settlement under the first stabilizer	
Θ	Inclination of the borehole on the vertical	
Λ	Dimensionless position of the *RSS* actuator	$\mathcal{O}(10^{-1})$
Ξ	Overgauge factor	$\mathcal{O}(10^{-5})$
Π	Dimensionless weight-on-bit	$\mathcal{O}(10^{-1} \sim 10)$
Υ	Dimensionless rigidity of the *BHA*	$\mathcal{O}(10^{-3} \sim 1)$
Φ	Dimensionless force applied by the *RSS* actuator	$\mathcal{O}(10^{-1})$
Φ_l	Dimensionless left support reaction of the outer housing on the shaft	$\mathcal{O}(10^{-1})$
Φ_r	Dimensionless right support reaction of the outer housing on the shaft	$\mathcal{O}(10^{-1})$

a	Bit radius	$\mathcal{O}(100$ mm$)$
b	Bit gauge height	$\mathcal{O}(100$ mm$)$
d_1	Axial depth of cut per revolution	$\mathcal{O}(1$ mm/rev$)$
d_2	Transverse depth of cut per revolution	$\mathcal{O}(10^{-2}$ mm/rev$)$
f_2	Dimensionless transverse force	$\mathcal{O}(10^{-1})$
ℓ	Length of *BHA* between the bit and the second stabilizer	$\mathcal{O}(10$ m$)$
m	Dimensionless moment	$\mathcal{O}(10^{-2})$
s	Curvilinear coordinate along the *BHA* (with origin at the bit)	
w	Weight per unit length of the *BHA*	$\mathcal{O}(10^3$ N/m$)$
A	Borehole radius	$\mathcal{O}(100$ mm$)$
E	Young's modulus	$210,000$ N/mm^2
$\breve{F}$	Force applied by the *RSS* actuator	$\mathcal{O}(10$ kN$)$
F_1	Axial force	
F_2	Transversal force	$\mathcal{O}(10$ kN$)$
G_0	Threshold contact moment	$\mathcal{O}(10$ kN$)$
G_1	Threshold axial contact force	
G_2	Threshold transverse contact force	
$\mathcal{H}_i, \mathcal{G}_i$	Bitmetrics coefficients	
I	Moment of inertia of the *BHA*	
K	Curvature of the borehole	$\mathcal{O}(10^{-5}$ m$^{-1})$
M_3	Bending moment	$\mathcal{O}(10$ kN.m$)$
S	Curvilinear coordinate along the borehole (with origin at the surface)	
T	Torque-on-bit	$\mathcal{O}(1 \sim 10^2$ kN.m$)$
W	Weight-on-bit	$\mathcal{O}(10^5$ kg$)$

Abbreviations

BHA	Bottom Hole Assembly
DC	Drill Collar
DP	Drill Pipe
HWDP	Heavy Wall Drill Pipe
MD	Measured Depth
PDC	Polycrystalline Diamond Compact
ROP	Rate Of Penetration
RSS	Rotary Steerable System
TVD	True Vertical Depth
WOB	Weight-On-Bit

SI Metric Conversion Factors

degrees (deg)	×	1.745 329	E−02	=	radian (rad)
feet (ft)	×	3.048*	E−01	=	meters (m)
inches (in)	×	2.54*	E+00	=	centimeters (cm)
lbm	×	4.535 924	E−01	=	kg
psi	×	6.894 757	E+00	=	kPa

* Conversion factor is exact.

Part I

Introduction

The use of energy has been a key in the development of the human society. All around the world and throughout history, human activity consumes energy. Managing the production and the consumption of energy is essential in the industrialized world of today since all economic activities require energy resources. The rise of the oil importance was mostly due to the invention of the internal combustion engine and the popularization of the commercial aviation. Currently, the main source of energy is fossil which includes coal, gas and petroleum. In 2008, the worldwide energy consumption was 474.10^{18} Joules with 80 to 90 percent derived from the combustion of fossil fuels (BP, 2010). Petroleum plays an essential role in economy, politics and technology. On top of that, it is also the raw material for many chemical products, including pharmaceuticals, solvents, fertilizers, pesticides and plastics. In summary, its qualities (dense and portable source of energy) to power the vast majority of vehicles[1] combined to the fact that it constitutes the base of many industrial chemicals makes it one of the world's most important commodities.

The demand for oil is highly dependent on the global macroeconomic conditions. According to the International Energy Agency (2004), high oil prices generally have a large negative impact on the global economic growth. The oil price from 1861–2008 presented in Figure 1(a) highlights the correlation between world events and crude oil prices. E.g., it shows sharp increases in 1973 and 1979 during the energy crises. The major trade movements, presented in Figure 1(b), calls attention to the global aspect of the oil inter-area movements.

The increasing use of energy resources since the *Industrial Revolution* has an effect on the environment. Fossil fuels do not only generate air pollutants like carbon dioxide (CO_2), sulphur dioxide and trioxide (SO_x) or nitrogen oxides (NO_x) but also releases traces of metals. The significant increase of greenhouse gases emission (like carbon dioxide) is thought to be responsible for some fraction of the rapid increase in global warming seen especially in the temperature records during the 20th century.

[1] Today, about 90% of transportation fuel needs are fulfilled by oil.

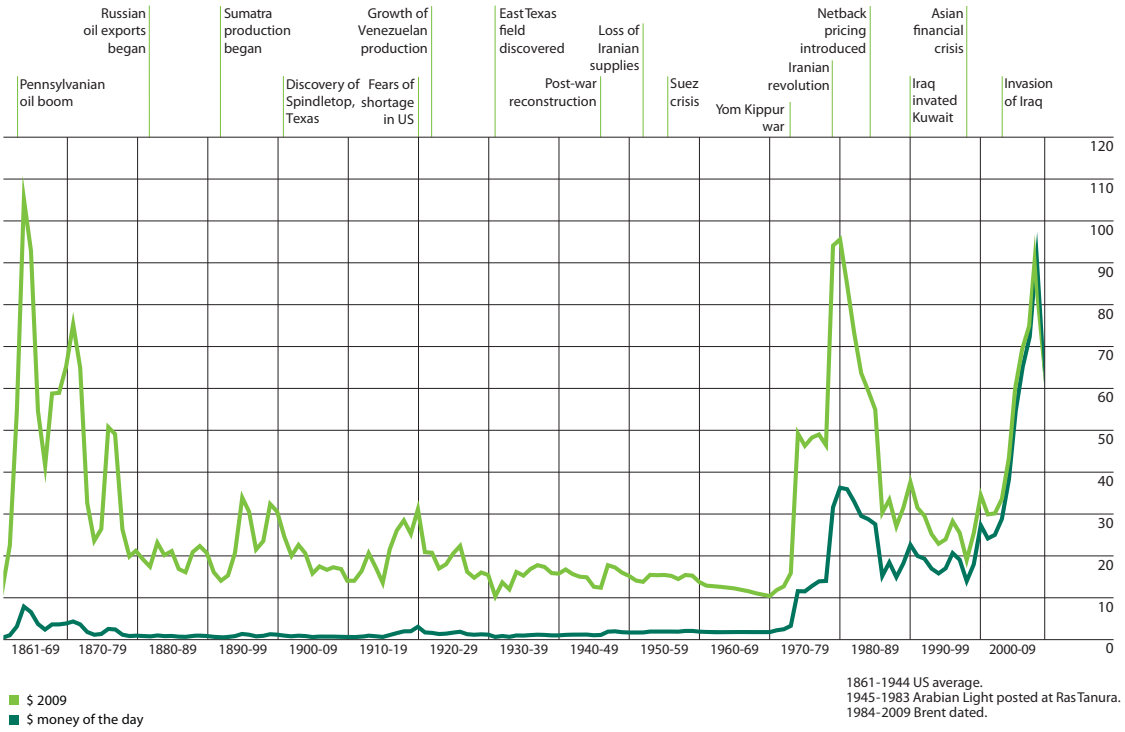

(a) Crude oil prices 1861-2009: US dollars per barrel - World events

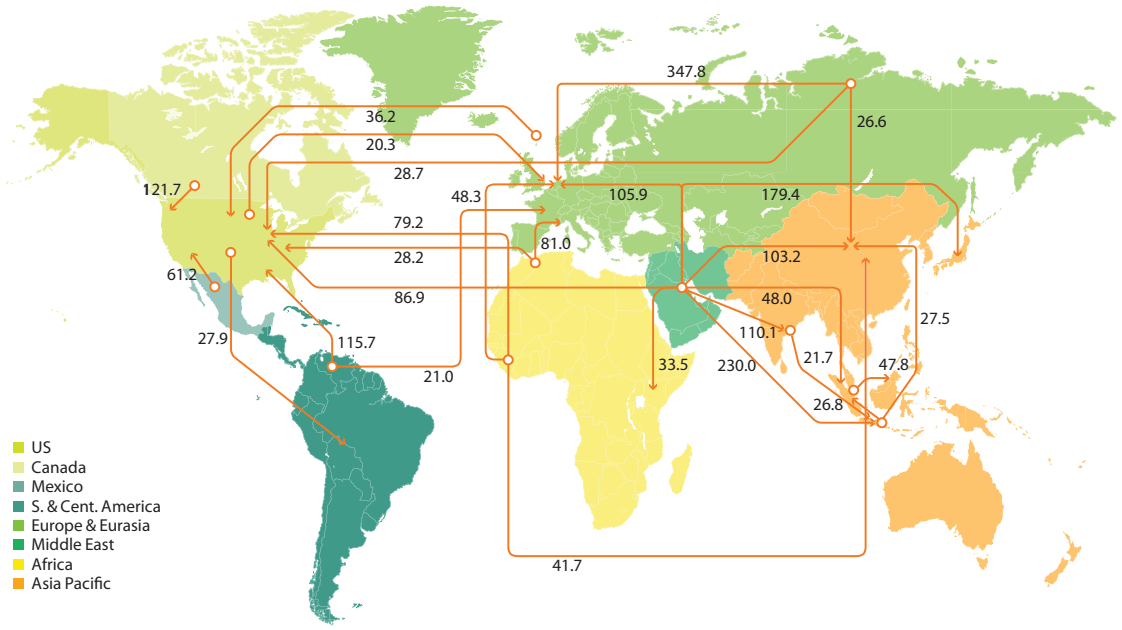

(b) Major trade movements 2009 (million tonnes)

Figure 1: Oil prices and trade flows worldwide (BP, 2010)

The consumption of energy at a greater rate than its regeneration leads the gas and petroleum reserves to decrease. For the first time, the physical limits of the Earth are met under the combination of finite resources and gas emissions. According to the Society of Petroleum Engineers et al. (2007), contingent resources are quantities of petroleum estimated to be potentially recoverable but which are not currently considered to be commercially recoverable due to one or more contingencies. On the other side, reserves are those quantities of petroleum anticipated to be commercially recoverable by application of development projects to known accumulations from a given date forward under defined conditions. In other words, reserves are all resources attainable with the current technology and for profit while reserves are not currently considered lucrative. The global distribution of oil proved reserves at the end of 2009 are presented in Figure 2(a) while the evolution of this distribution is presented in Figure 2(b).

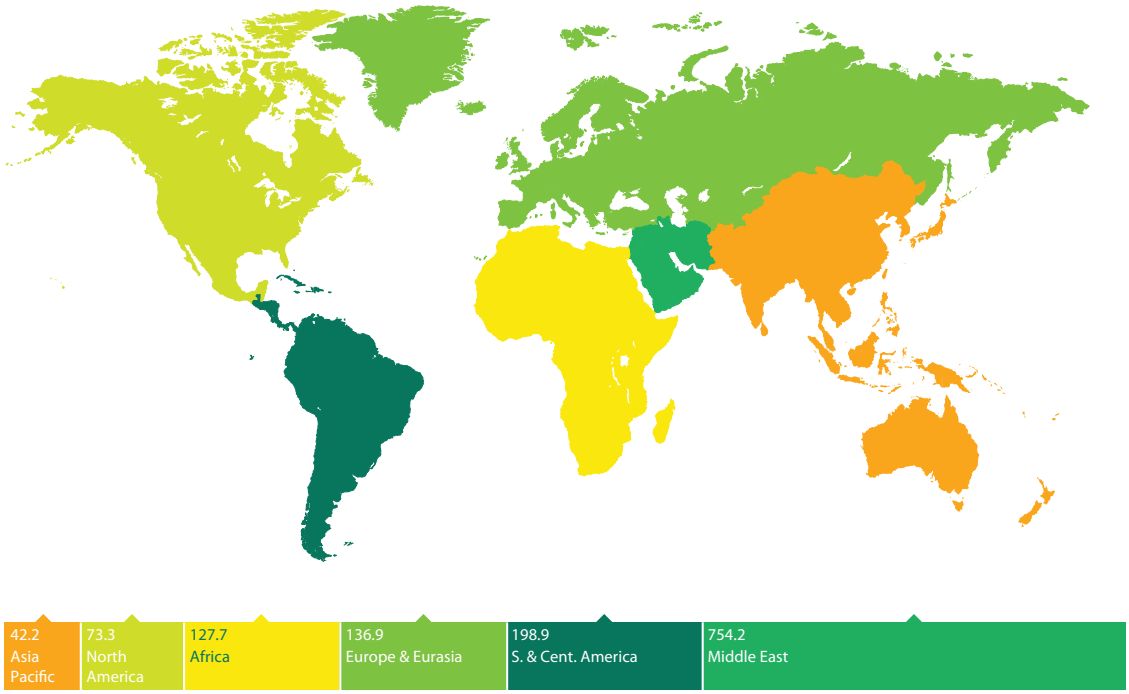

(a) Proved reserves at end 2009 (Thousand million barrels)

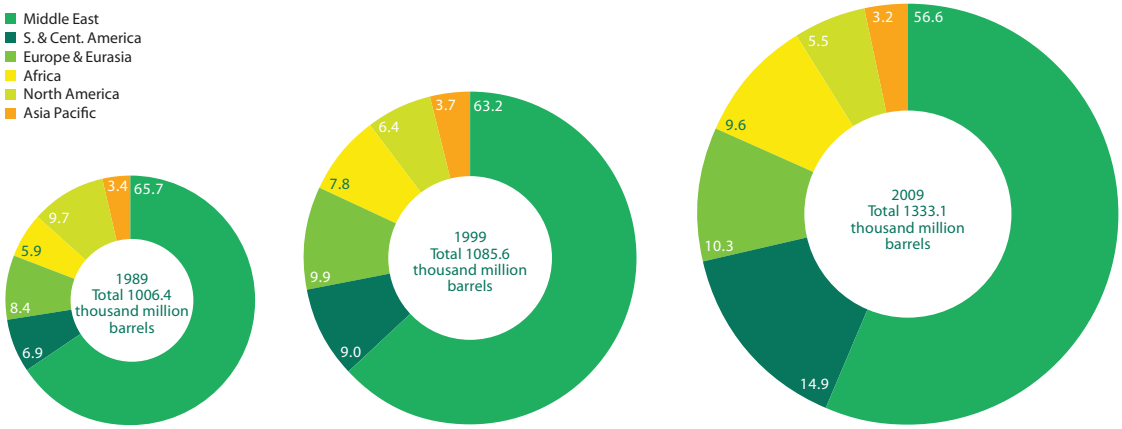

(b) Distribution of proved reserves in 1989, 1999 and 2009 (Percentage)

Figure 2: Oil proved reserves distribution and evolution (BP, 2010)

Demand in products derived from crude oil and the decrease of the gas and petroleum re-

serves boost the petroleum industry to always beat back the limit between reserves and resources. Now, the drilling industry meets more challenging drilling objectives everyday, which explains the growing interest for directional drilling during the last decades.

1 Drilling

Well drilling is the process of building a hole in the ground in order to extract a natural resource (such as ground water, natural gas or petroleum) or for the exploration of the nature. Two main technologies have been invented: the percussion and the rotating drilling. Nowadays, most common rigs in use are rotary drilling rigs. Their mechanics are quite simple: a rotating bit breaks loose the rock at the bottom of the hole while the rock fragments are swept away and lifted out of the hole by the mud stream. The main tasks of a rotary rig are to create rotation of the drillstring, to provide the infrastructure to advance and lift the drillstring and to establish the casing. The rotation of the drillstring is obtained by means of a rotary drive[2] system which can be at the surface but could also be at the bottom hole (downhole motor). Downhole motors are special engines located above the bit to promote bit rotation, they convert hydraulic power of the drilling fluid into mechanical power.

The mud consists generally of water with viscosifiers and weighting materials. In addition to clean, cool and lubricate the bit, it maintains the stability of the borehole walls by exerting a sufficient hydrostatic pressure. Powerful pumps, usually located at the derrick floor, are used to inject the drilling fluids to the bit through the drillstring and then flow up between the drillstring and the borehole.

One of the largest portion of the total cost of a drilling project return to the casing of steel pipes which is put in place to stabilize the borehole walls. The clearance between the casing and the borehole is filled with cement. As the well becomes deeper, the diameter of the casing used gets smaller, the diameter of the well can vary from 30 to 4 in, or from 76 to 10 cm (Sampaio, 2008).

1.1 The Drillstring

The purpose of the drillstring is to transmit axial force, torque, and drilling fluid (hydraulic power) to the bit. A basic drillstring is schematically presented in Figure 3, it is composed of the following components:

The swivel is suspended by the hook of the traveling block and allows the drill-string to rotate as drilling fluid is pumped to within the drillstring. It also supports the axial load of the drillstring.

The kelly is a long four-sided (square) or six-sided (hexagon) steel bar with a hole drilled through the middle for a fluid path. The purpose of the kelly is to transmit rotary motion and torque to the drillstring (and consequently to the drill bit), while allowing the drillstring to be lowered or raised during rotation. The length overall of the kelly is about 50 ft (15 m).

Drill pipes (DP) generally compose the upper (right bellow the kelly assembly) and longer portion of the drillstring, usually about $15,000$ ft ($4,500$ m). They must be light and strong. The outside diameter usually varies from $2^3/_8$ to $6^5/_8$ in (or 6 to 17 cm).

Drill collars (DC) are thick and heavy pipes normally located right above the bit. The purpose of the drill collars is to provide the axial force to the bit, *i.e.,* the weight on bit (WOB).

[2]The rotary speed at the surface is between 50 and 200 revolutions per minute for usual bits while the torque required to rotate the string at surface may vary between 0.5 and 50 kN.m. The torque on the bit varies between 0.5 and 10 kN.m.

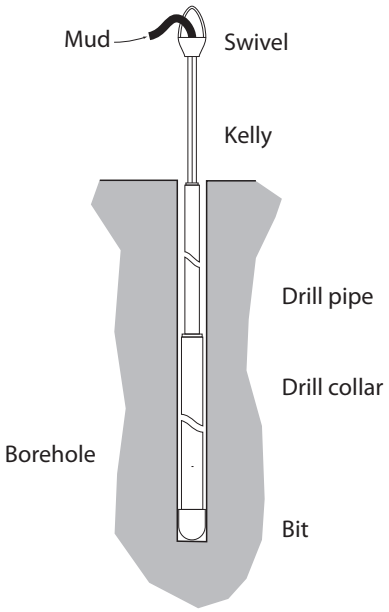

Figure 3: A basic drillstring and its components

Sometimes, heavy wall drill pipes ($HWDP$) are used in addition. They are strong enough to be under compression and they are flexible enough to be used in directional drilling. The overall length of DC is usually about $10,000$ ft ($3,000$ m).

Stabilizers are used to provide localized supports to the drillstring. They are essential in directional drilling and their space distribution highly conditions the behaviour of the bottom hole assembly. In vertical drilling, they can be used to limit low vibrations frequency while drilling. Different kinds of stabilizers are shown in Figure 4.

Figure 4: Different kinds of stabilizers

The bottom hole assembly (BHA) consists in the lower part of the drillstring. It is composed of drill collars, stabilizers and heavy wall drill pipes. This part is loaded in compression and can be several hundred meters long. The WOB has a typical value between 0 and 250 kN.

1.2 Drill Bits

Drill bits are connected to the lower end of the drill collars. There are a large variety of bits. Each type is designed to drill rocks of different hardness, composition, abrasiveness, etc. encountered during drilling operations but the selection of the appropriate bit depends also on the expected drill trajectory and the diameter of the borehole. The choice of the appropriate bit is extremely important. Drilling bits constitute just a fraction (one to five percent) of total well costs but are a critical component. Indeed, total well cost is widely dependent of the performance of the bit, *i.e.,* the time required to drill the well (the bit's efficiency and the bit life).

Drill bits can be classified in two main families: roller cone bits and fixed cutter bits (or drag bits).

1.2.1 Roller Cone Bits

Roller cone bits consist in rotating conical cutters or cones. The rotation of the cones, caused by the rotation of the drillstring, brings new teeth in contact with the bottom of the hole. The concentrated weight on those teeth crushes the rock and break it up into small pieces. This kind of bit required thus a heavy *WOB*. As the cone rolls, the torque needed at the bit is small.

There are two main types of roller cone bits, steel milled-tooth bits and carbide insert bits while the number of cone can vary between two and four. Two roller-cone bits are shown in Figure 5.

Figure 5: Tricone drill bits

1.2.2 Drag Bits

In the beginning of the drilling industry, all the bits were of the drag type. Drag bits have an integral cutting element and no moving parts. They drill with a shearing action under the action of axial force and rotation. This shearing process requires usually less *WOB* than the indenting process of roller-cone bits but a larger torque.

Drag bits can be split in two main classes: diamond impregnated bits and polycrystalline diamond compact bits. All of them take advantage of the properties of diamonds like extreme hardness, compressive strength, and thermal conductivity.

Polycrystalline diamond compact bits

Polycrystalline diamond compact (*PDC*) bits have been used since late 70's. They are usually

more expensive than roller-cone bits but have a better rate of penetration (ROP) and longer life in some hard and abrasive formations.

PDC bits shear the rock with a continuous scrapping motion by means of cutters made of synthetic diamond disk, see Figure 6(a). The cutters are about 1/8 in (3, 2 mm) thick and about 1/2 to 1 in (12, 7 to 25, 4 mm) in diameter. The number, size, position and shape of the chips are important parameters in *PDC* bits performances.

Diamond impregnated bits

The objective of diamond impregnated bits is to provide a sharp cutting edge at any moment. The cutting elements are made of (synthetic) diamonds suspended in a tungsten-carbide matrix, see Figure 6(b). The matrix erodes when diamonds become worn and blunt in order to expose new sharp diamonds.

Primarily those bits were used exclusively in hard and abrasive formations, where *PDC* bits are too slow and roller-cones wear out quickly, and for coring. However, nowadays some of them are designed to drill also medium hard formations.

(a) Polycrystalline diamond bits (b) Diamond impregnated bits

Figure 6: Drag bits

1.3 Directional Drilling

Directional drilling started as corrective operations occurring during drilling, as sidetracks due to fishing operation failures. But the drilling industry started really to take an interest in this technology, in the late 1920's, when there were several lawsuits about wells drilled from a rig on one property that had crossed the boundary and were penetrating a reservoir on an adjacent property. The 1970's and their energy crisis initiated this technology to be profitable, especially for offshore reserves. In the 1990's the introduction of the commercial rotary steerable system (RSS) revolutionized directional drilling. Nowadays, directional drilling is so efficient that it is becoming the benchmark for the industry. More than 75% of the well drilled from offshore rigs are directional wells.

Directional drilling offers substantial increases in production over vertical wells. Drilling trough the reservoir at an angle, and thus increasing the exposed section trough the reservoir, allows drainage improvements of the oil slick. Reservoirs where vertical access is difficult or not possible

(for instance an oilfield under a town, under a lake, or underneath a difficult to drill formation) are now accessible. Allowing more wellheads to be grouped together on one surface location can allow fewer rig moves, less surface area disturbance, and make it easier and cheaper to complete and produce the wells.

Several methods and equipments are available to steer the borehole and impose the trajectory of the bit. According to Sampaio (2008), the main families are presented below.

Whipstocks are the oldest technique but the most time consuming. A whipstock can be described as a wedge placed in the borehole to force the drill bit to start drilling in a direction away from the borehole axis. It produces a kick-off point with exact depth control and a precise direction.

The Hydraulic Method or jetting requires the use of a jetting bit to wash away the formation. This technique can only be used in soft–medium formation in which hydraulic power can be used to wash away a lateral "pocket" of the formation to initiate deflection.

Downhole Motors or mud motors are designed to turn the bit without the need to rotate the drill string. Thus, it is possible to orient the bit in a desired direction, and maintain it in this direction throughout the bit run. There are two types of downhole motors:

- Positive Displacement Motors are rotor-stator assemblies, consisting of a helical rotor that moves within a molded, elastomer–lined stator. In general, more torque will be generated by configurations employing greater numbers of lobes.
- Turbine Motors consist of multistage motor, each stage comprising a rotor a stator. They operate at relatively high rotary speeds, and so are run exclusively with fixed cutter bits.

Rotary Steerable Systems allow continuous rotation of the drillstring while steering the bit (3D directional control). The drilling efficiency they provide leads to tangible improvements in cost-per-foot and drilling optimization. Rotary steerable systems use a subassembly behind the bit, which can be operated from the surface. They can be divided in two main groups:

- The Point-The-Bit System steers the bit by tilting the bit in the direction of the desired curve, see Figure 7(a). Usually the bit is tilted by bending the transmission shaft inside a non-rotating housing.
- The Push-The-Bit System steers the bit by applying a side load that forces the bit laterally in the direction of the desired curve, see figure 7(b). A system of hydraulic actuated pads located close to the bit creates the lateral force with controlled direction and magnitude at the bit, which causes the deviation.

There are advantages and disadvantages to both systems. The choice between those two systems depends widely on the situation: the tortuosity of the path, the kind of bit, etc.

Whipstocks and the hydraulic method fell into disuse with the advent of downhole motors in the 1970's. Twenty years later, the introduction of commercial rotary steerable systems revolutionized directional drilling. Nowadays, the process of drilling highly deviated wells is almost automated thanks to these devices. Actually more than one million feet of well-bore are drilled every year using rotary steerable systems and application of such systems has now spread to many of the major oilfields in the world.

The number of stabilizers, their positions and the stiffness of the elements of the *BHA*, *i.e.,* the geometry of the *BHA*, influence widely the directional behaviour of the drilling system and so the trajectory of the well.

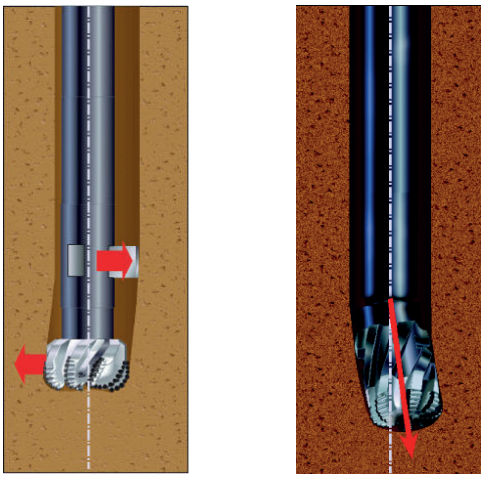

(a) The point-the-bit system (b) The push-the-bit system

Figure 7: Schematic description of the two main rotary steerable systems (*RSS*)

1.4 A Bit of History

Contrary to what we would expect, the drilling industry is not recent. Despite it involves relatively complex processes, drilling oil wells originated more than 1,500 years in China, where the oil was burned to evaporate brine and produce salt. The evolution of the drilling industry through the ages, especially through the last century, is phenomenal. Drilling methods are now far from the use of sharpened bamboos and involve high-tech systems to reach unimaginable depths or extended-reaches. A non exhaustive time-line is presented below, it parallels some technological advances or highlights related to the oil industry.

347 Oil wells are drilled in China up to 800 ft (240 m) deep using bits attached to bamboo poles;

1845 The rotary drilling method is patented in England;

1846 Canadian Abraham Gesner develops a process to distil kerosene (coal oil) from coal and bituminous shale;

1876 Nicolaus Otto invents the first four-stroke internal combustion engine, the Otto Cycle Engine, which he uses to build a motorcycle;

1893 Drilling depths reach $6,575$ ft (2004 m);

1896 Henry Ford builds his *"quadricycle"*;

1897 The first offshore drilling is done off the coast of Santa Barbara, California;

1908 First rock bit use;

1927 Charles Lindberg makes the first non-stop solo flight across the Atlantic;

1933 Tricone bits are introduced;

1947 Drilling depths reach $17,776$ ft (5418 m);

1953 The first fully hydraulic rig is introduced;

1958 More than a million passengers fly over the Atlantic Ocean, surpassing the total of Atlantic steamship passengers for the first time;

1973 *PDC* bits are introduced;

1974 Drilling depths of $31,441$ ft ($9,558$ m) are accomplished in Oklahoma. The Bertha Rogers well encountered enormous pressure, almost $25,000$ psi (172 kPa);

1989 The Kola Superdeep Borehole, SG-3, reaches $40,230$ ft ($12,262$ m), it is the deepest hole ever drilled . High unexpected temperatures (180 °C) at this depth and location prevents to drill deeper;

2008 In the Al Shaheen oil field (north east of Qatar), the GSF Rig 127 sets a world record for the longest extended-reach well ever drilled at $40,320$ ft ($12,289$ m) measured depth[3] with a $35,770$ ft ($10,902$ m) horizontal section.

Nowadays, the drilling industry handles dimensions and times that cover several order of magnitude. The time scale ranges from seconds for the bit revolution to days for the drilling of a well, while the length scale ranges from hundredth of millimetres for the penetration parameters of a bit in a rock formation to kilometres for the length of a drillstring. This makes the drilling industry such an unfamiliar field which confronts engineers to unconventional challenges.

[3]The measured depth, *MD*, is the length of the path of the wellbore. This measurement differs from the true vertical depth of the well in all but vertical wells.

Part II

Mathematical Model

Initial mathematical models of drilling assembly were analytical or semi-analytical, they were developed during the 50's and 60's by Lubinski and Woods (1953) followed by Murphey and Cheatham (1965). Those theories offer qualitative explanations or a means for calculating solutions to deviations problems for certain restricted conditions (such as straight inclined holes).

With the advent of finite element methods in the industry during the late 70's to 80's, Amoco Production group produced an important contribution through the publications of Millheim (1977-1981), Brett et al. (1986) and Warren (1987). The first boundary condition involving bit rock interaction laws is added by Brett et al. (1986).

In the late 80's and the early 90's, Ho contributed widely to the modelling of the bit rock interaction, see Ho (1986; 1987; 1989; 1995). However, the procedure to propagate the borehole and determine the evolution of the complete system (*BHA* structure and bit-rock interactions) is not described in his publications or patents.

The University of Braunschweig and the mud motor and rotary steerable division of Baker Hughes (Inteq) worked essentially on the active control of trajectory with rotary steerable system. A set of publications were published through this German collaboration (Heisig et al., 1996; Neubert and Heisig, 1996; Neubert, 1997; Pastusek et al., 2005; Neubert et al., 2005).

More recently, the very active Paris School of Mines pursues the work undergone at the French oil company Elf in the mid 80's by Birades and Fenoul (Birades, 1986; Birades and Fenoul, 1986 and 1988). The main contribution concerns the characterisation of the bit rock interface. Although they present some results of numerical simulations of borehole trajectories (Menand et al., 2002, 2003, 2006; Boualleg et al., 2006), mathematical details of the model are available only in Ph.D theses (Simon, 1996; Maouche, 1999).

All models described in the literature differ by the type of model used to described the mechanical response of the *BHA* and by the boundary conditions4 nature applied. The vast majority

of the models account only for the lower part of the drillstring, *i.e.,* from the drill bit up to the last considered stabilizer or up to the *point of tangency*, but they can diverge on

- the nature of the trajectory: planar or 3D;
- the behaviour of the solution: dynamic or static;
- the method used to solve the equations: analytic, finite elements or finite differences;
- the number of stabilizer;
- the presence of a rotary steerable system;
- the nature of the boundary conditions applied at the lower point (the bit) and at the upper point;
- etc.

But the main purpose of those models is to relate the loads applied on the drillstring to the forces acting on the bit.

The directional behaviour of a drilling assembly depends not only on the drillstring but also on the bit, these two components are mechanically linked. Indeed the forces acting on the bit are transmitted by the drillstring while the behaviour of the drillstring depends on its boundary conditions at the bit. When a bit-rock interaction model (which predict the drill ahead tendency of the bit) is coupled with a drillstring model, the propagation of the borehole and the future trajectory of the bit can be estimated.

The theory initiated by Detournay (2007) lead to the development of a rigorous directional drilling model. This mathematical model consists of three interacting components (see Figure 8):

- The equations governing the geometrical evolution of the borehole, which includes the relationships between the kinematical state variables characterizing the penetration of the bit in the rock and the geometrical quantities describing the borehole.
- The laws that link the kinematical bit/rock penetration variables to the forces on the bit. The characterization of the bit in the bit-rock interaction law is compatible with the mechanical description of the *BHA*, which is typically modelled within the framework of beam theory.
- The relationships between the forces on the bit and the loads on the *BHA*. Evidently, these relations involves the elastic response of the *BHA* and the contacts between the drillstring and the borehole wall.

This model distinguishes especially from the *traditional* models by the nature of the boundary conditions considered at the bit for the beam problem. Indeed, in view of the bit-rock interaction feature developed in this theory, force-velocity (penetration per revolution) boundary conditions substitute the classical force-displacement boundary conditions.

This part of the work proposes to develop a mathematical model of drilling assembly equipped with a point-the-bit system based on the theory established by Detournay. The originality of this work lies in the fact that the literature covers exclusively drilling assembly equipped with a push-the-bit system. No (mathematical) model of point-the-bit system has been developed up to this point or at least has been published, to our knowledge.

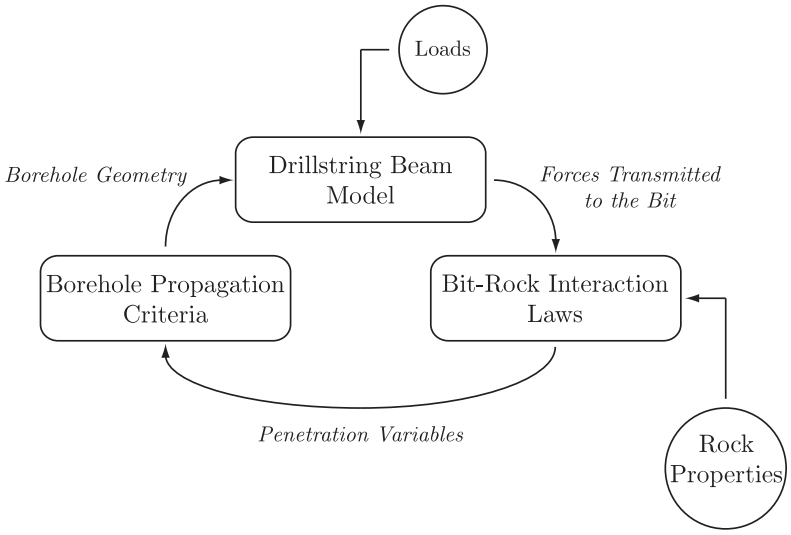

Figure 8: Schematic description of the complete mathematical model of a drilling assembly equipped with a rotary steerable system

1 Problem Definition

1.1 Point-the-Bit System Description

It is commonly accepted in the industry that point-the-bit system steer the bit by "tilting" the bit in the direction of the desired curve. We distinguish two main methods to "tilt" the bit:

- The drive shaft is bended inside a non-rotating housing as in Figure 9(a);
- A pre-determined bias is hold by a geo-stationary unit inside a rotating housing as in Figure 9(b).

But this work will focus on the first technology which is currently more common in the industry. We will thus only consider the configuration in which the bit tilt is obtained by imposing a deflection to the transmission shaft by means of *eccentric rings* or *pads*. These actuators are usually controlled through a hydraulic system.

(a) Internally deflected driveshaft on a non-rotating housing

(b) Geo-stationary unit keeps bit tilt angle in a rotating section

Figure 9: Point-the-bit systems: two main methods to tilt the bit (Sugiura, 2008)

This technology incorporates two adjacent stabilizers to maintain the system inside the borehole. It is commonly accepted in the industry and by drillers that the near-bit stabilizer acts as a fulcrum point[4] and orients the drill bit axis in the desired direction. From this point of view

[4]A fulcrum point is a fixed point of support of a lever which acts as the pivot about which the lever turns.

and considering the "Force and Levers" theory, the shorter the distance between the bit and the fulcrum point, the less force has to be developed by the actuator at the steering unit for the same side force acting at the bit. For this reason, some drillers prefer to use long passive gauge bits in order to reduce the length between the bit and the fulcrum point. Influences of those parameters are investigated in the parametric analysis (Part III) and in the case study (Part IV) of this work.

1.2 Reduced Problem

This report focuses on the **near-bit region** of the borehole that contains the *BHA* segment with the bit and the two first stabilizers. However the complete version of this problem would include the complete description of the drillstring (from the bit to the rig) and the entire geometry of the borehole, the reduced problem presented in this work is likely to be sufficient to predict the borehole evolution. Influence of the *BHA* and the drillstring above the second stabilizer is bracketed by the consideration of two limiting boundary conditions at the upper stabilizer, either zero moment or zero rotation relative to the borehole axis. Moreover, we consider no penetration of the stabilizers into the rock and that their diameter is close to the borehole diameter, meaning that drillstring is compelled to lie on the borehole axis at the stabilizers.

We further assume that the bit follows a **plane trajectory**, *i.e.,* that the borehole axis is a plane curve. Since all quantities (such as forces or velocities) used in the model are averaged over at least one revolution of the bit, bit-rock interaction laws involve the same set of parameters both in planar than in non-planar borehole geometries. Consequently, this assumption does not trivialize the boundary conditions at the bit-rock interface.

Finally, we focus on the equilibrium points of the dynamical system, *i.e.,* on the **stationary solutions** of the problem. Due to the changing orientation of the borehole with respect to the gravitational field, the only stationary solutions for planar borehole are the trivial cases of a straight borehole. Nevertheless, in most situations, solutions of the evolutionary system can be estimated as a sequence of stationary solutions. The stationary solutions are the equilibrium points of the system of equations (3), they obviously correspond to segments of borehole characterized by a constant curvature and by a constant diameter (see section 2, Geometrical Problem of the Borehole).

In the following sections we expand the three interacting components of the mathematical model. Firstly the borehole propagation criteria is introduced, this leg of the complete model relates the borehole geometry to the penetration variables of the bit. Secondly we establish the bit-rock interaction laws which associates the forces acting on the bit to the penetration variables of the bit. Finally we develop the drillstring beam model, this third leg establishes the relations between the loads applied on the drillstring and the forces and moments acting on the bit.

Notation adopted

Generally, capital letters (from Latin and Greek alphabet) are adopted to denote quantities referring to the borehole. Contrary, lower case letters denote quantities referring to the drillstring or the bit. Characters overhung by a hat apply to quantities evaluated at the bit, while characters overhung by a bar (two bars) apply to quantities evaluated at the first (second) stabilizer above the bit.

2 Geometrical Problem of the Borehole

At the lengthscale of its current length (L) and in the context of planar trajectories, the borehole is a 1D object. Its geometry can be thus completely defined by the inclination angle $\Theta(S)$

corresponding to the curvilinear coordinate S, see Figure 10(a). Associating $S = 0$ to the borehole entry on the earth surface and $S = L$ to the current hole bottom, $\Theta(S)$ is a function defined on $0 \leq S \leq L$.

If we consider now the borehole at the lengthscale of the bit radius (a), this 1D description is not sufficient to catch the clearance between the bit and the borehole which affects the tilt of the bit ψ, see Figure 10(b). The overgauge factor $\Xi(S)$ is thus introduced

$$\Xi(S) = \frac{A(S)}{a} - 1 \tag{1}$$

with $A(S)$ denoting the mean borehole radius at coordinate S. For apparent technological reasons, the overgauge cannot be negative.

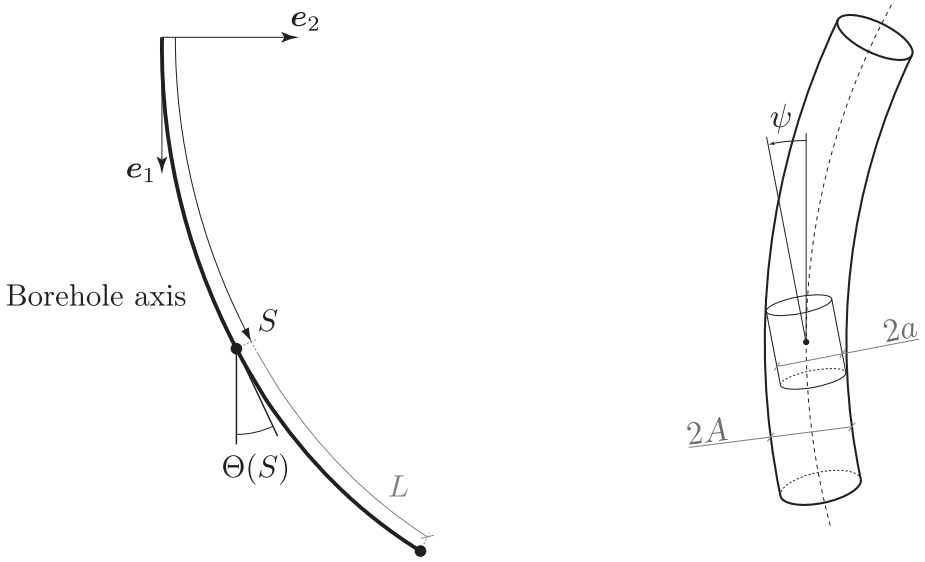

(a) Definition of the curvilinear coordinate S, the length of the borehole L and the inclination angle Θ

(b) Correlation between the bit tilt ψ and the clearance between the bit and the borehole

Figure 10: Geometrical problem of the borehole

In summary, modelling directional drilling requires to consider the borehole as a "1D+ε" object in order to distinguish both lenghtscale L and a. The borehole geometry is then completely described by the two functions $\Theta(S)$ and $\Xi(S)$. The borehole curvature $K(S)$ is also introduced

$$K(S) = \frac{\mathrm{d}\Theta(S)}{\mathrm{d}S} \tag{2}$$

In term of the borehole propagation problem we need to formulate the evolution of the borehole geometry when its length grows from L to $L + \Delta L$. As shown by Detournay (2007), the borehole propagation problem can be cast mathematically as a spatial evolution problem described by a system of two differential equations, a second order one in $\Theta(S)$ and a first order one in $\Xi(S)$

$$\frac{\mathrm{d}^2\Theta}{\mathrm{d}S^2} = F(S) \qquad \text{and} \qquad \frac{\mathrm{d}\Xi}{\mathrm{d}S} = G(S) \tag{3}$$

It is now obvious that the stationary solutions of the problem, corresponding to the equilibrium points of this system of equations, is characterized by a constant curvature and by a constant diameter.

3 Bit-Rock Interaction Problem

As we already pointed out, one particularity of this theory is that the bit-rock interactions at the bit are force-velocity boundary conditions. Indeed a pseudo time is involved in the laws relating forces on the bit to the penetration *per revolution*. This penetration of the bit in the rock over one revolution involves removal rock and is associated to the incremental propagation of the borehole. The kinematics of the bit is described by the penetration vector $\boldsymbol{d}$ and the angular penetration vector $\boldsymbol{\varphi}$ which are linked to the velocity $\boldsymbol{v}$ and spin $\boldsymbol{\omega}$ vectors:

$$\boldsymbol{d} = \frac{2\pi \boldsymbol{v}}{\Omega} \qquad \text{and} \qquad \boldsymbol{\varphi} = \frac{2\pi \boldsymbol{\omega}}{\Omega} \tag{4}$$

and where Ω is the magnitude of the bit angular velocity vector $\boldsymbol{\Omega}$.

Due to the assumption of plane trajectories, the vector $\boldsymbol{d}$ is restrained in the plane of the borehole axis while the vector $\boldsymbol{\varphi}$ is orthogonal to that plane. Those vectors can be expressed in the director basis associated to the bit $(\hat{\boldsymbol{\imath}}_1, \hat{\boldsymbol{\imath}}_2, \hat{\boldsymbol{\imath}}_3)$. The penetration per revolution of the bit is then described by three quantities (for planar trajectories): *(i)* the axial penetration d_1, *(ii)* the lateral penetration d_2 and *(iii)* the angular penetration φ_3, see Figure 11. The penetration vector $\boldsymbol{d}$ is tangent to the borehole axis, its inclination β on the axis of revolution of the bit $\hat{\boldsymbol{\imath}}_1$ is given by

$$\beta = \arctan\left(\frac{d_2}{d_1}\right) \tag{5}$$

and is related to the bit tilt by the relation

$$\psi + \beta = 0 \tag{6}$$

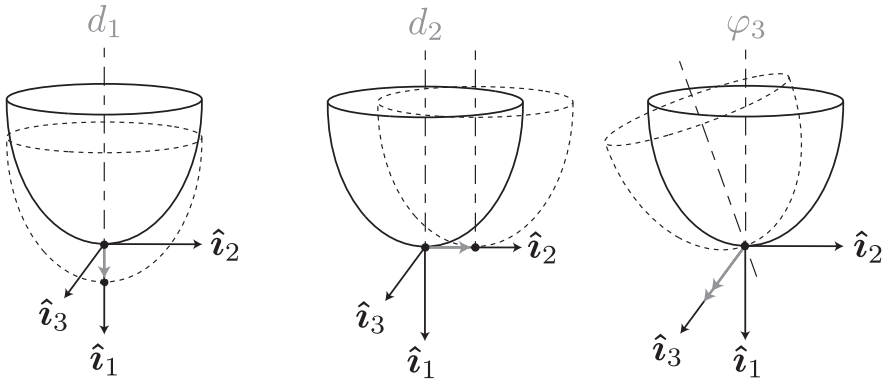

Figure 11: Penetration parameters for a plane trajectory. Definition of the axial penetration d_1, the lateral penetration d_2 and the angular penetration φ_3 (Perneder, 2008a)

3.1 Interface Laws for Space Trajectories

Bit-rock interface laws are the relations between the kinematic parameters of the bit and the dynamic quantities acting on the bit, *i.e.,* the forces and moments. The general formulation of the bit-rock interface laws links the vector of the generalized forces applied on the bit $\boldsymbol{\mathcal{F}}$ and the generalized penetration vector $\boldsymbol{\mathcal{D}}$ by the expression

$$\boldsymbol{\mathcal{F}} = \boldsymbol{\mathcal{H}}(\boldsymbol{\mathcal{D}}) \tag{7}$$

In the general context of a 3D trajectory, the two generalized vectors are defined as

$$\boldsymbol{\mathcal{F}} = \left\{\hat{F}_1, \hat{F}_2, \hat{F}_3, \hat{M}_2, \hat{M}_3\right\}^T \tag{8}$$

$$\boldsymbol{\mathcal{D}} = \left\{d_1, d_2, d_3, \varphi_2, \varphi_3\right\}^T \tag{9}$$

Considerations about the bit symmetry, the nature of the interaction (see Appendix A) and the assumed rock isotropy allow to express the general formulation (7) as a linear relationship between $\boldsymbol{\mathcal{F}}$ and $\boldsymbol{\mathcal{D}}$. It has been shown by Detournay (2007) that this linear relationship can be written as

$$\begin{Bmatrix} \hat{F}_1 \\ \hat{F}_2 \\ \hat{F}_3 \\ \hat{M}_2 \\ \hat{M}_3 \end{Bmatrix} = - \begin{Bmatrix} \mathcal{G}_1 \\ \mathcal{G}_2 \\ \mathcal{G}_3 \\ \mathcal{G}_4 \\ \mathcal{G}_5 \end{Bmatrix} - \begin{bmatrix} \mathcal{H}_{11} & 0 & 0 & 0 & 0 \\ 0 & \mathcal{H}_{22} & \mathcal{H}_{23} & \mathcal{H}_{24} & \mathcal{H}_{25} \\ 0 & \mathcal{H}_{32} & \mathcal{H}_{33} & \mathcal{H}_{34} & \mathcal{H}_{35} \\ 0 & \mathcal{H}_{42} & \mathcal{H}_{43} & \mathcal{H}_{44} & \mathcal{H}_{45} \\ 0 & \mathcal{H}_{52} & \mathcal{H}_{53} & \mathcal{H}_{54} & \mathcal{H}_{55} \end{bmatrix} \begin{Bmatrix} d_1 \\ d_2 \\ d_3 \\ \varphi_2 \\ \varphi_3 \end{Bmatrix} \tag{10}$$

where the coefficients of the matrices $\boldsymbol{\mathcal{G}}$ and $\boldsymbol{\mathcal{H}}$ depend on the bit tilt.

The existence of off-diagonal terms reflects the non-coaxiality between dynamic and the kinematic quantities. Indeed, the terms $\mathcal{H}_{23} = \mathcal{H}_{32}$ express the non-coaxiality of the side force vector $(\hat{F}_2, \hat{F}_3)$ and the lateral penetration vector (d_2, d_3). This phenomenon, which is called *bit walk*, results from the rotation of the drill bit and is characterized by the bit walk angle α between the side force vector and the lateral penetration vector (see Figure 12). Comparably, the existence of the off-diagonal terms $\mathcal{H}_{45} = \mathcal{H}_{54}$ lead to the non-coaxiality of moment vector $(\hat{M}_2, \hat{M}_3)$ and the rotation vector of the bit (φ_2, φ_3).

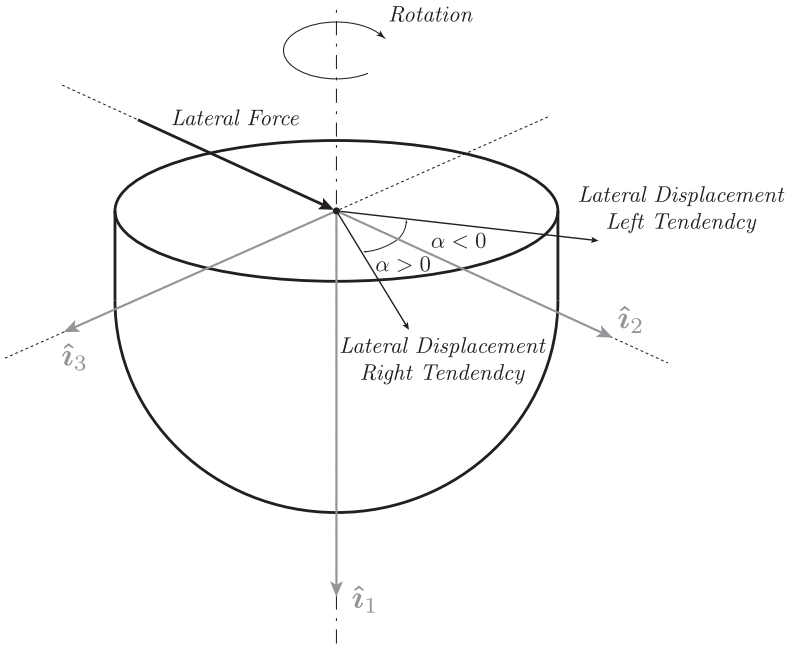

Figure 12: Definition of the left and right walk tendency of a bit and of the walk angle α (Perneder, 2008a)

Perneder (2008a) determined the expression of the elements $\mathcal{H}_{ij}$ and $\mathcal{G}_i$ and showed that the matrix $\boldsymbol{\mathcal{H}}$ is not symmetric.

3.2 Interface Laws for Plane Trajectories

In the context under consideration, *i.e.,* a plane trajectory contained in the plane $(\hat{\boldsymbol{\imath}}_1, \hat{\boldsymbol{\imath}}_2)$, both penetration variables d_3 and φ_2 vanish[5]. The general formulation of the bit-rock interactions given by Equation (10) can thus be simplified as

$$\begin{Bmatrix} \hat{F}_1 \\ \hat{F}_2 \\ \hat{M}_3 \end{Bmatrix} = - \begin{Bmatrix} \mathcal{G}_1 \\ \mathcal{G}_2 \\ \mathcal{G}_0 \end{Bmatrix} - \begin{bmatrix} \mathcal{H}_{11} & 0 & 0 \\ 0 & \mathcal{H}_{22} & \mathcal{H}_{25} \\ 0 & \mathcal{H}_{52} & \mathcal{H}_{55} \end{bmatrix} \begin{Bmatrix} d_1 \\ d_2 \\ \varphi_3 \end{Bmatrix} \tag{11}$$

Moreover when the origin of the director basis is located at the geometric centre of the bit, the therms $\mathcal{H}_{25}$ and $\mathcal{H}_{52}$ are both null. In the following developments, the notations $\mathcal{H}_i = \mathcal{H}_{ii}$, $\mathcal{H}_{55} = \mathcal{H}_0$ and $\mathcal{G}_5 = \mathcal{G}_0$ have been adopted for concision considerations.

Considering that under stationary conditions the axial force at the bit $\hat{F}_1$ is constant and equal to the opposite of the weight on bit W, the bitmetrics laws can be written as

$$W = \mathcal{G}_1 + \mathcal{H}_1 d_1 \,, \qquad \hat{F}_2 = -\mathcal{G}_2 - \eta \mathcal{H}_1 d_2 \,, \qquad \hat{M}_3 = -\mathcal{G}_0 - h^2 \mathcal{H}_1 \varphi_3 \tag{12}$$

where two quantities reflecting the geometry of the bit have been introduced

$$\eta = \frac{\mathcal{H}_2}{\mathcal{H}_1} \qquad \text{and} \qquad h = \sqrt{\frac{\mathcal{H}_0}{\mathcal{H}_1}} \tag{13}$$

Ideally, the *WOB* is greater than the threshold force $\mathcal{G}_1 = W_*$ and the axial penetration occurs in Regime II. In contrast, it can be assumed that the lateral and angular penetrations are both dominated by the contact process (Regime I). Meaning that the coefficients $\mathcal{G}_0$ and $\mathcal{G}_2$ are null. However, the formulation (12) will be maintained by concerns of generality.

4 Mechanical Problem of the Drillstring

The last component of the complete model is the drillstring model. It relates the loads applied on the drillstring to the forces and moment acting on the bit. As it has already been noticed, we focus on the near-bit region of the drillstring, *i.e.,* the *BHA* segment between the bit and the second stabilizer. Moreover we assume that those stabilizers are perfectly fitted to the borehole. Finally, we neglect the frictional resistance and so consider that all the axial force is transmitted to the bit.

In the context of planar trajectories, the drillstring is a 1D object and is thus completely defined by its inclination $\theta(s)$ corresponding to the curvilinear coordinate[6] s. Considering that the current length of the drillstring is ℓ, the function $\theta(s)$ is defined between the bit in $s = 0$ and the second stabilizer in $s = \ell$, see Figure 13. The position of the first stabilizer along the drillstring is $s = \lambda_1$. According to the adopted notation, the length of the borehole axis is given by $\hat{S} - \bar{\hat{S}} = L$ while the length of the drillstring is given by $\bar{\hat{s}} - \hat{s} = \ell$. Nonetheless, when the bit is drilling, those two lengths are nearly equal $L \simeq \ell$.

The bit tilt introduced as a consequence of the clearance between the bit and the borehole can now be defined as the difference between the inclination of the drillstring at the bit $\theta(\hat{s})$ and the inclination of the borehole at the bit $\Theta(\hat{S})$

$$\psi = \hat{\theta} - \hat{\Theta} \tag{14}$$

[5]It does not indicate that the force $\hat{F}_3$ and the moment $\hat{M}_2$ are null but the mathematical model of the drillstring does not take them into account.

[6]The drillstring curvilinear coordinate s is running in the opposite direction compared to the borehole curvilinear coordinates S.

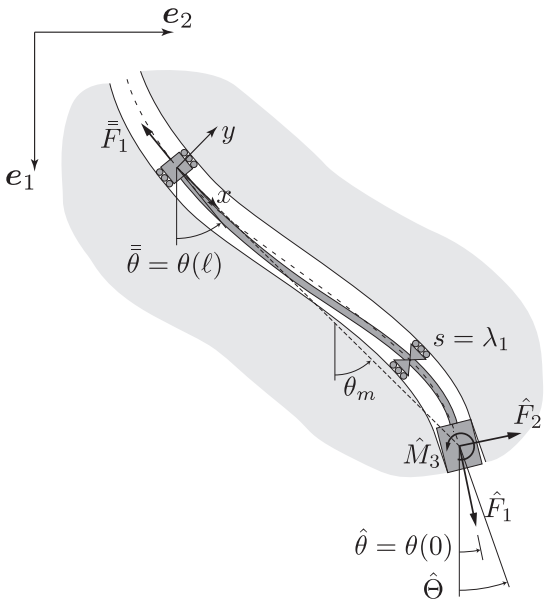

Figure 13: Description of the simplified problem for the drillstring model

Since the drillstring is moving along the borehole (either during drilling of during a trip up), all the quantities associated to the drillstring are functions of both the space s and the "time" L. However this work focus on the behaviour of the *BHA* when the bit is drilling, *i.e.,* when $\hat{S} = L$, and the "time" component can be ignored.

4.1 Formulation within St-Venant Beam Theory

Assuming small rotations and small displacement by reference to an initial configuration, the elastic response of the drillstring is expressed in the framework of St-Venant beam theory, which is an approximation of the more rigorous Kirchhoff's theory. This approximation is lawful when the shear deformation can be neglected compare to the bending deformation, this is usually the case with circular and tubular cross sections.

The deformation of the *BHA* segment is analysed by choosing the chord linking the bit and the second stabilizer as reference configuration. Since the bit and the second stabilizer are compelled to lie on the borehole axis, their positions in the fixed cartesian coordinate system $(\boldsymbol{e}_1, \boldsymbol{e}_2)$ defined in Figure 13 are known. Considering that the coordinates of the bit are $(\hat{X}, \hat{Y})$ and those of the second stabilizer are $(\bar{\bar{X}}, \bar{\bar{Y}})$, the inclination θ_m of the chord on the $\boldsymbol{e}_1$-axis is given by

$$\theta_m = \arctan\left(\frac{\hat{Y} - \bar{\bar{Y}}}{\hat{X} - \bar{\bar{X}}}\right) \tag{15}$$

A new coordinate system $(\boldsymbol{x}, \boldsymbol{y})$ is defined to characterize the beam deflection. Its origin is chosen at the second stabilizer and with the x-axis coinciding with the chord and pointing towards the bit (see Figure 13). The reference configuration of the *BHA* segment is thus the part of the $\boldsymbol{x}$-axis defined by $0 \leq x \leq \ell$, $y = 0$, and any deformation of the beam corresponds to a transverse deflection $U(x)$, taken positive in the direction of the $\boldsymbol{y}$-axis.

We can assert that any transverse displacement imposed to a point of a beam is equivalent in terms of internal efforts to introduce an adequate kink angle at this point while keeping this one seating on the reference configuration. Indeed, the two configurations shown in Figure 14 lead to

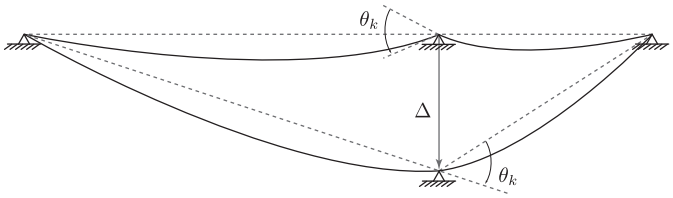

Figure 14: Two equivalent configurations of a beam in terms of internal shear and moment

the same shear and moment diagrams along the beam. The *settlement* Δ requisite to keep the stabilizer on the borehole axis can thus be advantageously substituted by the kink angle θ_k given by

$$\theta_k = \theta_{m,1} - \theta_{m,2} \tag{16}$$

where $\theta_{m,1}$ and $\theta_{m,2}$ are defined in Figure 15 for the stationary solution characterised the constant curvature $K = R^{-1}$

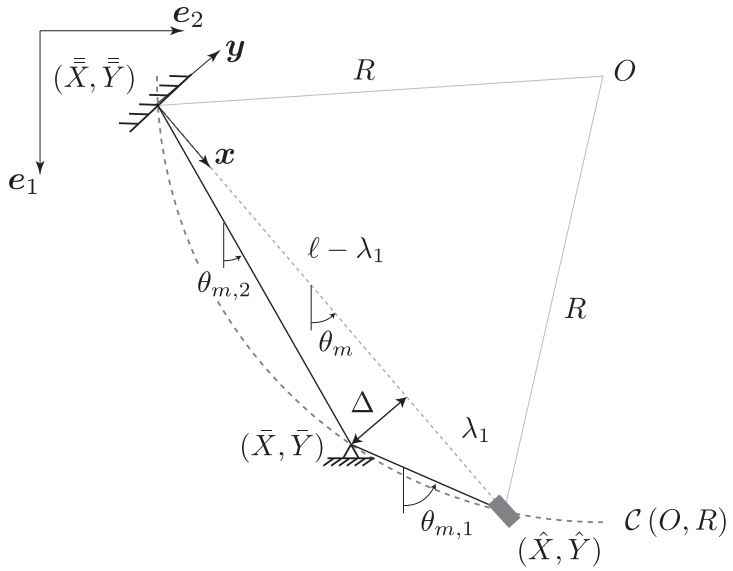

Figure 15: Definition of angles $\theta_{m,1}$ and $\theta_{m,2}$ for the stationary solution characterised the constant curvature $K = R^{-1}$

4.2 Geometrical & Loading Considerations

The free body diagram presented in Figure 16 highlights the parameters involved in the relationships governing the drillstring model. This figure parallels the free body diagram and the sketch of a real point-the-bit system, the "Well-Guide RSS" commercialised by *Girodata*. To our knowledge, all point-the-bit systems are significantly identical in their design and operating principle.

To bracket the effect of the drillstring above the second stabilizer, two limiting boundary conditions will be considered at this stabilizer: either zero moment or zero rotation relative to the borehole axis.

Devices that control the deflection of the transmission shaft usually operate at imposed displacements because of their design. However we can transform this problem to an equivalent one

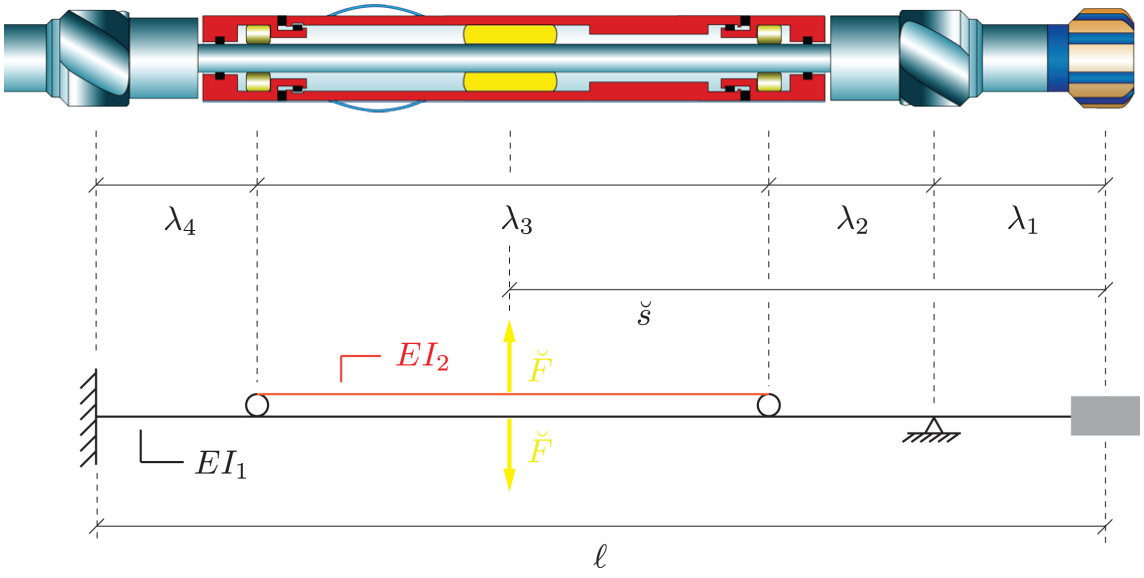

Figure 16: The "Well-Guide RSS" designed by *Girodata* and the free body diagram considered to develop the *BHA* model

that operates at imposed forces and calculate the displacements retrospectively. We will therefore suppose that the force $\breve{F}$ applied by this device is known.

On the free body diagram, the upper beam (the red one) is kinematically determinate, *i.e.,* we can immediately find its support reactions which have to be considered as forces acting on the transmission shaft (the black beam in Figure 16). The Figure 17 depicts how to calculate these reactions. We can thus replace the outer housing by a couple of reactions (functions of the force $\breve{F}$) on the transmission shaft.

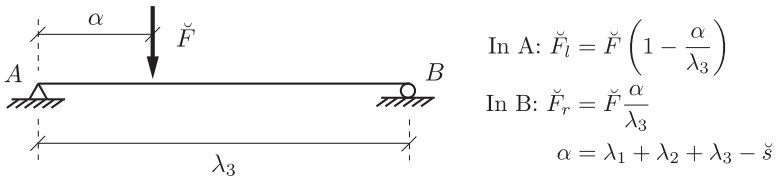

Figure 17: Reactions $\breve{F}_l$ and $\breve{F}_r$ of the outer housing on the transmission shaft

4.3 Governing Equations

To write the equation governing the deflection of the beam, we use the fundamental relation between the curvature K and the moment M. In the context of small rotations and small displacement by reference to the initial configuration, the exact expression of the curvature can be approximated by the second derivative with respect to coordinate x

$$M_3 = EI\,\frac{\mathrm{d}^2U}{\mathrm{d}s^2} \simeq EI\,\frac{\mathrm{d}^2U}{\mathrm{d}x^2} \tag{17}$$

where E is Young's modulus and I is the area moment of inertia. The rigidity EI is assumed to be constant along the beam.

The beam is subjected to gravity loading and to the transverse forces $\breve{F}$, $\breve{F}_l$ and $\breve{F}_r$ respectively at $x = \ell - \breve{s}$, $x = \lambda_4$ and $x = \lambda_4 + \lambda_3$. Considering that the gravity field is inclined by an angle $-\theta_m$

on the $\boldsymbol{x}$-axis and if we denote the weight per unit length of the beam by w, then the transverse lineic force is $-w \sin\theta_m$.

Considering now the balance of forces and moments we can write

- the moment equilibrium:

$$\frac{\mathrm{d}M_3}{\mathrm{d}x} + F_2 = 0 \tag{18}$$

- the transverse force equilibrium:

$$\frac{\mathrm{d}F_2}{\mathrm{d}x} + \breve{F}_l \delta_{\lambda_4} - \breve{F} \delta_{\ell - \breve{s}} + \breve{F}_r \delta_{\lambda_4 + \lambda_3} - w \sin\theta_m = 0 \tag{19}$$

  where δ_λ denotes the Dirac delta function at $x = \lambda$;

- the axial force equilibrium:

$$\frac{\mathrm{d}F_1}{\mathrm{d}x} + w \cos\theta_m = 0 \tag{20}$$

Combining equations (17) to (19) and considering that the beam is also submitted to the kink angle θ_k at the first stabilizer, *i.e.,* in $x = \ell - \lambda_1$, we obtain

$$EI \frac{\mathrm{d}^4 U}{\mathrm{d}x^4} - \breve{F}_l \delta_{\lambda_4} + \breve{F} \delta_{\ell - \breve{s}} - \breve{F}_r \delta_{\lambda_4 + \lambda_3} + w \sin\theta_m - \theta_k \delta_{\ell - \lambda_1} = 0 \tag{21}$$

The axial equilibrium (20) is simply integrated to yield

$$\hat{F}_1 = \bar{\bar{F}}_1 - x.w \cos\theta_m \tag{22}$$

4.4 Boundary Conditions

The solution of the governing equation involves four integration constants, we need thus four boundary conditions. Those conditions are imposed deflection (U), rotation ($\mathrm{d}U/\mathrm{d}x$) or moment ($\sim \mathrm{d}^2U/\mathrm{d}x^2$) at each end. Rotations are taken positive counterclockwise and are relative to the inclination of the chord linking the bit to the second stabilizer.

The boundary conditions are

- At the bit ($x = \ell$):

$$U = 0 \tag{23}$$

$$\frac{\mathrm{d}U}{\mathrm{d}x} = \hat{\Theta} + \psi - \theta_m \tag{24}$$

- At the second stabilizer ($x = 0$):

$$U = 0 \tag{25}$$

$$\frac{\mathrm{d}U}{\mathrm{d}x} = \bar{\bar{\Theta}} - \theta_m \quad \text{or} \quad \frac{\mathrm{d}^2U}{\mathrm{d}x^2} = 0 \tag{26}$$

  depending if the second stabilizer is assumed to blocked or hinged.

In the problem under consideration, the shaft is also maintained on the borehole axis by the first stabilizer. Since this constraint has been substituted by imposing an adequate kink angle while the stabilizer is compelled to lie on the reference configuration, a fifth boundary condition is imposed at $x = \ell - \lambda_1$:

$$U = 0 \tag{27}$$

4.5 Scaling

The governing equations can advantageously be scaled. The characteristic quantities are defined as, respectively for the length, the deflection, the force and the moment,

$$L_* = \ell \qquad U_* = \frac{w\ell^4}{EI} \qquad F_* = w\ell \qquad M_* = w\ell^2 \tag{28}$$

The dimensionless position, deflection, shear force and moment are then defined as

$$\xi = \frac{x}{L_*} \qquad u = \frac{U}{U_*} \qquad f_2 = \frac{F_2}{F_*} \qquad m = \frac{M}{M_*} \tag{29}$$

With the scaling (28), the dimensionless moment and shear force are related to the deflection by the relations

$$m = \frac{\mathrm{d}^2 u}{\mathrm{d}\xi^2} \qquad\qquad f_2 = -\frac{\mathrm{d}^3 u}{\mathrm{d}\xi^3} \tag{30}$$

According to Figure 18 and considering $\varkappa_i = \dfrac{\lambda_i}{\ell}$, the governing equation (21) becomes then

$$\frac{\mathrm{d}^4 u}{\mathrm{d}\xi^4} - \Phi_l \delta_{\varkappa_4} + \Phi \delta_\Lambda - \Phi_r \delta_{\varkappa_3+\varkappa_4} + \sin\theta_m - \theta_k \Upsilon \delta_{1-\varkappa_1} = 0 \tag{31}$$

with the scaled distance Λ between the stabilizer and the actuator and the dimensionless rigidity of the shaft Υ, which are given by

$$\Lambda = 1 - \frac{\breve{s}}{\ell} \qquad\qquad \Upsilon = \frac{EI}{w\ell^3} \tag{32}$$

and with the scaled forces

$$\Phi_l = \frac{\breve{F}_l}{w\ell} \quad , \quad \Phi = \frac{\breve{F}}{w\ell} \quad \text{and} \quad \Phi_r = \frac{\breve{F}_r}{w\ell} \tag{33}$$

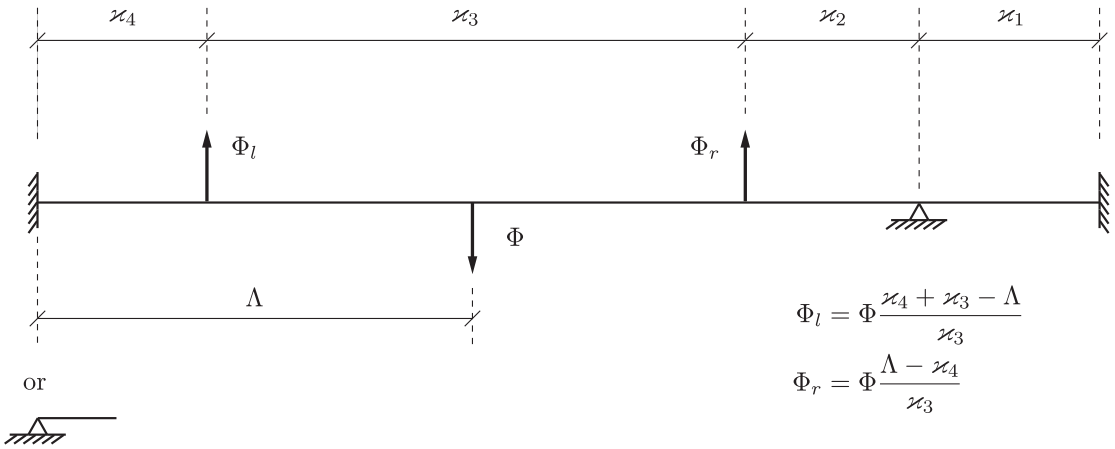

Figure 18: Free body diagram of the scaled problem

Boundary conditions are now expressed as

- at the bit ($\xi = 1$):

$$\begin{aligned} u &= 0 \\ \frac{\mathrm{d}u}{\mathrm{d}\xi} &= \Upsilon\left(\hat{\Theta} + \psi - \theta_m\right) \end{aligned}$$

- at the first stabilizer ($\xi = 1 - \varkappa_1$):

$$u = 0$$

- at the second stabilizer ($\xi = 0$):

$$\begin{aligned} u &= 0 \\ \frac{\mathrm{d}u}{\mathrm{d}\xi} = \Upsilon\left(\bar{\bar{\Theta}} - \theta_m\right) \quad &\text{or} \quad \frac{\mathrm{d}^2u}{\mathrm{d}\xi^2} = 0 \end{aligned}$$

The governing equation (31) is of fourth order, its integration involves thus four integration constants while we have five boundary conditions to impose. This difficulty is circumvented by means of a method called the *force method* or *method of consistent deformations*. This method consists in making the beam isostatic by releasing appropriate boundary conditions and externalize those by external forces. Amplitudes of those external forces are determined by imposing consistent deformations according to the released boundary conditions through a system of equations. This method is explained in details for the problem under consideration in Appendix B.

Equation (31) can be solved with the boundary conditions expressed above. According to the borehole evolution problem, the relevant elements of the solution are the expressions of the efforts on the bit, the moment $\hat{M}_3$ and the transverse force $\hat{F}_2$. Due to the superposition principle and the linearity of the beam problem, the solution can be written as the sum of five terms, each expressing either a boundary condition or a load.

$$\frac{\hat{F}_2}{w\ell} = \mathcal{F}_b\Upsilon\left(\hat{\Theta} + \psi - \theta_m\right) + \mathcal{F}_s\Upsilon\left(\bar{\bar{\Theta}} - \theta_m\right) + \mathcal{F}_k\Upsilon\theta_k + \mathcal{F}_w\sin\theta_m + \mathcal{F}_r\Phi \tag{34}$$

$$\frac{\hat{M}_3}{w\ell^2} = \mathcal{M}_b\Upsilon\left(\hat{\Theta} + \psi - \theta_m\right) + \mathcal{M}_s\Upsilon\left(\bar{\bar{\Theta}} - \theta_m\right) + \mathcal{M}_k\Upsilon\theta_k + \mathcal{M}_w\sin\theta_m + \mathcal{M}_r\Phi \tag{35}$$

The first term corresponds to the rotation imposed at the bit, the second to the rotation at the second stabilizer, the third brings out the effect of the kink angle θ_k, the fourth express the influence of the distributed load w, and the fifth highlights the effect of the load Φ applied by the actuator.

The coefficients $\mathcal{F}$'s and $\mathcal{M}$'s are functions of only $\varkappa_1$ except $\mathcal{F}_\Phi$ and $\mathcal{M}_\Phi$, which are also functions of $\varkappa_2$, $\varkappa_3$, $\varkappa_4$ and Λ. Naturally the coefficients $\mathcal{F}_s$ and $\mathcal{M}_s$ are equal to zero when the second stabilizer is assumed to be hinged. The expressions of those coefficients are given in Table 1 for the two limiting cases, *i.e.,* blocked rotation at the second stabilizer ($\bar{\bar{\theta}} = \bar{\bar{\Theta}} - \theta_m$) and free rotation at the second stabilizer ($\bar{\bar{M}}_3 = 0$).

The particular problem corresponding to the *BHA* without the first stabilizer can also be treated. Coefficients $\mathcal{F}$'s and $\mathcal{M}$'s corresponding to this situation are given in Table C.1, Appendix C. This solution is immediate and the coefficients are numbers except $\mathcal{F}_\Phi$ and $\mathcal{M}_\Phi$ which are still functions of $\varkappa_3$, $\varkappa_4$ and Λ.

5 Stationary Solutions

Stationary solutions of the problem are practically significant, they correspond to the equilibrium points of equations (3) and are characterized by a constant curvature and diameter. As it has already been explained, stationary solutions in the context of planar borehole axis do not exist, except the trivial cases of straight borehole. Nonetheless, they are of prime interest since solutions of the evolving problem can often be approximated by sequences of stationary solutions.

	Blocked rotation	Free rotation
$\mathcal{F}_b$	$-\frac{3(\varkappa_1+1)}{\varkappa_1^2}$	$\frac{6(\varkappa_1+2)}{(\varkappa_1-4)\varkappa_1^2}$
$\mathcal{F}_s$	$\frac{3}{\varkappa_1}$	0
$\mathcal{F}_k$	$\frac{6}{\varkappa_1}$	$-\frac{18}{(\varkappa_1-4)\varkappa_1}$
$\mathcal{F}_w$	$\frac{2\varkappa_1^2+3\varkappa_1-1}{8\varkappa_1}$	$\frac{\varkappa_1^3-\varkappa_1^2-9\varkappa_1+3}{4(\varkappa_1-4)\varkappa_1}$
$\mathcal{F}_r$	$-\frac{3(\Lambda-\varkappa_4)(\Lambda-\varkappa_3-\varkappa_4)(\Lambda-\varkappa_2+\varkappa_4)}{2(\varkappa_1-1)\varkappa_1}$	$\frac{3(\Lambda-\varkappa_4)(\Lambda-\varkappa_3-\varkappa_4)(\Lambda+\varkappa_3+2\varkappa_4)}{\varkappa_1\left(\varkappa_1^2-5\varkappa_1+4\right)}$
$\mathcal{M}_b$	$\frac{3}{\varkappa_1}+1$	$-\frac{12}{(\varkappa_1-4)\varkappa_1}$
$\mathcal{M}_s$	-1	0
$\mathcal{M}_k$	-2	$\frac{6}{\varkappa_1-4}$
$\mathcal{M}_w$	$\frac{(1-3\varkappa_1)}{24}$	$\frac{\varkappa_1^2-3\varkappa_1+1}{16-4\varkappa_1}$
$\mathcal{M}_r$	$\frac{(\Lambda-\varkappa_4)(\Lambda-\varkappa_3-\varkappa_4)(\Lambda-\varkappa_2+\varkappa_4)}{2(\varkappa_1-1)}$	$-\frac{(\Lambda-\varkappa_4)(\Lambda-\varkappa_3-\varkappa_4)(\Lambda+\varkappa_3+2\varkappa_4)}{\varkappa_1^2-5\varkappa_1+4}$

Table 1: Coefficients $\mathcal{F}$'s and $\mathcal{M}$'s when the first stabilizer is imposed to stay on the chord

In situations of steady state, the loads acting on the *BHA* do not fluctuate and its deformed shape is invariant during drilling. The *BHA* movement can thus be akin to a rigid body motion while the forces and moments acting on the bit are invariant meaning that the penetration variables are constant. Indeed, introducing the δ-operator to denote the variation of a quantity over one revolution of the bit, it appears

$$\delta d = \delta\beta = \delta\varphi_3 = 0 \tag{36}$$

which means that those quantities do not vary over one bit revolution, *i.e.,*

$$d = d_s \quad , \qquad \beta = \beta_s \quad , \qquad \varphi_3 = \varphi_s \tag{37}$$

where d is the magnitude of the penetration vector $\boldsymbol{d}$. On the other side, the variation of the absolute bit inclination and the increment of the borehole length after one bit revolution can be expressed as

$$\delta\hat{\theta} = \varphi_3 \qquad , \qquad \delta L = d \tag{38}$$

The expression (2) of the borehole curvature can be expressed in terms of the δ-variation of the borehole inclination at the bit $\hat{\Theta}$ and the penetration d according to

$$\hat{K} = \frac{\delta\hat{\Theta}}{d} \tag{39}$$

Using equations (6), (14) and (38) we can determine the expression of the constant curvature $\hat{K}$ as

$$\hat{K} = \frac{\varphi_3 + \delta\beta}{d} = \frac{\varphi_s}{d_s} \tag{40}$$

while the constant diameter of the borehole lead to a constant expression of the overgauge factor

$$\Xi = \Xi_0 + \frac{2}{\pi}\nu|\beta_s| \tag{41}$$

where ν is the bit slenderness $\nu = b/a$.

5.1 Equations Governing the Stationary Problem

Considering that the borehole segment between the bit and the second stabilizer is a circular arc, the system of equations consisting of the relationships (40) and (41) between the borehole geometry and the penetration variables, the bit-rock interaction laws (12) and the solution (34)-(35) of the *BHA* problem can be simplified, see Appendix D. The inclination θ_m of the chord on the $\boldsymbol{e}_1$-axis can be expressed as

$$\theta_m = \frac{1}{2}\left(\hat{\Theta} + \bar{\Theta}\right) \tag{42}$$

and $\left(\hat{\Theta} + \bar{\Theta}\right)$ as

$$\left(\hat{\Theta} + \bar{\Theta}\right) = K\ell \tag{43}$$

After introducing the dimensionless curvature κ

$$\kappa = K\ell \tag{44}$$

we can write

$$\hat{\Theta} - \theta_m = \frac{\kappa}{2} \qquad , \qquad \bar{\Theta} - \theta_m = -\frac{\kappa}{2} \tag{45}$$

while the kink angle θ_k can be expressed as

$$\theta_k = \frac{\kappa}{2} \tag{46}$$

Finally the system of equations governing the equilibrium solution is summarized below, where we assume that drilling takes place in regime II, *i.e.,* that the weight on bit W is larger than the threshold contact force $\mathcal{G}_1$.

- Bit-rock interaction:

$$W = \mathcal{G}_1 + \mathcal{H}_1 d_1 \,, \qquad \hat{F}_2 = -\mathcal{G}_2 - \eta \mathcal{H}_1 d_2 \,, \qquad \hat{M}_3 = -\mathcal{G}_0 - h^2 \mathcal{H}_1 \varphi_3 \tag{47}$$

- Relationship between bit penetration and borehole geometry:

$$\kappa = \frac{\varphi_3 \ell}{d} \qquad , \qquad \Xi = \Xi_0 + \frac{2}{\pi} \nu |\beta| \tag{48}$$

- Drillstring equilibrium:

$$\frac{\hat{F}_2}{w\ell} = \frac{1}{2}\mathcal{F}_b \Upsilon \left(\kappa - 2\beta\right) - \frac{1}{2}\mathcal{F}_s \Upsilon \kappa + \frac{1}{2}\mathcal{F}_k \Upsilon \kappa + \mathcal{F}_w \sin\theta_m + \mathcal{F}_r \Phi \tag{49}$$

$$\frac{\hat{M}_3}{w\ell^2} = \frac{1}{2}\mathcal{M}_b \Upsilon \left(\kappa - 2\beta\right) - \frac{1}{2}\mathcal{M}_s \Upsilon \kappa + \frac{1}{2}\mathcal{M}_k \Upsilon \kappa + \mathcal{M}_w \sin\theta_m + \mathcal{M}_r \Phi \tag{50}$$

The system of equations (47)-(50) is closed in terms of the unknowns κ and β, *i.e.,* in terms of the dimensionless borehole curvature and the penetration inclination (or equivalently the bit tilt).

5.2 Equilibrium Borehole Curvature and Radius

We are now in position to calculate both the equilibrium curvature κ_s and overgauge Ξ_s, which is directly related to the penetration inclination β_s (itself equal to the opposite of the bit tilt ψ_s).

The bit-rock interaction laws (47) and the penetration relationships (48) can be combined to express the lateral force on bit, $\hat{F}_2$, and the moment on bit $\hat{M}_3$ in terms of the weight on bit W. The following approximations are used

$$d_2 \simeq \beta d_1 \qquad , \qquad \varphi_3 \simeq \frac{\kappa d_1}{\ell} \tag{51}$$

both on account that $\beta \ll 1$. Hence,

$$\hat{F}_2 = -\mathcal{G}_2 - \beta\eta \left(W - \mathcal{G}_1\right) \tag{52}$$

$$\hat{M}_3 = -\mathcal{G}_0 - \kappa\chi \left(W - \mathcal{G}_1\right)\ell \tag{53}$$

where η and χ denote the lateral and angular steering resistances respectively. The are defined as

$$\eta = \frac{\mathcal{H}_2}{\mathcal{H}_1} \qquad , \qquad \chi = \left(\frac{h}{\ell}\right)^2 = \frac{\mathcal{H}_0}{\mathcal{H}_1 \ell^2} \tag{54}$$

Next, $\hat{F}_2$ and $\hat{M}_3$ are eliminated between (49), (50), (52) and (53), to yield a linear system of equations in terms of β and κ

$$\begin{bmatrix} M_{\beta\beta} & M_{\beta\kappa} \\ M_{\kappa\beta} & M_{\kappa\kappa} \end{bmatrix} \begin{Bmatrix} \beta \\ \kappa \end{Bmatrix} = \begin{Bmatrix} N_\beta \\ N_\kappa \end{Bmatrix} \tag{55}$$

where the coefficients M's are given by

$$M_{\beta\beta} = \mathcal{F}_b - \eta\Pi_c \tag{56}$$

$$M_{\beta\kappa} = \frac{\Upsilon}{2}\left(\mathcal{F}_s - \mathcal{F}_b - \mathcal{F}_k\right) \tag{57}$$

$$M_{\kappa\beta} = \Upsilon\mathcal{M}_b \tag{58}$$

$$M_{\kappa\kappa} = \frac{\Upsilon}{2}\left(\mathcal{M}_s - \mathcal{M}_b - \mathcal{M}_k\right) - \chi\Pi_c \tag{59}$$

where Π_c denotes the dimensionless fraction of the weight-on-bit mobilized by the cutting process

$$\Pi_c = \Pi - \Gamma_1 \tag{60}$$

and Π is the dimensionless weight-on-bit

$$\Pi = \frac{W}{w\ell} \tag{61}$$

It is interesting to note that the matrix of coefficients $\boldsymbol{M}$ is never diagonal. The coefficients N's are given by

$$N_\beta = \Gamma_2 + \mathcal{F}_w \sin\theta_m + \mathcal{F}_r\left(\Lambda\right)\Phi \tag{62}$$

$$N_\kappa = \Gamma_0 + \mathcal{M}_w \sin\theta_m + \mathcal{M}_r\left(\Lambda\right)\Phi \tag{63}$$

where

$$\Gamma_0 = \frac{\mathcal{G}_0}{w\ell^2} \quad , \qquad \Gamma_1 = \frac{\mathcal{G}_1}{w\ell} \quad , \qquad \Gamma_2 = \frac{\mathcal{G}_2}{w\ell} \tag{64}$$

The equilibrium solution κ_s and β_s is then deduced from (55) to be

$$\beta_s = \frac{M_{\kappa\kappa}N_\beta - M_{\beta\kappa}N_\kappa}{M_{\beta\beta}M_{\kappa\kappa} - M_{\beta\kappa}M_{\kappa\beta}} \qquad , \qquad \kappa_s = \frac{M_{\beta\beta}N_\kappa - M_{\kappa\beta}N_\beta}{M_{\beta\beta}M_{\kappa\kappa} - M_{\beta\kappa}M_{\kappa\beta}} \tag{65}$$

Part III

Parametric Analysis

In this part of the work, we conduct a parametric analysis of the mathematical model developed in the previous part. The analysis is restricted to planar borehole trajectories and stationary solutions. In this context, solutions of the problem correspond to *BHA* segments of constant deformed shape moving into boreholes of constant curvature and radius. Moreover, it is assumed that the lateral and angular penetrations are both dominated by the contact process (Regime I). Meaning that the coefficients $\mathcal{G}_0$ and $\mathcal{G}_2$ present in the bit-rock interaction laws (47) are null.

The problem being fully symmetric with respect to the vertical axis, this parametric analysis considers only the cases where the inclination of the chord θ_m is positive. Indeed, solutions for $\theta_m < 0$ are identical to solution for $\theta_m > 0$ with the opposite sign for the resulting curvature and bit tilt. A positive curvature (increasing borehole inclination Θ) corresponds thus to a curvatures oriented in the direction of the director vector $\hat{\mathbf{i}}_2$. Therefore, build-up and drop-off tendencies correspond to positive and negative curvature, respectively.

This parametric analysis focus on the borehole curvature which is the most relevant output of the mathematical model from a directional driller perspective. We first determine the combination of parameters that control the directional tendency of the drilling assembly, *i.e.,* the sign of the borehole curvature. Then, the effects of the parameters on its magnitude are studied. The analysis is conducted for the two configurations of the *BHA*: blocked and free rotation at the second stabilizer.

This part is divided in four sections. The first one introduces the range of amplitude of the parameters governing the solutions that are representative of field cases. The second section deals with the behaviour of the *BHA* without the rotary steerable system (*i.e.,* $\breve{F} = 0$), general comments are made about the solution and results of simulations are presented. The more complex configuration corresponding to the *BHA* equipped with a rotary steerable system is approached in the third section.

1 Range of Amplitude of the Governing Parameters

In the framework of the mathematical model, the solution of the problem is expressed in terms of the dimensionless borehole curvature κ and the penetration inclination β which is directly related to the bit tilt ψ. This solution is controlled by twelve dimensionless parameters that can be classified into three different categories:

Three bit-rock interactions parameters: the lateral η and the angular χ steering resistances are two numbers introduced to characterised the steerability of the system. The dimensionless fraction of the weight-on-bit mobilized by frictional contact between the rock and the bit on surfaces such as wear flat is designated by Γ_1.

Two control parameters: the dimensionless weight-on-bit Π and steering force Φ are the only parameters controlled by the driller during drilling.

Seven *BHA* parameters: the inclination of the chord θ_m, the dimensionless position of the *RSS* actuator Λ, the dimensionless distances $\varkappa_i$ $(i = 1 \dots 4)$ and the dimensionless *BHA* stiffness Υ are used to specify the geometry of the *BHA*. Note that the dimensionless distances between the stabilizers must satisfy

$$\varkappa_4 + \varkappa_3 + \varkappa_2 + \varkappa_1 = 1 \tag{66}$$

Finally, we introduce the number Ψ defined as

$$\Psi = \frac{\Pi_c}{\Upsilon} \tag{67}$$

which affects greatly the directional behaviour of the drilling assembly as it will be shown in the analysis and where Π_c designates the dimensionless fraction of the weight-on-bit mobilized by the cutting process $\Pi_c = \Pi - \Gamma_1$

1.1 Bit-Rock Interaction Properties

The lateral steering resistance η is defined as the ratio between the two bitmetric coefficients $\mathcal{H}_2$ and $\mathcal{H}_1$. For simple *PDC* bit geometry, it can be expressed as

$$\eta = \frac{1}{2}\xi\nu \tag{68}$$

where ν is the bit aspect ratio and ξ is defined as the ratio between two numbers characterizing the interactions between the rock and the different part of the bit

$$\nu = \frac{b}{a} \qquad , \qquad \xi = \frac{\zeta}{\zeta'} \tag{69}$$

Indeed, ζ depicts the interactions between the cutting structure and the rock while the number ζ' considers the interactions between the gauge and the rock. In the typical field of directional drilling, the bit aspect ratio usually varies between 1/5 and 2. On the other side, laboratory tests conducted by Menand et al. (2002) indicate that ξ takes values of order $\mathcal{O}(10)$ for "active" gauge and of order $\mathcal{O}(10^2)$ for "passive" gauge. In summary, the lateral steering resistance η covers typically two orders of magnitude $\mathcal{O}(1 \sim 10^2)$.

The expression of the angular steering resistance χ is also derived from the bitmetric coefficients but depends besides of the scaling ℓ

$$\chi = \left(\frac{h}{\ell}\right)^2 \qquad \text{with} \quad h = \sqrt{\frac{\mathcal{H}_0}{\mathcal{H}_1}} \tag{70}$$

In the particular case of simple *PDC* bit geometry it can be expressed as

$$\begin{aligned}\chi &= \frac{1}{6}\left(\frac{a}{\ell}\right)^2 + \frac{2}{3}\left(\frac{b}{\ell}\right)^2 \eta \\ &\simeq \frac{2}{3}\left(\frac{b}{\ell}\right)^2 \eta \end{aligned} \tag{71}$$

Considering that the length of point-the-bit systems ranges usually from 3 to 10 meters and that the bit gauge height (for *PDC* bit) embraces generally values between 0.1 and 1.5 ft (3 cm and 50 cm), the angular steering resistance χ covers six orders of magnitude $\mathcal{O}(10^{-3} \sim 50)$. Table 2 resumes the orders of magnitude for the two steering resistances η and χ.

ν	$0.2 - 2.0$
ξ	$10 - 100$
η	$1 - 100$
χ	$0.001 - 50$

Table 2: Range of amplitude of the bit-rock interactions properties

As mentioned earlier, the lateral and angular penetrations are assumed to be both dominated by the contact process (Regime I) meaning that the two bitmetric coefficients $\mathcal{G}_0$ and $\mathcal{G}_2$ are set to zero for this analysis. Contrariwise, the axial penetration occurs ideally in Regime II and the bitmetric coefficient $\mathcal{G}_1$ is not null. Detournay (2007) shows that the fractions of the weight-on-bit mobilized by frictional contact between the rock and the bit on surfaces such as wear flat, can be expressed as

$$\mathcal{G}_1 = \sigma a \ell_1 \tag{72}$$

where σ is the contact strength, *i.e.,* the maximum pressure that can be transmitted at the interface between the wearflat and the rock, a is the bit radius and ℓ_1 denotes the contact length which is an objective measure of the bit bluntness. For problems under consideration, the typical order of magnitude of $\mathcal{G}_1$ is 10 kN.

1.2 Rotary Steerable Specifications

This work focus on *BHA*s equipped with point-the-bit rotary steerable systems. The most part of borehole drilled by means of *RSS* have sections of diameter from $6^{1/4}$ to $12^{1/4}$ inches. The real dimensions of steerable systems are generally well-kept secrets. However manufacturers specify the stiffness of their systems in term of equivalent drill collar, *i.e.,* the *RSS* is assimilated to a pipe of internal diameter d_i and external diameter d_e. Table 3 summarizes point-the-bit systems specifications for such borehole size, these ranges are suggested by several field data as well as specifications given by manufacturers.

The *BHA* beam model involves several parameters to describe the complete geometry of the rotary steerable system. Relying on several field observations, some additional assumptions can be emitted about the distances λ_i. Indeed, the two distances λ_2 and λ_4 are commonly equal while the force $\breve{F}$ is usually applied at the middle of the segment λ_3 of the *BHA*. We obtain thus the two new relations

$$\varkappa_4 = \varkappa_2 \tag{73}$$

$$\Lambda = \varkappa_2 + \frac{\varkappa_3}{2} \tag{74}$$

Hole Size (in)	$6^{1/4}$	$8^{1/2}$	$8^{1/4}$
d_i (mm)	$31.8 - 44.5$	$41.3 - 63.5$	$50.8 - 71.5$
d_e (mm)	$120.7 - 133.4$	$171.5 - 193.7$	$209.6 - 269.9$
ℓ (m)	$3 - 10$		
w (N/m)	$775 - 1034$	$1563 - 2207$	$2392 - 4330$
EI/w ($\times 10^3$ m^3)	$2.8 - 3.1$	$5.6 - 6.6$	$8.2 - 12.6$
Υ	$3 - 120$	$5 - 245$	$8 - 470$

Table 3: Range of amplitude of the *BHA* specifications (density is taken as $\rho = 8000$ kg/m^3)

Meaning that the relation (66) becomes

$$\varkappa_1 + 2\Lambda = 1 \tag{75}$$

Usually the segment of the *BHA* joining the bit to the second stabilizer is smaller than the segment joining the two stabilizers. In this work we consider ranges from 0 to 0.4 for the dimensionless length $\varkappa_1$, corresponding to a dimensionless position of the *RSS* actuator Λ varying between 0.3 and 0.5, while the dimensionless length $\varkappa_2$ runs from 0 to 0.3.

1.3 Control Parameters

Drillers can only acts on two parameters during drilling, the weight-on-bit W through the tension applied at the hook and the transverse force $\breve{F}$ applied by the actuator of the *RSS*. The minimum *WOB* is defined so that the axial penetration occurs in Regime II, *i.e.,* it should ideally be greater than the threshold force $\mathcal{G}_1 = W_*$. It is thus function of the drill bit properties and the rock. On the opposite, the maximum *WOB* that can be applied is defined based on buckling considerations and is conditioned by the stiffness of the steerable system. Others considerations about bit cleaning, vibrations, rate of penetration, etc. can also influence the range of weight-on-bit applied.

The transverse force used to bend the transmission shaft is generally applied and controlled by means of a hydraulic system. The maximum force that can be applied as well as the accuracy with which it is applied are thus dependant to the specifications of this hydraulic system. Usually the hydraulic system embedded is function of the bit diameter and the force $\breve{F}$ is equal to 5, 10, 20 kN for $6^{1/4}$, $8^{1/2}$ and $12^{1/4}$ bit size, respectively.

Hole Size (in)	$6^{1/4}$	$8^{1/2}$	12
WOB (*kN*)	$50 - 150$	$100 - 250$	$200 - 450$
Π	$4.5 - 63.5$	$4.5 - 52.5$	$4.5 - 61.5$
$\breve{F}$ (kN)	± 5	± 10	± 20
$\lvert\Phi\rvert$	$0 - 3$		

Table 4: Range of amplitude of the control parameters

1.4 General Comments about the Solution

Regarding the general expression of the equilibrium solution (65), we notice that the curvature and the penetration inclination have both the same denominator $\left(M_{\beta\beta}M_{\kappa\kappa} - M_{\beta\kappa}M_{\kappa\beta}\right)$. The sign of this denominator is positive and independent of the magnitude of the parameters governing the model. The drilling tendency is then entirely controlled by the numerator $\left(M_{\beta\beta}N_{\kappa} - M_{\kappa\beta}N_{\beta}\right)$ which appears to be independent of the angular steering resistance χ.

Table 5 summarizes the ranges of amplitude for the parameters governing the solution of the mathematical model presented in the second part of this work (Mathematical Model).

Hole Size (in)	$6^{1/4}$	$8^{1/2}$	$12^{1/4}$
η	$1 - 100$		
χ	$10^{-3} - 50$		
Γ_1	$1 - 4.3$	$0.45 - 2.15$	$0.2 - 1.4$
Π	$4.5 - 63.5$	$4.5 - 52.5$	$4.5 - 61.5$
$\lvert\Phi\rvert$	$0 - 3$		
$\sin\theta_m$	$0 - 1$		
Υ	$3 - 120$	$5 - 245$	$8 - 470$
Π_c	$0.4 - 63$	$2 - 52$	$3 - 61$
Ψ	$0.004 - 22.5$	$0.01 - 9.3$	$0.007 - 7.5$
$\varkappa_1$	$0 - 0.4$		
$\varkappa_2$	$0 - 0.3$		
Λ	$0.3 - 0.5$		

Table 5: Range of amplitude of the governing parameters

2 *BHA* without Rotary Steerable System ($\Phi = 0$)

The comprehension of the *BHA* behaviour when no force is developed by the actuator is of prime importance. Indeed, the solution corresponding to $\Phi = 0$ consists of a simplification of the general solution (65) since the gravity is the only load acting on the *BHA*. Moreover, the drilling tendency of the *BHA* and how it behaves when the *RSS* is not activated are also significant from a directional driller perspective.

In this context, the equilibrium solution is computed considering $\Phi = 0$ in the general solution (65) and the expressions of the $\mathcal{F}$'s and $\mathcal{M}$'s coefficients given in Table 1. This solution (κ_s, β_s) or equivalently (κ_s, ψ_s) is determined for the two boundary conditions considered at the upper stabilizer, either blocked (κ_b, ψ_b) or free rotation (κ_f, ψ_f) relative to the borehole axis. The

dimensionless curvature is given by

$$\kappa_b = -\frac{\Big(\eta\Psi(1-3\varkappa_1)\varkappa_1^2+6\left(\varkappa_1^3+3\varkappa_1^2+3\varkappa_1-1\right)\Big)\sin\theta_m}{12\Upsilon\left(2\eta\Psi^2\chi\varkappa_1^2+3\Psi\left(\eta\varkappa_1+2\chi(\varkappa_1+1)\right)+6\right)} \tag{76}$$

$$\kappa_f = -\frac{\Big(\eta\Psi\left(\varkappa_1^2-3\varkappa_1+1\right)\varkappa_1^2+6\left(\varkappa_1^2+3\varkappa_1-1\right)\Big)\sin\theta_m}{4\Upsilon\left(\eta\Psi^2\chi(4-\varkappa_1)\varkappa_1^2+3\Psi\left(\eta(2-\varkappa_1)\varkappa_1+2\chi(\varkappa_1+2)\right)+18\right)} \tag{77}$$

while the bit tilt is given by

$$\psi_b = \frac{\Big(\chi\Psi\varkappa_1\left(2\varkappa_1^2+3\varkappa_1-1\right)+\left(3\varkappa_1^2+3\varkappa_1-1\right)\Big)\sin\theta_m}{4\Upsilon\left(2\eta\Psi^2\chi\varkappa_1^2+3\Psi\left(\eta\varkappa_1+2\chi(\varkappa_1+1)\right)+6\right)} \tag{78}$$

$$\psi_f = -\frac{\Big(\chi\Psi\varkappa_1\left(\varkappa_1^3-\varkappa_1^2-9\varkappa_1+3\right)+3\left(\varkappa_1^3-\varkappa_1^2-3\varkappa_1+1\right)\Big)\sin\theta_m}{4\Upsilon\left(\eta\Psi^2\chi(4-\varkappa_1)\varkappa_1^2+3\Psi\left(\eta(2-\varkappa_1)\varkappa_1+2\chi(\varkappa_1+2)\right)+18\right)} \tag{79}$$

2.1 Drilling Tendency

Regarding the expressions (76) and (77) of the dimensionless curvature κ_s, it is now obvious that the drilling tendency is independent of the angular steering resistance χ. Moreover, it appears that the sign of the curvature is entirely governed by the only two numbers $\eta\Psi$ and $\varkappa_1$. As shown in Figure 19, two distinct regions can be identified in the space defined by these two numbers $(\varkappa_1, \eta\Psi)$. The boundaries between the regions can be derived analytically for the two limiting cases:

- If the rotation of the upper stabilizer is blocked, any combination of the numbers $\eta\Psi$ and $\varkappa_1$ complying with the relation

$$\eta\Psi = \frac{6\left(\varkappa_1^3+3\varkappa_1^2+3\varkappa_1-1\right)}{\varkappa_1^2(3\varkappa_1-1)} \tag{80}$$

  corresponds to a curvature κ_b null, *i.e.,* to a holding assembly. In Figure 19(a), we observe a window of the parameter $\varkappa_1$ in which the borehole curvature is always negative regardless of the magnitude of the number $\eta\Psi$. Indeed, for a range of the parameter

$$\varkappa_1 \in \left[\sqrt[3]{2}-1;\frac{1}{3}\right] \simeq [0.260; 0.333] \tag{81}$$

  the assembly is always characterised by a dropping tendency.

- If the upper stabilizer is free to rotate, the combination the numbers $\eta\Psi$ and $\varkappa_1$ corresponding to a curvature κ_s^f null is

$$\eta\Psi = -\frac{6\left(\varkappa_1^2+3\varkappa_1-1\right)}{\varkappa_1^2\left(\varkappa_1^2-3\varkappa_1+1\right)} \tag{82}$$

  In Figure 19(b) now, we observe again a window of the parameter $\varkappa_1$ in which the borehole curvature is always negative regardless of the magnitude of the number $\eta\Psi$. This range of the parameter $\varkappa_1$ corresponding to a dropping tendency is

$$\varkappa_1 \in \left[\frac{1}{2}\left(\sqrt{13}-3\right);\frac{1}{2}\left(3-\sqrt{5}\right)\right] \simeq [0.302; 0.382] \tag{83}$$

The drilling tendency is then independent of the *BHA* mean inclination θ_m, which affects only the magnitude of the curvature. It means that, for any inclination θ_m, a combination of the numbers $\eta\Psi$ and $\varkappa_1$ complying with the relation (80) or (82), depending of the boundary condition at the upper stabilizer, always yields to a borehole curvature null. This unintuitive observation can readily be explained. When the curvature is null, the moment $\hat{M}_3$ acting on the bit is null as well and the *BHA* can be viewed as a beam on three supports uniformly loaded by $\sin\theta_m$. Considering the linearity of the problem if this load is doubled, the reaction $\hat{F}_2$ acting on the bit and the inclination of the deflection at the bit β are doubled too. This proportionality is also valid from a bit-rock interaction point of view. Indeed, if the weight-on-bit is constant, β is proportional to d_2 considering Equation (51) and d_2 is proportional to $\hat{F}_2$ with respect to Equation (47). Meaning that β and F_2 are proportional in the two legs of the model and that it corresponds to an equilibrium solution.

On the other side, for both boundary conditions, the dimensionless curvature κ_s is positive when $\varkappa_1$ tends to zero. Meaning that the *BHA* is always characterised by a building tendency when the length λ_1 is sufficient small compared to the *BHA* length ℓ, whatever the magnitude of the number $\eta\Psi$ which can be written as

$$\eta\Psi = \eta\frac{\ell^2 W_c}{EI} \tag{84}$$

where W_c is the fraction of the weight-on-bit mobilized by the cutting process.

Considering expression (84) we notice that the definition (67) of Ψ can be rewritten as

$$W_c = \Psi\frac{EI}{\ell^2} \tag{85}$$

which is strangely resembling to the critical load defined by Euler[7] for the buckling of homogeneous and perfectly straight columns. Indeed, the drillstring can be assimilated to a slender beam loaded by an axial force which is the fraction of the weight-on-bit mobilized by the cutting process.

2.2 Build-Up Rate

The drilling tendency is not the only relevant output of the mathematical model, the magnitude of the borehole curvature is highly significant for the drilling industry. The parametric analysis presented below has been conducted considering a $8^{1/2}$ inches borehole diameter and for the range of parameters listed in Table 5. In the industry, the radius of curvature is not popular and the build-up rate or dog leg severity are usually preferred. They are expressed in degrees per 100 feet (or 30 meters) of borehole drilled and correspond to the rate of change of the inclination of the tangent to the borehole with the borehole length. Practically, a build-up rate of 1° per 100 ft corresponds to a radius $R = 1765$ m.

In the following paragraphs, the influence of the main parameters governing the model is investigated. However, since the magnitude of the borehole curvature is proportional to the sine of the *BHA* mean inclination, the influence of the parameter θ_m is not studied.

2.2.1 Influence of the Parameter $\varkappa_1$

The distance λ_1 between the bit and the first stabilizer is of prime importance. *BHA* assemblies described by low values of the parameter $\varkappa_1$ are not only mainly characterized by a building tendency but it also appears that the magnitude of the borehole curvature increases quickly for

[7] The critical buckling load is given by Euler's formula:

$$F_{cr} = \pi^2\frac{EI}{\ell^2}$$

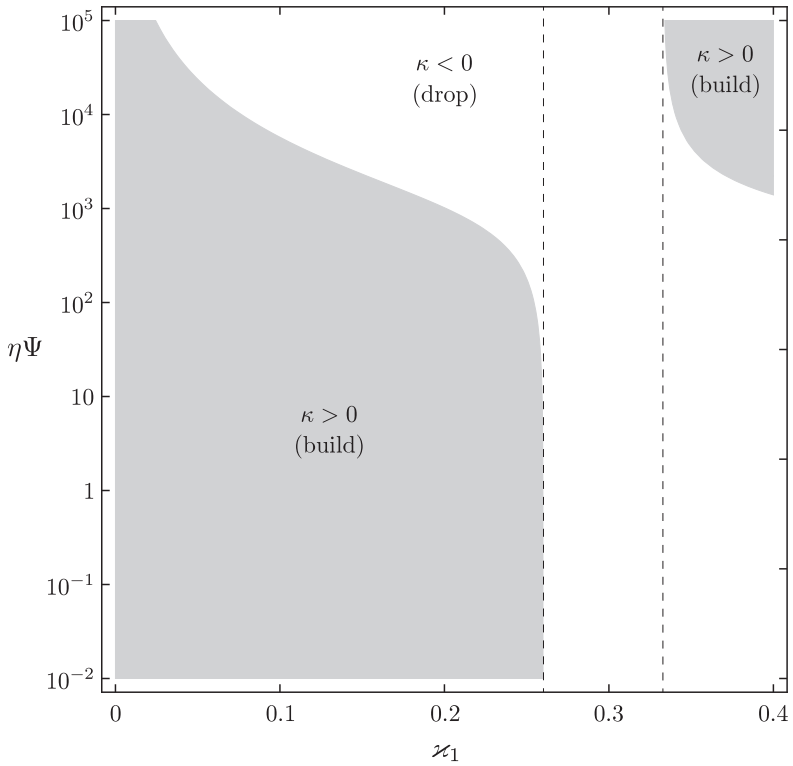

(a) The upper stabilizer is blocked in rotation (κ_b)

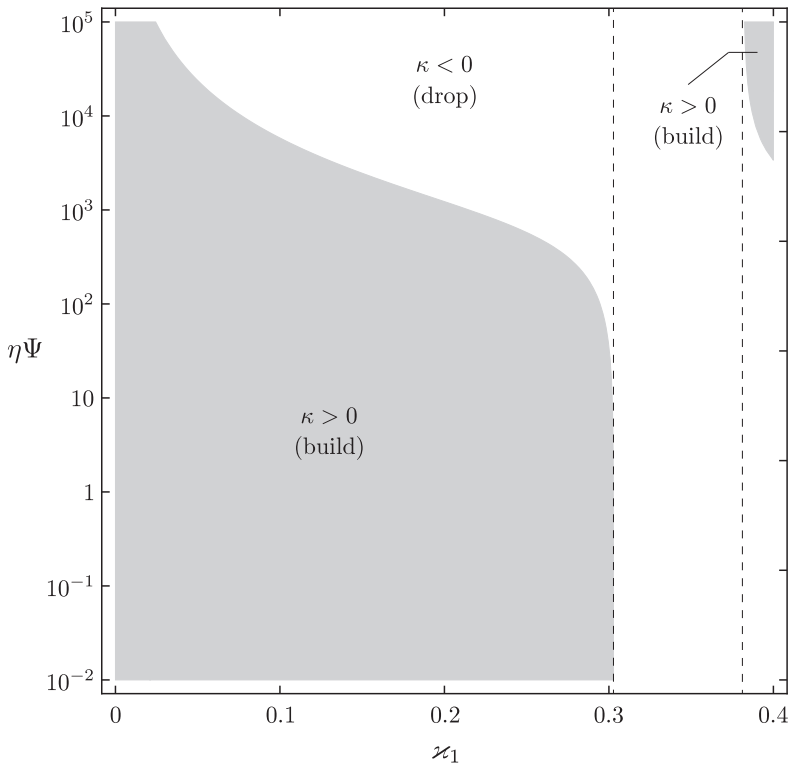

(b) The upper stabilizer is free to rotate (κ_f)

Figure 19: Sign of the borehole curvature κ_s in the space $(\varkappa_1, \eta\Psi)$ considering $\Phi = 0$

values of $\varkappa_1$ approaching zero (see Figure 20, 21, 22 and 23). This observation reflects the behaviour of the beam model. Indeed, for decreasing values of the parameters $\varkappa_1$, the transversal force acting on the bit $\hat{F}_2$ increases (see Appendix E), involving an intensification of the the lateral penetration d_2 according to Equation (47) resulting in the growth of the curvature κ_s.

In the limiting case of $\varkappa_1$ tending to zero, the borehole curvature and the penetration inclination are independent of the lateral steering resistance and are moreover mainly conditioned by the ratio between the stiffness and the mean inclination of the *BHA*

$$\lim_{\varkappa_1 \to 0} \kappa_b = \frac{\sin\theta_m}{12\Upsilon(\chi\Psi+1)} \tag{86}$$

$$\lim_{\varkappa_1 \to 0} \beta_b = \frac{\sin\theta_m}{24\Upsilon(\chi\Psi+1)} \tag{87}$$

$$\lim_{\varkappa_1 \to 0} \kappa_f = \frac{\sin\theta_m}{4\Upsilon(2\chi\Psi+3)} \tag{88}$$

$$\lim_{\varkappa_1 \to 0} \beta_f = \frac{\sin\theta_m}{8\Upsilon(2\chi\Psi+3)} \tag{89}$$

Extremely long *BHA* assemblies compared to the distance between the bit and the first stabilizer ($\varkappa_1 \ll 1$) are then always characterised by a building tendency. Furthermore, we observe that the ratios between the curvature and the penetration inclination are equal and constant for the two boundary conditions considered at the upper stabilizer

$$\frac{\beta_b}{\kappa_b} = \frac{\beta_f}{\kappa_f} = 2 \tag{90}$$

On the other hand, as soon as the bit and the stabilizer become too close, allow the bit to have a transverse depth of cut per revolution, d_2, and compel the stabilizer to lie on the borehole axis can not be considered realistic. Limits of the mathematical model are met. Both, the stabilizer and the bit, have to be viewed as a unique tool.

2.2.2 Influence of the Weight-On-Bit

The influence of the *WOB* is studied through the dimensionless fraction of the weight-on-bit mobilized by the cutting process $\Pi_c = \Pi - \Gamma_1$. Indeed, it is commonly accepted that the fractions of the weight-on-bit mobilized by frictional contact between the rock and the bit is readily constant for a given state of wear (taken here as $\mathcal{G}_1 = 10$ kN).

Figure 20 illustrates the effects of the parameters $\varkappa_1$ on the curvature for various values of Π_c. Comparing Figures 20(a) and 20(b), we observe that the solutions are only slightly affected by the boundary conditions considered at the upper stabilizer. Since these two boundary conditions have been chosen to bracket the effect of the drillstring above the second stabilizer, it suggests that considering only the first two stabilisers is probably sufficient to predict the borehole curvature.

Increase of the *WOB* tends to reduce the magnitude of the borehole curvature and to amplify the influence of the distance between the bit and the first stabilizer. Especially, for extremely high values of Π_c, the borehole axis becomes straight

$$\lim_{\Pi_c \to \infty} \kappa_b = \lim_{\Pi_c \to \infty} \kappa_f = 0 \tag{91}$$

On the opposite when the fraction of the *WOB* mobilized by the cutting process takes extremely small values compare to the fraction mobilized by frictional contact (*i.e.,* $\Pi_c \to 0$ or $\Pi \to \Gamma_1$), the magnitude of the curvature becomes independent of the steering resistances and is fully conditioned

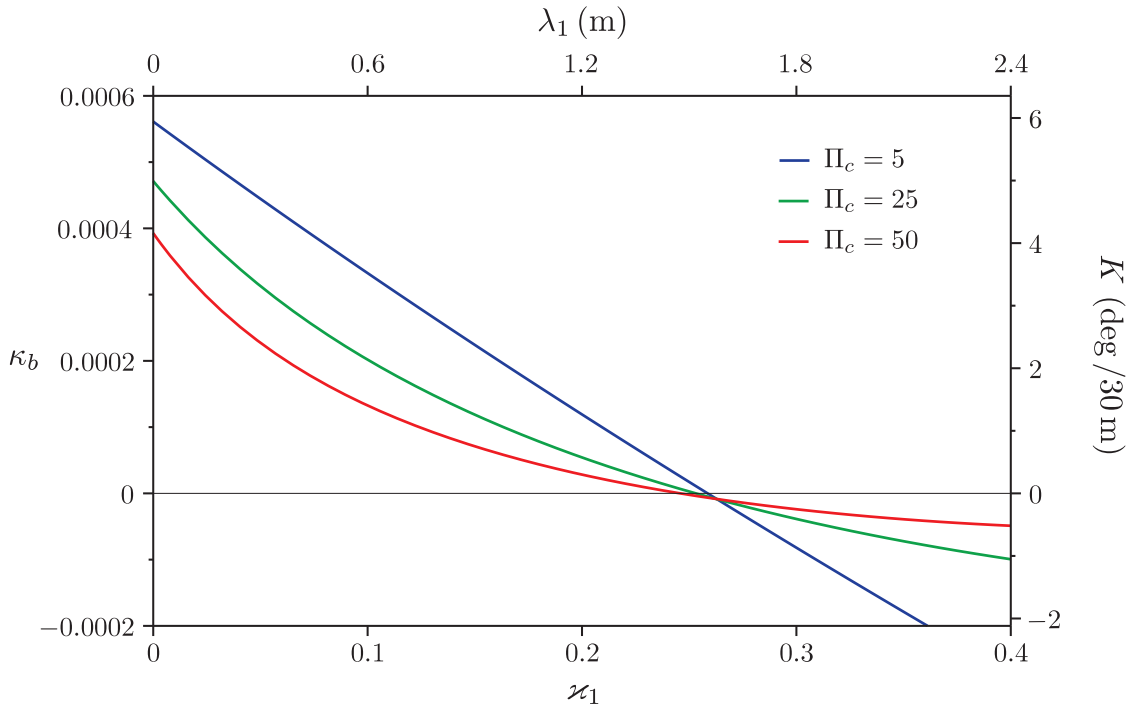

(a) The upper stabilizer is blocked in rotation

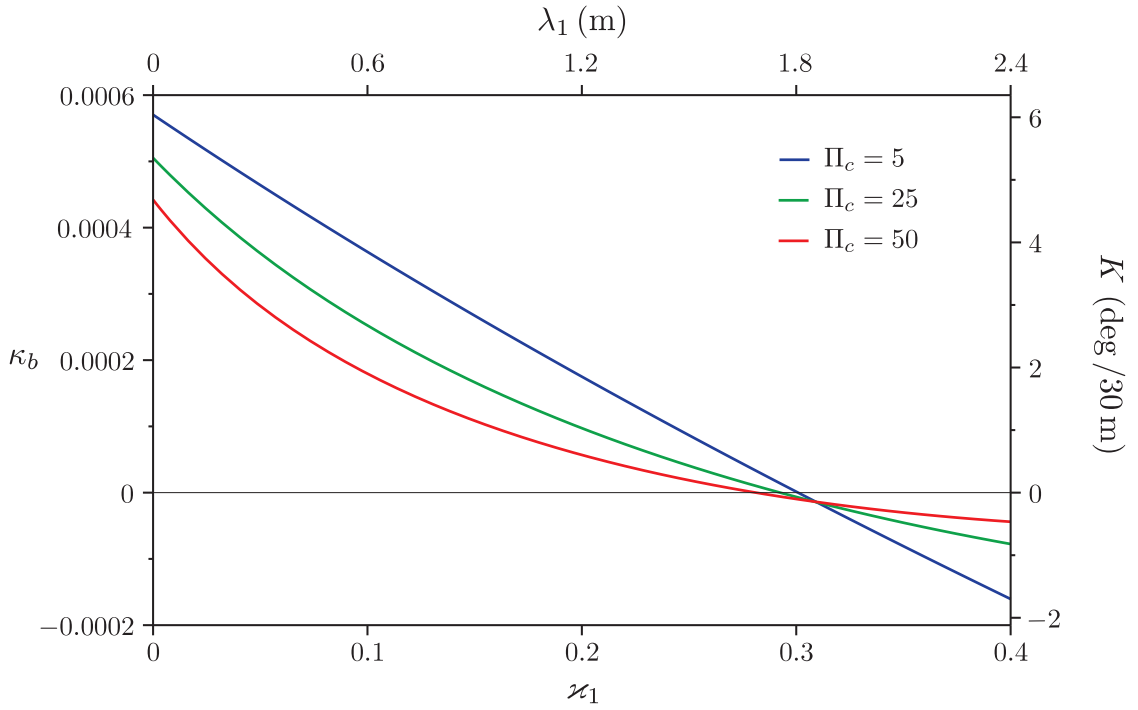

(b) The upper stabilizer is free to rotate

Figure 20: Effect of the parameter $\varkappa_1$ on the borehole curvature for various Π_c and for $\chi = 1$, $\eta = 50$, $\Upsilon = 100$ and $\theta_m = \pi/4$. The length λ_1 and the curvature K are given for a *BHA* length $\ell = 6$ m

by the three parameters θ_m, Υ and $\varkappa_1$

$$\lim_{\Pi_c \to 0} \kappa_b = -\frac{\left(\varkappa_1^3 + 3\varkappa_1^2 + 3\varkappa_1 - 1\right)\sin\theta_m}{12\Upsilon} \tag{92}$$

$$\lim_{\Pi_c \to 0} \kappa_f = -\frac{\left(\varkappa_1^2 + 3\varkappa_1 - 1\right)\sin\theta_m}{12\Upsilon} \tag{93}$$

Moreover when the length between the first stabiliser and the bit becomes small compare to the length of the *BHA* (*i.e.,* $\varkappa_1 \ll 1$), the curvature of the borehole does not depend on the boundary condition considered at the upper stabilizer

$$\lim_{\substack{\Pi_c \to 0 \\ \varkappa_1 \to 0}} \kappa_b = \lim_{\substack{\Pi_c \to 0 \\ \varkappa_1 \to 0}} \kappa_f = \frac{\sin\theta_m}{12\Upsilon} \tag{94}$$

For moderate values of the angular steering resistance, *i.e.,* for the range of amplitude given in Table 5, it exists a value of the parameter $\varkappa_1$ for which the curvature can be considered as independent of the weight-on-bit. Indeed for this value of $\varkappa_1$, it appears that the curvature is essentially conditioned by the stiffness Υ while the terms in $\eta\Pi_c$ and $\chi\Pi_c$ can be neglected. This particular value of $\varkappa_1$ depends on the boundary conditions considered at the upper stabilizer, it correspond to the third root of the polynomial (95) if the rotation at the upper stabilizer is blocked and to the second root of the polynomial (96) if the upper stabilizer is free to rotate.

$$3\varkappa_1^3 + 12\varkappa_1^2 + 8\varkappa_1 - 3 = 0 \tag{95}$$

$$-\varkappa_1^3 + \varkappa_1^2 + 3\varkappa_1 - 1 = 0 \tag{96}$$

The curvature degenerates then to the expression (92) where $\varkappa_1$ is equal to

$$\varkappa_1 = \frac{1}{6}\left(\sqrt{21} - 3\right) \simeq 0.264 \tag{97}$$

or to the expression (93) where $\varkappa_1$ is equal to

$$\varkappa_1 = \frac{1}{3} + \sqrt{\frac{10}{3}}\sin\left(\frac{1}{3}\tan^{-1}\left(3\sqrt{111}\right)\right) - \frac{1}{3}\sqrt{10}\cos\left(\frac{1}{3}\tan^{-1}\left(3\sqrt{111}\right)\right) \simeq 0.311 \tag{98}$$

depending on the boundary conditions considered at the upper stabilizer. The curvature is thus given by

$$\kappa_b = -\frac{\left(2\sqrt{21} - 9\right)\sin\theta_m}{108\Upsilon} \simeq -\frac{0.0015\sin\theta_m}{\Upsilon} \tag{99}$$

$$\kappa_f \simeq -\frac{0.0025\sin\theta_m}{\Upsilon} \tag{100}$$

2.2.3 Influence of the Stiffness

Effects of the parameter $\varkappa_1$ on the curvature are given in Figure 21 for different values of the dimensionless stiffness. We notice again that the curvature is only slightly affected by the boundary conditions considered at the upper stabilizer.

Generally, an increase of Υ (all other parameters being equal) causes a decrease of the curvature. We notice also a decrease of the dependence on the dimensionless distance between the bit and the first stabilizer when the stiffness increases. Conversely, for magnitudes of the stiffness met on the field and for values of the parameters $\varkappa_1$ superior to 0.2, the curvature seems to be essentially conditioned by the *BHA* mean inclination and the steering resistances.

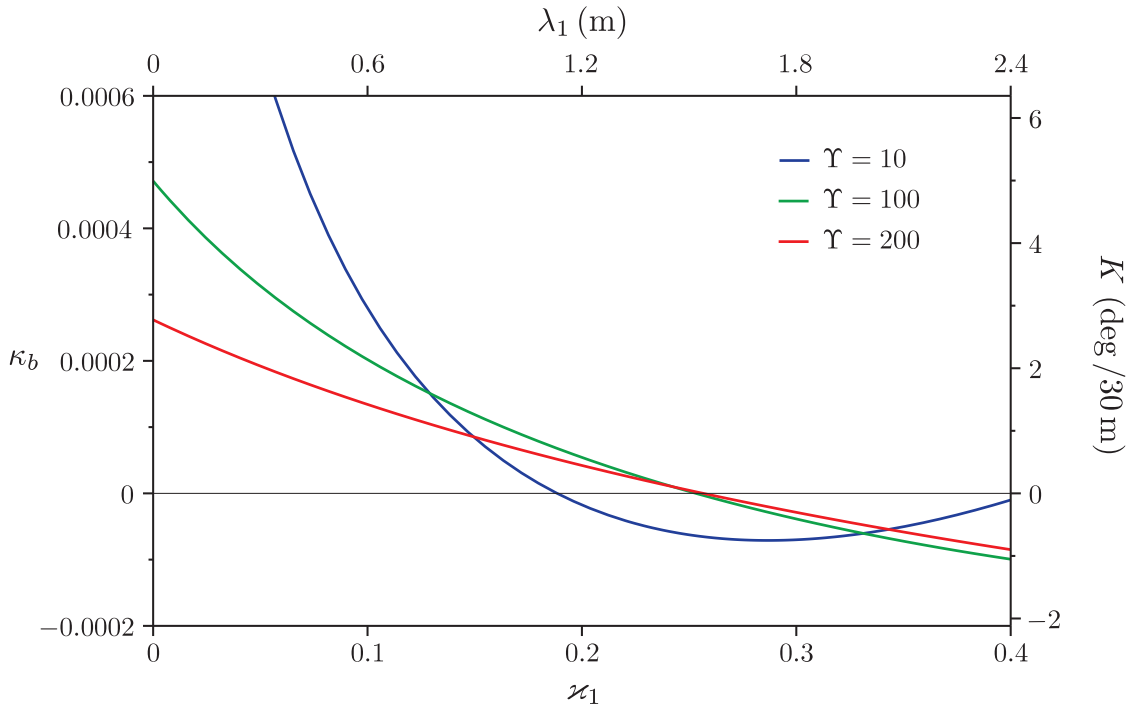

(a) The upper stabilizer is blocked in rotation

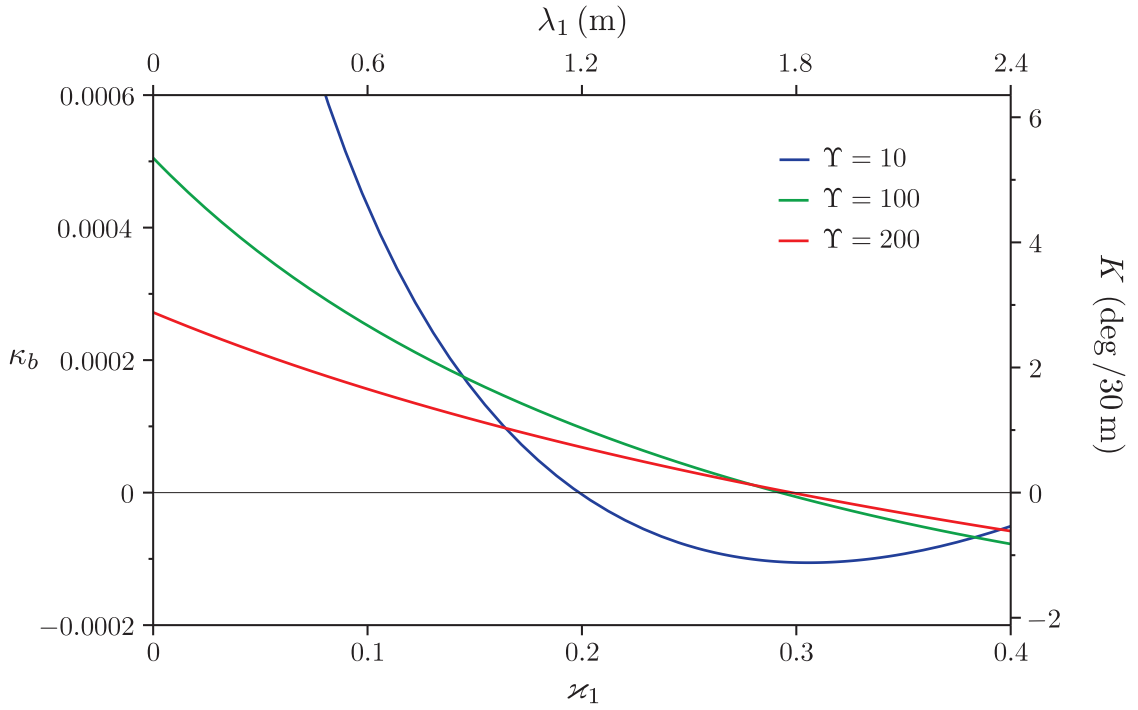

(b) The upper stabilizer is free to rotate

Figure 21: Effect of the parameter $\varkappa_1$ on the borehole curvature for various Υ and for $\chi = 1$, $\eta = 50$, $\Pi_c = 25$ and $\theta_m = \pi/4$. The length λ_1 and the curvature K are given for a *BHA* length $\ell = 6$ m

Considering now the limiting case of an extremely stiff *BHA*, the borehole axis degenerates to a straight line for both boundary conditions considered at the upper stabilizer and for any value of $\varkappa_1$

$$\lim_{\Upsilon\to\infty} \kappa_b = \lim_{\Upsilon\to\infty} \kappa_f = 0 \tag{101}$$

On the other side, for low values of the stiffness, two different assemblies ($\varkappa_1 \neq$) may produce the same borehole curvature. In the limiting case of a *BHA* hugely flexible, the borehole curvature is independent of the lateral steering resistance but is inversely proportional to $\Pi_c\chi$, meaning large magnitude of the borehole curvature

$$\lim_{\Upsilon\to 0} \kappa_b = \frac{(3\varkappa_1 - 1)\sin\theta_m}{24\Pi_c\chi} \tag{102}$$

$$\lim_{\Upsilon\to 0} \kappa_f = \frac{\left(\varkappa_1^2 - 3\varkappa_1 + 1\right)\sin\theta_m}{4\Pi_c\chi(\varkappa_1 - 4)} \tag{103}$$

Moreover, for extremely long *BHA* compared to the length between the bit and the first stabilizer (*i.e.,* $\varkappa_1 \ll 1$), the borehole curvature is independent of any parameters related to the *BHA*

$$\lim_{\substack{\Upsilon\to 0\\ \varkappa_1\to 0}} \kappa_b = \frac{\sin\theta_m}{24\Pi_c\chi} \tag{104}$$

$$\lim_{\substack{\Upsilon\to 0\\ \varkappa_1\to 0}} \kappa_f = \frac{\sin\theta_m}{16\Pi_c\chi} \tag{105}$$

2.2.4 Influence of the Steering Resistances

The lateral and the angular steering resistances involves several parameters characterizing the bit or the interactions between the rock and the different part of the bit. Moreover η and χ are linked by the relation (71), meaning that a variation of one of these parameters may induce variations of both steering resistances which are not necessarily of the same magnitude. Considering independently every parameters (a, b or ξ), we can establish the following relations relating the variation of this parameter to the variations of steering resistances

- A variation of the bit radius Δa implies

$$\begin{aligned} \Delta\eta &\propto -\frac{\Delta a}{a^2} \\ \Delta\chi &\propto -\frac{\Delta a}{a^2} \end{aligned} \tag{106}$$

- A variation of the bit gauge Δb implies

$$\begin{aligned} \Delta\eta &\propto \Delta b \\ \Delta\chi &\propto b^2\Delta b \end{aligned} \tag{107}$$

- A variation of the ratio $\Delta\xi$ implies

$$\begin{aligned} \Delta\eta &\propto \Delta\xi \\ \Delta\chi &\propto \Delta\xi \end{aligned} \tag{108}$$

Considering that the definition of the angular steering resistance (71) involves the length of the *BHA*, it appears that a variation $\Delta\ell$ implies

$$\begin{aligned} \Delta\eta &\propto 0 \\ \Delta\chi &\propto -\frac{\Delta\ell}{\ell^3} \end{aligned} \tag{109}$$

Finally, in the expressions of the dimensionless curvature (76) and (77), the lateral and angular steering resistances appear only as coefficients of the parameter Π_c meaning that their effects on the curvature are amplified by large value of the weight-on-bit.

Figures 22 and 23 depict the effects of the parameters $\varkappa_1$ on the curvature for various values of the steering resistances η and χ, respectively. As expected since η and χ express the difficulty to steer the bit, an increase of those parameters involves a decrease of the borehole curvature. These figures confirm that the drillstring above the second stabilizer has a weak influence on the borehole curvature.

Similarly to the effects of the weight-on-bit, an increase of the lateral steering resistance reduces the magnitude of the curvature. Figure 22 highlights also that, for $\varkappa_1 \to 0$, the borehole curvature do not depend on η. The lateral steering resistance is the only parameters who does not modify the intersection of the curve $\kappa_s(\varkappa_1)$ with the ordinates axis.

For extremely high values of η, it appears that the borehole curvature has a weak dependence on $\varkappa_1$

$$\lim_{\eta\to\infty} \kappa_b = -\frac{\varkappa_1(1-3\varkappa_1)\sin\theta_m}{12\Upsilon(2\chi\Psi\varkappa_1+3)} \tag{110}$$

$$\lim_{\eta\to\infty} \kappa_f = -\frac{\varkappa_1\left(\varkappa_1^2-3\varkappa_1+1\right)\sin\theta_m}{4\Upsilon\left(\chi\Psi(4-\varkappa_1)\varkappa_1+3(2-\varkappa_1)\right)} \tag{111}$$

and *BHA* assemblies are always characterized by a dropping tendency for $\varkappa_1 < 0.333$ or $\varkappa_1 < 0.382$ depending on the boundary condition considered at the upper stabilizer.

On the opposite for extremely low values of the lateral steering resistance, the borehole curvature is still highly dependent on $\varkappa_1$

$$\lim_{\eta\to 0} \kappa_b = -\frac{\left(\varkappa_1^3+3\varkappa_1^2+3\varkappa_1-1\right)\sin\theta_m}{12\Upsilon\left(\chi\Psi(\varkappa_1+1)+1\right)} \tag{112}$$

$$\lim_{\eta\to 0} \kappa_f = -\frac{\left(\varkappa_1^2+3\varkappa_1-1\right)\sin\theta_m}{4\Upsilon\left(\chi\Psi(\varkappa_1+2)+3\right)} \tag{113}$$

Influences of the angular steering resistance is similar to the influence of the weight-on-bit. Generally, an increase of the angular steering resistance involves a decrease of the curvature magnitude. Especially, for extremely high values of χ, the borehole axis becomes straight

$$\lim_{\chi\to\infty} \kappa_b = \lim_{\chi\to\infty} \kappa_f = 0 \tag{114}$$

Figure 23 highlights that the combination of parameters corresponding to a holding assembly is independent of the angular steering resistance. Which is confirm by the expressions (80) and (82) corresponding to the boundaries between the regions defining the drilling tendency of the assembly.

2.3 Bit Tilt and Over-gauge

The drilling tendency and the borehole curvature are not the only relevant output of the mathematical model. Indeed, the bit tilt ψ_s (or equivalently the penetration inclination β_s) constraints the magnitude of the borehole diameter through the overgauge factor Ξ_s, see Equation 1. Since the clearance between the casing and the borehole is to be filled with cement, an important overgauge may lead to consequent extra costs.

Figure 24 pictures the evolution of the bit tilt with the dimensionless borehole curvature for varying values of the dimensionless length $\varkappa_1$. Seeing that this relation has a minor dependence on the type of boundary condition considered at the upper stabilizer, only the case corresponding

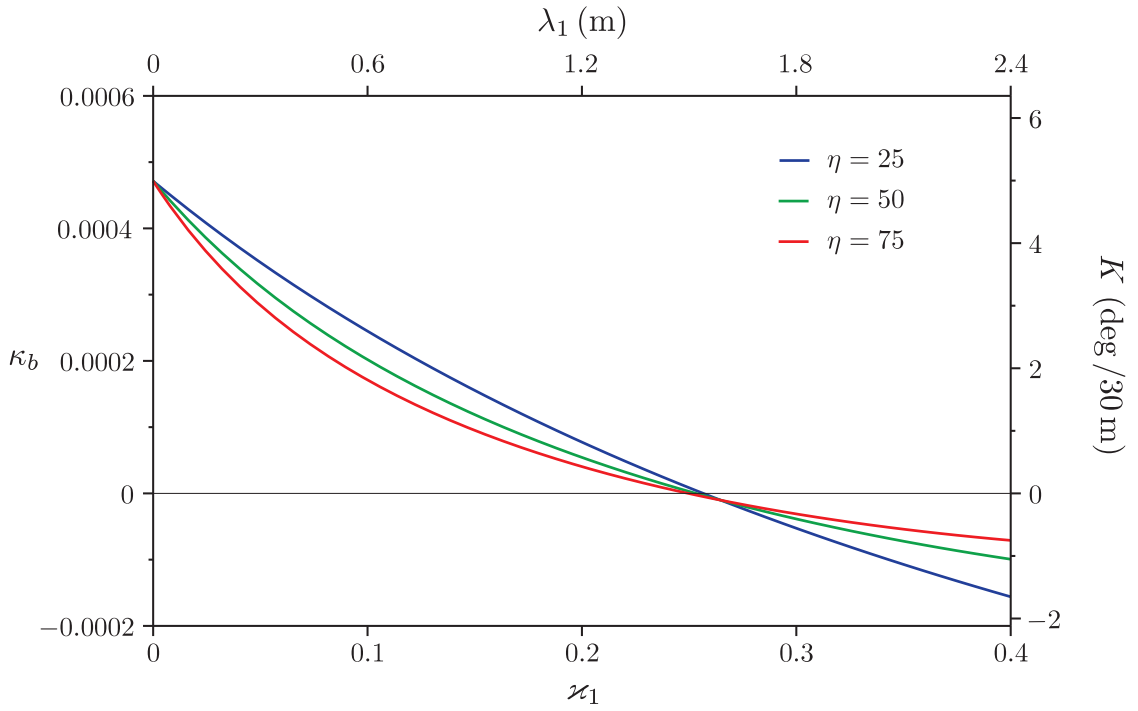

(a) The upper stabilizer is blocked in rotation

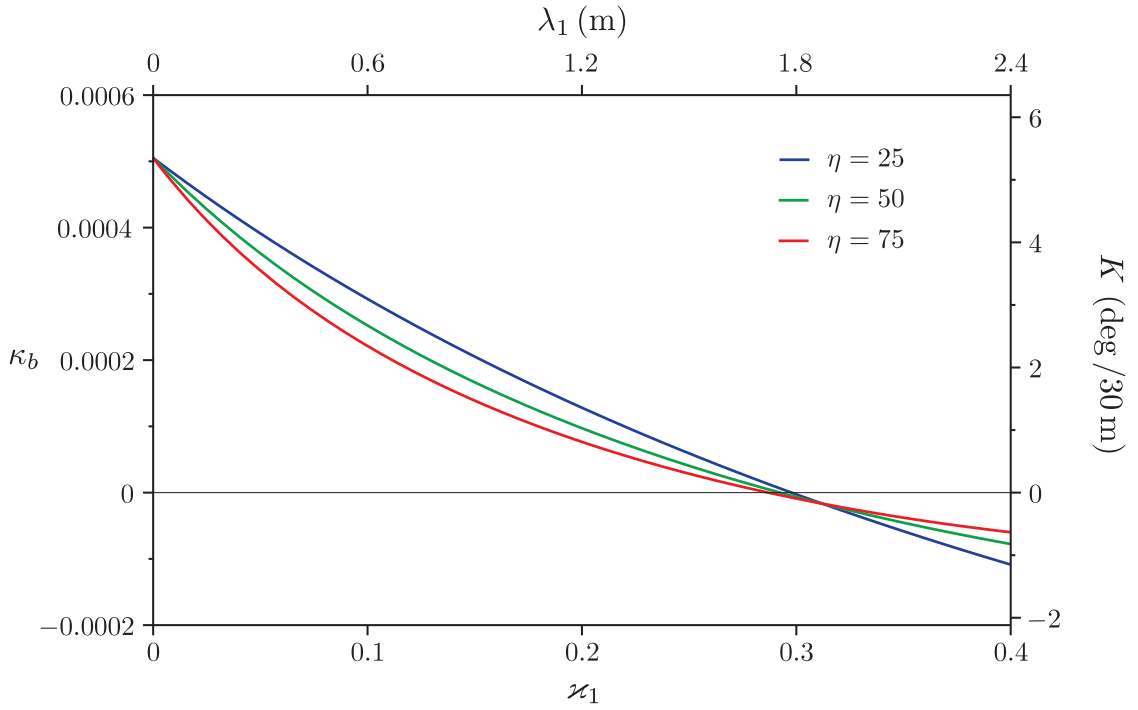

(b) The upper stabilizer is free to rotate

Figure 22: Effect of the parameter $\varkappa_1$ on the borehole curvature for various η and for $\chi = 1$, $\Pi_c = 25$, $\Upsilon = 100$ and $\theta_m = \pi/4$. The length λ_1 and the curvature K are given for a *BHA* length $\ell = 6$ m.

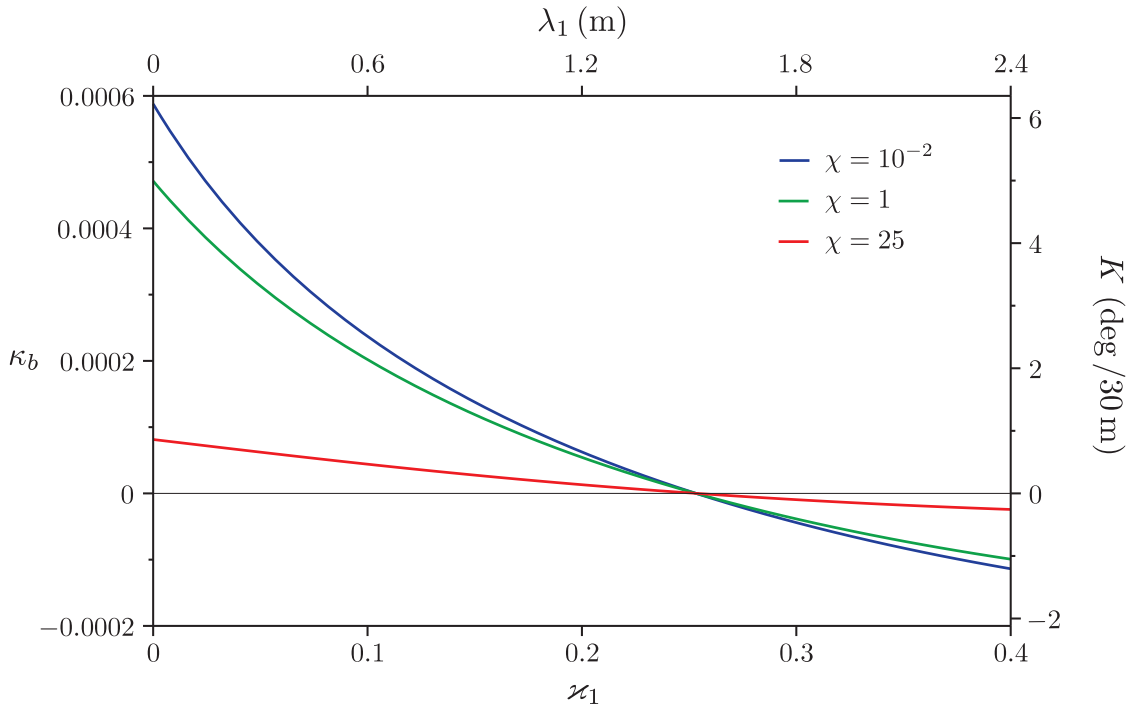

(a) The upper stabilizer is blocked in rotation

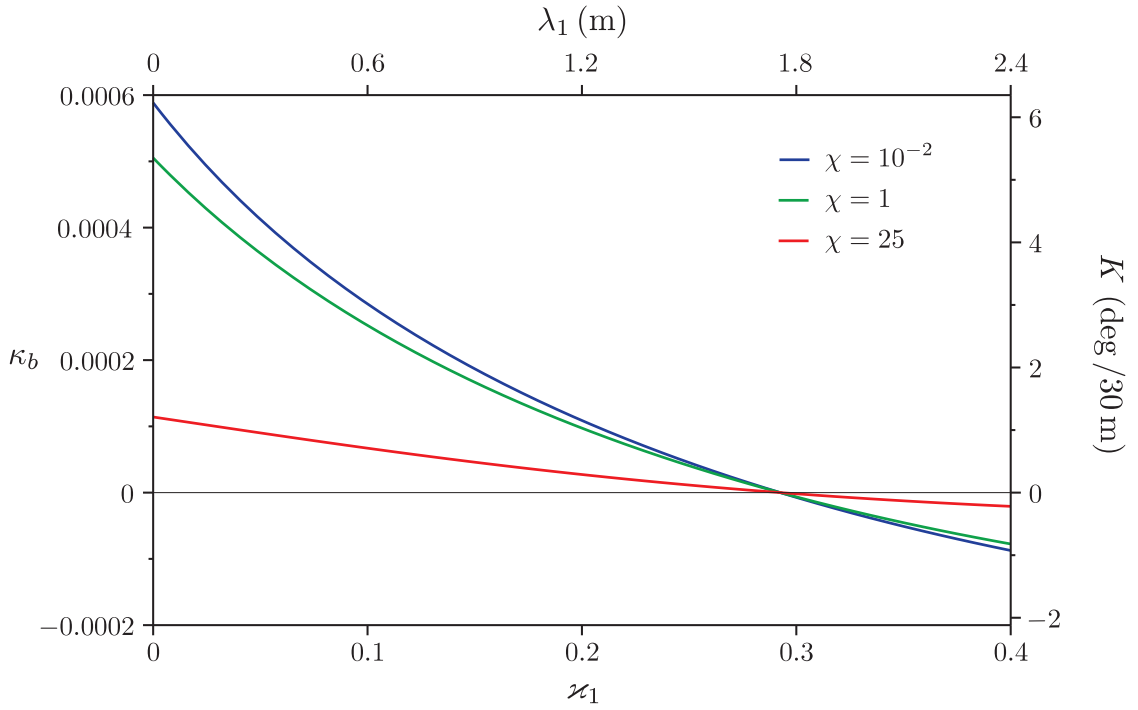

(b) The upper stabilizer is free to rotate

Figure 23: Effect of the parameter $\varkappa_1$ on the borehole curvature for various χ and for $\eta = 50$, $\Pi_c = 25$, $\Upsilon = 100$ and $\theta_m = \pi/4$. The length λ_1 and the curvature K are given for a *BHA* length $\ell = 6$ m.

to the upper stabilizer blocked in rotation is presented. However, the chart corresponding to the upper stabilizer free to rotate is given in Appendix F.1. Moreover, as the influence of the lateral steering resistance and the weight-on-bit (or similarly Π_c) are similar, only the impact of the last one is studied.

First, we notice that building tendencies, *i.e.,* positive values of the borehole curvature, correspond mostly to negative values of the bit tilt. Moreover, the magnitude of the bit tilt increases with the borehole curvature. Meaning also that the magnitude of the bit tilt decreases when the parameter $\varkappa_1$ increases.

The influence of the dimensionless fraction of the weight-on-bit mobilized by the cutting process is investigate in Figure 24(a). It appears that the impact of this parameter is mainly noticeable for high values of $\varkappa_1$, *i.e.,* for dropping assemblies. On the opposite, for positive values of the curvature, the parameter Π_c has a weak influence on the relation between the borehole curvature and the bit tilt.

Figure 24(b) depicts the effects of the dimensionless stiffness on the evolution of the bit tilt with the dimensionless borehole curvature. At constant curvature and considering a building assembly, an increase of the *BHA* stiffness produces a decrease of the magnitude of the bit tilt. On the other side, considering now dropping assemblies characterized by a low stiffness, it appears that two different bit tilts (sometimes of opposite sign) can be obtained for the same borehole curvature only by changing the magnitude of the parameter $\varkappa_1$, *i.e.,* the distance between the bit and the first stabilizer or the length of the *BHA*.

Finally, effects of the angular steering resistance are studied in Figure 24(c). As expected, an increase of the parameter χ involves not only a decrease of the borehole curvature but also of the bit tilt. For high values of the angular steering resistance and for positive curvature, two different curvature of the borehole may be obtained for the same bit tilt only by changing the magnitude of the ratio $\varkappa_1$. Those effects are obviously amplified by high values of the *WOB* since the angular steering resistance appears only as coefficients of the parameter Π_c.

3 *BHA* Equipped with a Rotary Steerable System

Consider now the more complex problem of a *BHA* equipped with a rotary steerable system. As mentioned earlier, this parametric analysis is led considering that the actuator exerts the force $\breve{F}$ equidistantly from the two stabilizers and that the two segments λ_2 and λ_4 have the same length, or in dimensionless form $\varkappa_2 = \varkappa_4$.

Under these assumptions, the equilibrium solution (65) can be, once again, determined for the two boundary conditions considered at the upper stabilizer remembering the expressions of the $\mathcal{F}$'s and $\mathcal{M}$'s coefficients given in Table 1. However, for brevity considerations and since the previous section highlighted a weak dependence of the solution on this boundary condition, the solution is only presented in the case of an upper stabilizer blocked in rotation. The solution corresponding to the upper stabilizer free to rotate is given in Appendix G.1. In this context, the borehole curvature can be written as

$$\kappa_b = \frac{\mathcal{C}_{\Phi,\kappa}\Phi + \mathcal{C}_{w,\kappa}\sin\theta_m}{\mathcal{C}_{\Upsilon,\kappa}\Upsilon} \tag{115}$$

with the coefficients

$$\begin{aligned}
\mathcal{C}_{\Phi,\kappa} &= 3(1-\varkappa_1-2\varkappa_2)\left(\eta\Psi(\varkappa_1+2\varkappa_2-1)\varkappa_1^2+6\left(1-\varkappa_1^2+\varkappa_1(\varkappa_2-4)+\varkappa_2\right)\right)\\
\mathcal{C}_{w,\kappa} &= -2\left(\eta\Psi(1-3\varkappa_1)\varkappa_1^2+6\left(\varkappa_1^3+3\varkappa_1^2+3\varkappa_1-1\right)\right)\\
\mathcal{C}_{\Upsilon,\kappa} &= 24\left(2\eta\Psi^2\chi\varkappa_1^2+3\Psi\left(\eta\varkappa_1+2\chi(\varkappa_1+1)\right)+6\right)
\end{aligned} \tag{116}$$

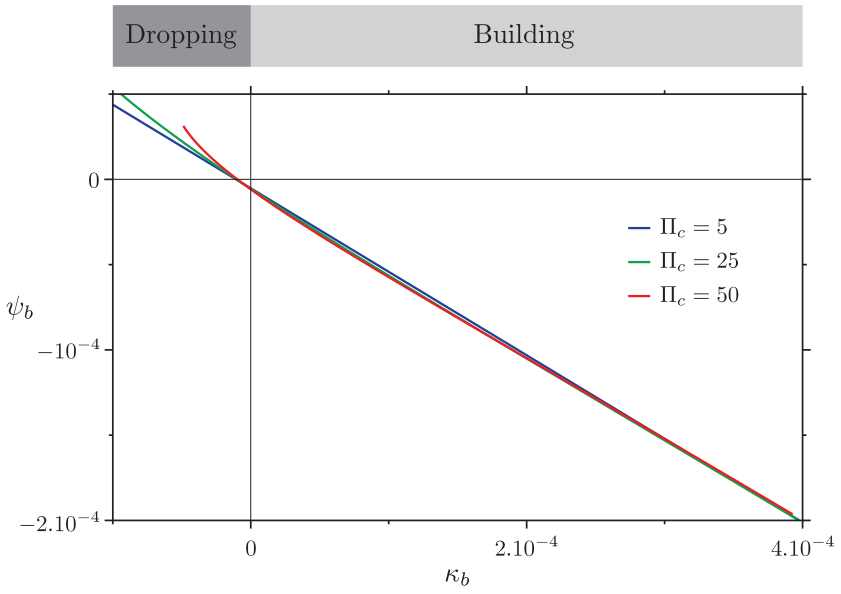

(a) For different values of the parameter Π_c

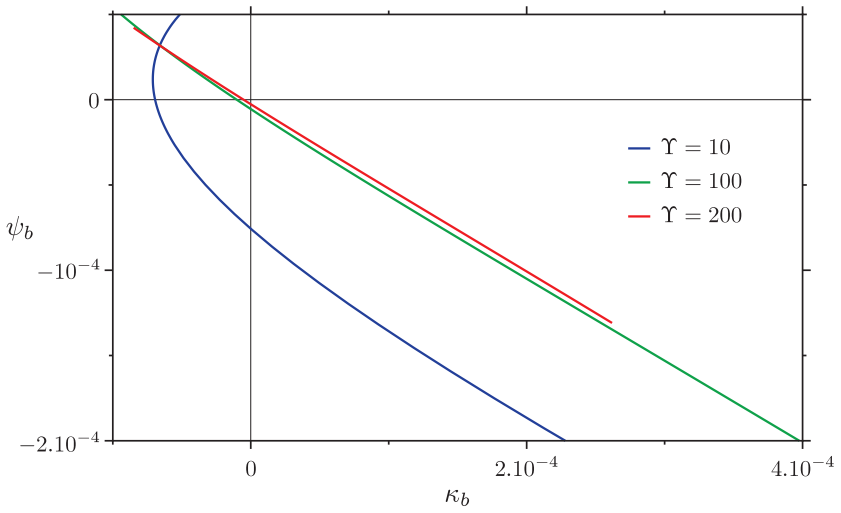

(b) For different values of the dimensionless stiffness Υ

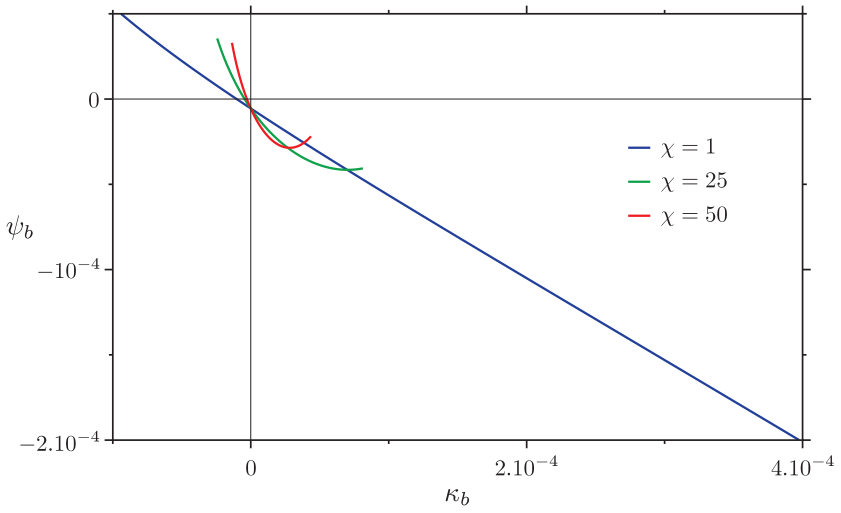

(c) For different values of the lateral steering resistance η

Figure 24: Evolution of the bit tilt with the dimensionless borehole curvature for varying $\varkappa_1$ and considering the upper stabilizer blocked in rotation ($\chi = 1$, $\eta = 50$, $\Pi_c = 25$, $\Upsilon = 100$ and $\theta_m = \pi/4$)

Similarly, the penetration inclination read

$$\beta_b = \frac{\mathcal{C}_{\Phi,\beta}\Phi + \mathcal{C}_{w,\beta}\sin\theta_m}{\mathcal{C}_{\Upsilon,\beta}\Upsilon} \tag{117}$$

with the coefficients

$$\begin{aligned}
\mathcal{C}_{\Phi,\beta} &= 3(1-\varkappa_1-2\varkappa_2)\left(\chi\Psi(1-3\varkappa_1)\varkappa_1 - 4\varkappa_1 + \varkappa_2 + 1\right)\\
\mathcal{C}_{w,\beta} &= -2\left(\chi\Psi\left(2\varkappa_1^2+3\varkappa_1-1\right)\varkappa_1 + 3\varkappa_1^2 + 3\varkappa_1 - 1\right)\\
\mathcal{C}_{\Upsilon,\beta} &= 8\left(2\eta\Psi^2\chi\varkappa_1^2 + 3\Psi\left(\eta\varkappa_1 + 2\chi(\varkappa_1+1)\right) + 6\right)
\end{aligned} \tag{118}$$

While the sign and the magnitude of the coefficients $\mathcal{C}_\Phi$'s and $\mathcal{C}_w$'s depend widely on the different parameters of the models, it appears that coefficients $\mathcal{C}_\Upsilon$'s are always positive, regardless to the magnitude of the parameters governing the mathematical model.

Solutions presented in the previous section and corresponding to a *BHA* without rotary steerable system can be easily recovered by choosing $\Phi = 0$ in the relations above. The influence of the *RSS* is then fully determined by the terms $\mathcal{C}_\Phi\Phi$ and the complete solution can be viewed as the sum of two terms: the curvature (penetration inclination) obtained due to the gravity field and the curvature (penetration inclination) obtained due to the application of the load Φ on the shaft.

3.1 Drilling Tendency

Since the product $\mathcal{C}_{\Upsilon,\kappa}\Upsilon$ is always positive, the sign of the borehole curvature and thus the drilling tendency is entirely conditioned by the numerator of the expression (115). Consequently, we can identify four distinct behaviours corresponding to the four combinations of signs for the two coefficients $\mathcal{C}_{\Phi,\kappa}$ and $\mathcal{C}_{w,\kappa}$

- $\mathcal{C}_{\Phi,\kappa} > 0$ and $\mathcal{C}_{w,\kappa} > 0$: the borehole curvature κ_s is positive for any positive values of the *RSS* force, meaning that the assembly is characterized by a building tendency whatever the magnitude of Φ, which can be written as $\kappa_s > 0$, $\forall\,\Phi > 0$.
- $\mathcal{C}_{\Phi,\kappa} > 0$ and $\mathcal{C}_{w,\kappa} < 0$: the borehole curvature κ_s is negative for any negative values of the *RSS* force, meaning that the assembly is characterized by a dropping tendency whatever the magnitude of Φ, which can be written as $\kappa_s < 0$, $\forall\,\Phi < 0$.
- $\mathcal{C}_{\Phi,\kappa} < 0$ and $\mathcal{C}_{w,\kappa} < 0$: the assembly is characterized by a dropping tendency for any negative values of Φ, thus $\kappa_s < 0$, $\forall\,\Phi > 0$.
- $\mathcal{C}_{\Phi,\kappa} < 0$ and $\mathcal{C}_{w,\kappa} > 0$: the assembly is characterized by a building tendency for any negative values of Φ, thus $\kappa_s > 0$, $\forall\,\Phi < 0$.

These four behaviours can be associated to four distinct regions in the space $(\eta\Psi, \varkappa_1)$ which are presented in Figures 25 and 26. The boundaries delimiting the regions are defined by

$$\eta\Psi = \frac{6\left(\varkappa_1^2 - \varkappa_1(\varkappa_2-4) - \varkappa_2 - 1\right)}{\varkappa_1^2(\varkappa_1+2\varkappa_2-1)} \tag{119}$$

$$\eta\Psi = \frac{6\left(\varkappa_1^3 + 3\varkappa_1^2 + 3\varkappa_1 - 1\right)}{\varkappa_1^2(3\varkappa_1-1)} \tag{120}$$

if the upper stabilizer is considered as blocked in rotation and by

$$\eta\Psi = \frac{6}{\varkappa_1^2} \tag{121}$$

$$\eta\Psi = -\frac{6\left(\varkappa_1^2+3\varkappa_1-1\right)}{\varkappa_1^2\left(\varkappa_1^2-3\varkappa_1+1\right)} \tag{122}$$

if it is free to rotate. These boundaries are all independent of the angular steering resistance, the *RSS* force and the *BHA* mean inclination. In the first case, the boundary depends on the parameter $\varkappa_2$ and the second region (defined by $\mathcal{C}_{\Phi,\kappa} > 0$ and $\mathcal{C}_{w,\kappa} < 0$) do not exist for low values of the $\varkappa_2$, see Figure 25(a).

Typical field assemblies used to drill $8^{1/2}$ inches diameter boreholes are characterized by values of the product $\eta\Psi$ fluctuating between 1 and 10^2 while the dimensionless distance between the bit and the first stabilizer ranges from 0.025 to 0.2. Considering this window in the space $(\varkappa_1, \eta\Psi)$ on Figures 25 and 26, it appears that the two coefficients $\mathcal{C}_{\Phi,\kappa}$ and $\mathcal{C}_{w,\kappa}$ are mostly positive. The behaviour of such an assembly corresponds then, for the most part, to the first region and the borehole angle builds up for any positive values of the *RSS* force. However, if the upper stabilizer is blocked in rotation, two distinct behaviours may occur in this window. Meaning that, even a weak variation of one of the parameters ($\varkappa_1$, $\varkappa_2$ or $\eta\Psi$), may result in a switch from one behaviour to another.

These results allow us to affirm that the knowledge of the force orientation is not completely sufficient to establish the drilling tendency. Indeed, considering an assembly characterized by $\mathcal{C}_{\Phi,\kappa} > 0$ and $\mathcal{C}_{w,\kappa} > 0$ (Region I), a downward force ($\Phi > 0$) produces a borehole curvature positive, or in other words the borehole angle builds up. If for some reasons the values of the product $\eta\Psi$ is modified (modification the weight-on-bit, of the rock properties or of the bluntness of the bit), the assembly can switch to Region IV and, for the same *RSS* force, produces a borehole curvature negative. Finally, considering the same assembly (Region I), the sign of the curvature produced by the application of an upward load ($\Phi < 0$) cannot be deduced from the sign of the the coefficients $\mathcal{C}_{\Phi,\kappa}$ and $\mathcal{C}_{w,\kappa}$ but depends also on the magnitude of the ratio $\Phi/\sin\theta_m$.

3.2 Build-Up Rate

The parametric analysis presented below has been conducted considering a $8^{1/2}$ inches borehole diameter and for the range of parameters listed in Table 5. Despite all the assumptions and simplifications made, the complete mathematical model remains relatively complex and involves several parameters. Unlike the parametric analysis led for the simple case of a *BHA* without rotary steerable system (see Section 2), the magnitude of the borehole curvature is not directly proportional to the sine of the *BHA* mean inclination but result from a balance between the different load acting on the shaft (the gravity field and the force applied by the *RSS*).

Considering that influences of parameters like the weight-on-bit, the stiffness or the steering resistances keep the same trend than in the precedent analysis (see Section 2) and since the borehole curvature can advantageously be expressed as (115), the influence of the different parameters is studied through the three coefficients $\mathcal{C}_{\Phi,\kappa}$, $\mathcal{C}_{w,\kappa}$ and $\mathcal{C}_{\Upsilon,\kappa}$. Only the parameters $\varkappa_1$ is treated separately, for which the particular behaviour of the *BHA* for $\varkappa_1$ approaching zero is investigated.

On Figures 27, 28 and 29, values of the numbers $\varkappa_1$ and $\eta\Psi$ characterizing typical field assemblies used to drill $8^{1/2}$ inches diameter boreholes are framed by a white rectangle.

3.2.1 Influence of the Parameter $\varkappa_1$

Several field data observations and manufacturers specifications suggest that the length between the bit and the first stabilizer is usually small compared to the length of the *BHA* assembly. The general expression of the solution can thus be expand for small values of the parameter $\varkappa_1$, expression (115) of the borehole curvature becomes

$$\kappa_b \quad = \quad \kappa_b^0 + \frac{\mathcal{C}'_{\Phi,\kappa}\Phi + \mathcal{C}'_{w,\kappa}\sin\theta_m}{\mathcal{C}'_{\Upsilon,\kappa}\Upsilon}\varkappa_1 + \mathcal{O}\left(\varkappa_1^2\right) \tag{123}$$

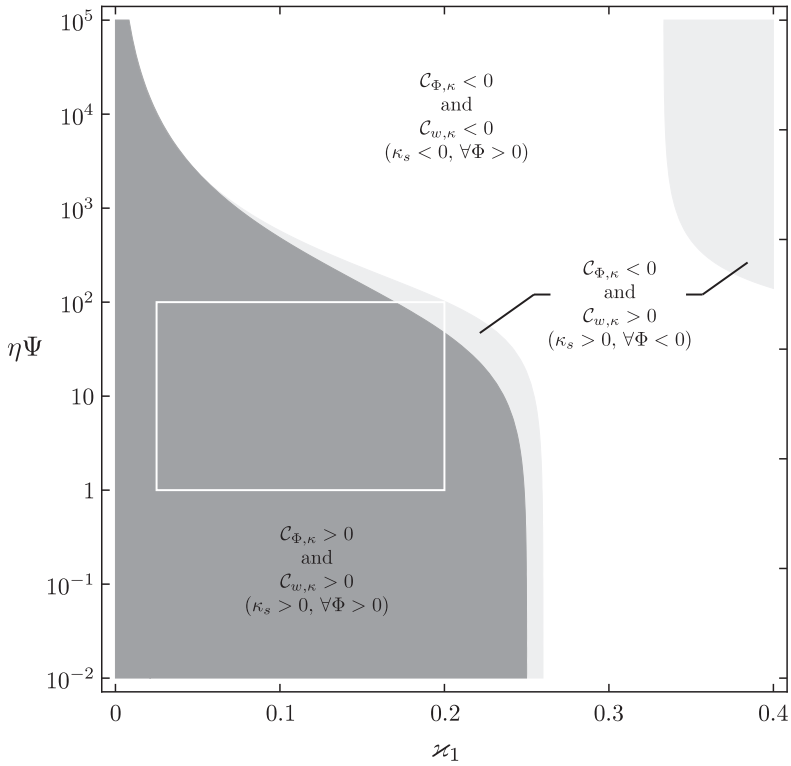

(a) The parameter $\varkappa_2$ is equal to 0.05

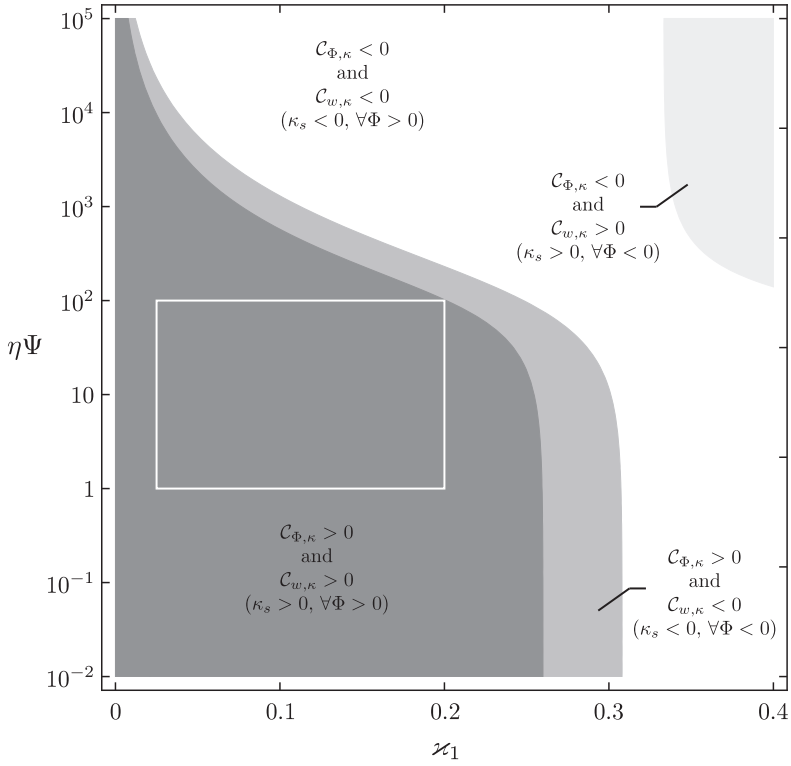

(b) The parameter $\varkappa_2$ is equal to 0.25

Figure 25: Sign of the coefficients $\mathcal{C}_{\Phi,\kappa}$ and $\mathcal{C}_{w,\kappa}$ and identification of the four regions in the space $(\varkappa_1, \eta\Psi)$ considering the upper stabilizer blocked in rotation

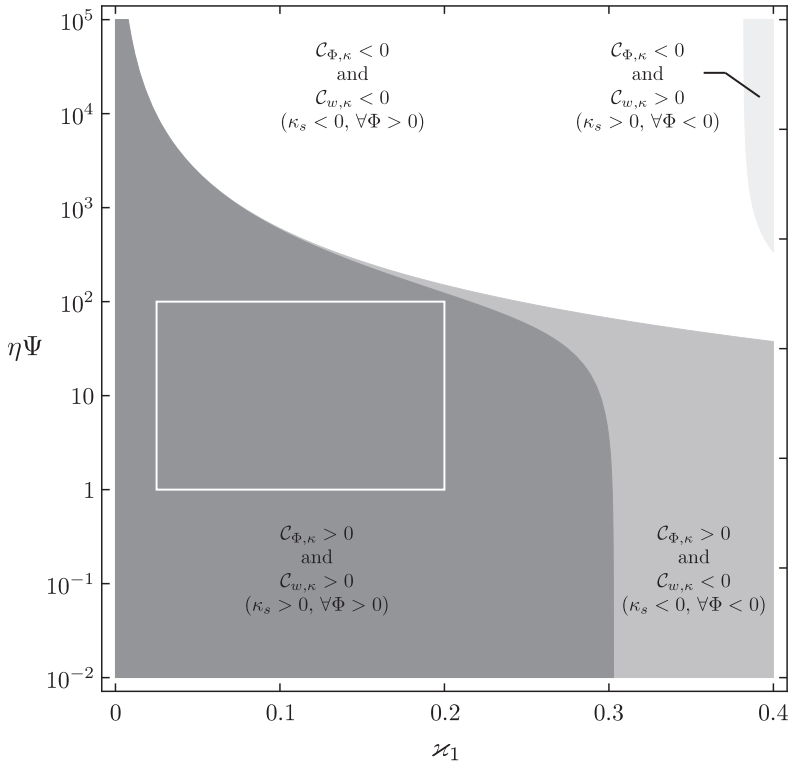

Figure 26: Sign of the coefficients $\mathcal{C}_{\Phi,\kappa}$ and $\mathcal{C}_{w,\kappa}$ and identification of the four regions in the space $(\varkappa_1, \eta\Psi)$ considering the upper stabilizer free to rotate

while the penetration inclination can be expressed as

$$\beta_b = \beta_b^0 + \frac{\mathcal{C}'_{\Phi,\beta}\Phi + \mathcal{C}'_{w,\beta}\sin\theta_m}{\mathcal{C}'_{\Upsilon,\beta}\Upsilon}\varkappa_1 + \mathcal{O}\left(\varkappa_1^2\right) \tag{124}$$

Where κ_b^0 and β_b^0 are the limit borehole curvature and penetration inclination, respectively, for $\varkappa_1$ tending to zero

$$\begin{aligned}\kappa_b^0 &= \lim_{\varkappa_1\to 0}\kappa_b \\ &= \frac{3\left(1-\varkappa_2-2\varkappa_2^2\right)\Phi + 2\sin\theta_m}{24\Upsilon(\chi\Psi+1)}\end{aligned} \tag{125}$$

$$\begin{aligned}\beta_b^0 &= \lim_{\varkappa_1\to 0}\beta_b \\ &= \frac{3\left(1-\varkappa_2-2\varkappa_2^2\right)\Phi + 2\sin\theta_m}{48\Upsilon(\chi\Psi+1)}\end{aligned} \tag{126}$$

which are independent of the lateral steering resistance. Similar expressions of the borehole curvature and the penetration inclination can be written if the second stabilizer is free to rotate. Coefficients $\mathcal{C}'_\kappa$'s and $\mathcal{C}'_\beta$'s are given in Appendix G.2 for both boundary conditions.

Like the curvature and the penetration inclination, the ratio κ_s/β_s can be written as a series expansion

$$\frac{\kappa_b}{\beta_b} = 2 + \mathcal{G}_b\varkappa_1 + \mathcal{O}\left(\varkappa_1^2\right) \tag{127}$$

$$\frac{\kappa_f}{\beta_f} = 2 + \mathcal{G}_f\varkappa_1 + \mathcal{O}\left(\varkappa_1^2\right) \tag{128}$$

where the two coefficients $\mathcal{G}_b$ and $\mathcal{G}_f$ are expressed as

$$\mathcal{G}_b = \frac{3\Phi(1-2\varkappa_2)(\chi\Psi-\varkappa_2) + 4\chi\Psi\sin\theta_m}{3\Phi\left(2\varkappa_2^2+\varkappa_2-1\right) - 2\sin\theta_m} \tag{129}$$

$$\mathcal{G}_f = -2\chi\Psi \tag{130}$$

and are generally non negligible, meaning that the terms associated with $\mathcal{F}_b$ and $\mathcal{M}_b$ in the expressions (49) and (50) of the transverse force and moment acting on the bit do not vanish. Finally, we notice that the ratio between the curvature and the penetration inclination is also constant and equal to 2 in the limiting case $\varkappa_1 \to 0$. Meaning that the ratio κ_s/β_s is not modified by the *RSS* force for this limiting behaviour.

As it has already been pointed out, as soon as the bit and the stabilizer become too close, limits of the mathematical model are met. Indeed, when $\varkappa_1$ tends to 0, the transverse force acting on the stabilizer becomes too large to consider no penetration of this one and both, the bit and the stabilizer, have to be viewed as a unique tool.

3.2.2 Coefficient $\mathcal{C}_{\Phi,\kappa}$

The coefficient $\mathcal{C}_{\Phi,\kappa}$ is the only term in the expression (115) of the borehole curvature involving the parameter $\varkappa_2$, meaning that the influence of the dimensionless length $\varkappa_2$ increases with high values of the *RSS* force. Figure 27 illustrates the magnitude of the coefficient $\mathcal{C}_{\Phi,\kappa}$ in the space $(\varkappa_1, \eta\Psi)$ for two distinct values of the parameter $\varkappa_2$ and considering the upper stabilizer blocked in rotation. The case corresponding to the second boundary condition is treated comparably in Appendix G.3.

The magnitude of coefficient $\mathcal{C}_{\Phi,\kappa}$ tends to decrease for increasing values of the parameter $\varkappa_2$. More specifically, for typical field assemblies characterized by values of $\varkappa_2$ superior to 0.15, the

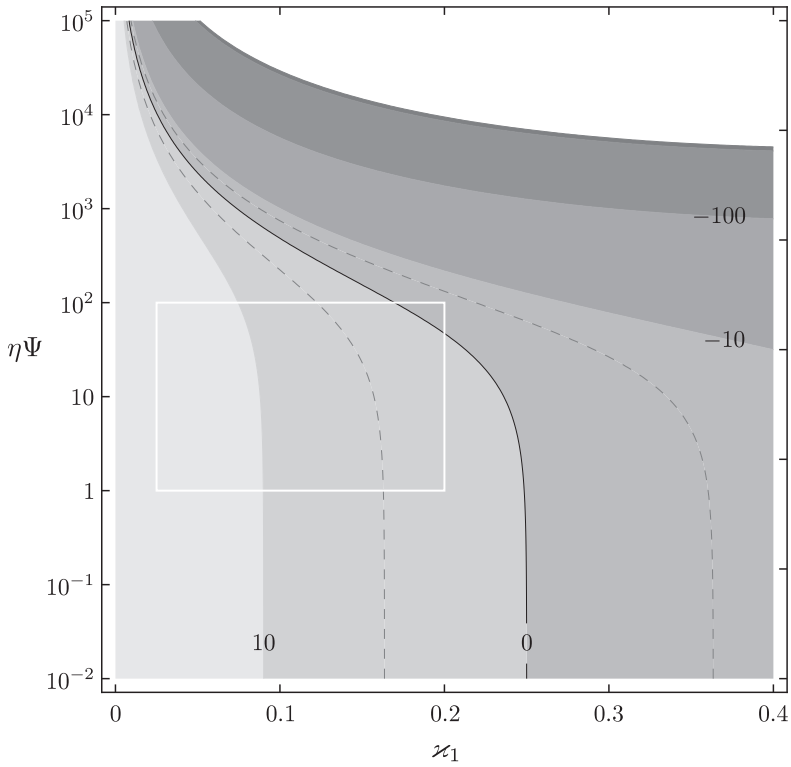

(a) The parameter $\varkappa_2$ is equal to 0.05

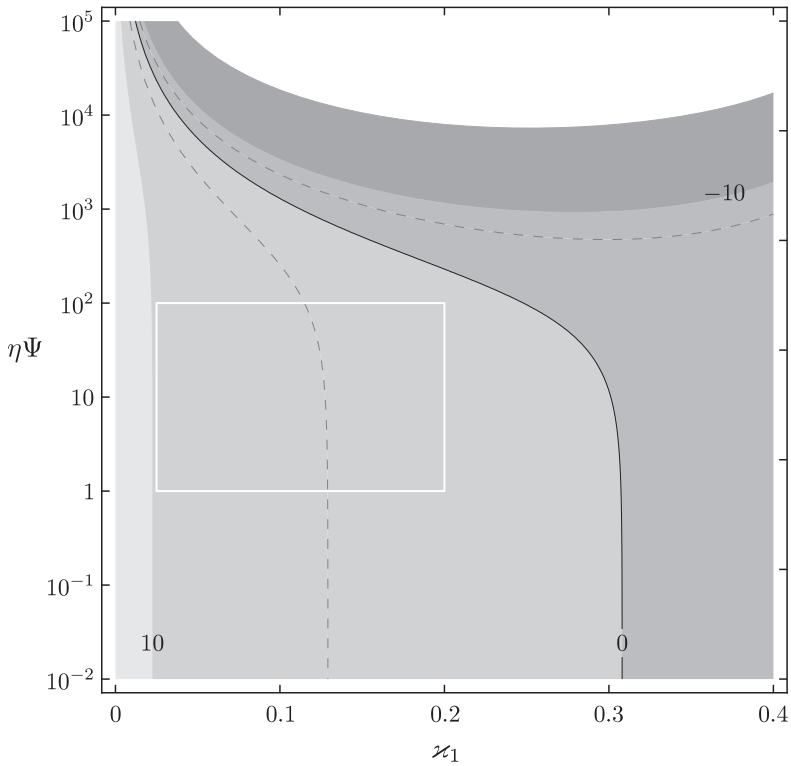

(b) The parameter $\varkappa_2$ is equal to 0.25

Figure 27: Magnitude of the coefficient $\mathcal{C}_{\Phi,\kappa}$ in the space $(\varkappa_1, \eta\Psi)$ considering the upper stabilizer blocked in rotation

coefficient $\mathcal{C}_{\Phi,\kappa}$ is always positive. Meaning that the borehole angle builds up for any positive values of the *RSS* force (Region I). If the upper stabilizer is free to rotate, typical field assemblies are always in Region I, regardless to the parameter $\varkappa_2$.

For typical field assemblies, the magnitude of the coefficient $\mathcal{C}_{\Phi,\kappa}$ ranges values from -5 to 50 for low values of $\varkappa_2$. While, for high values of this parameter, the magnitude of the coefficient run from 0 to 10.

Finally, in the limiting case corresponding to a length λ_2 null, the reactions Φ_l and Φ_r of the outer housing on the transmission shaft are transferred to the stabilizers and vanish from the transverse equilibrium (31). In this particular case, the behaviour of the *RSS* becomes similar to that of a point-the-bit system positioned between the two first stabilizer.

3.2.3 Coefficient $\mathcal{C}_{w,\kappa}$

Figure 28 pictures the magnitude of the coefficient $\mathcal{C}_{\Phi,\kappa}$ in the space $(\varkappa_1, \eta\Psi)$ considering the upper stabilizer blocked in rotation. For values of the parameters characterizing typical field assemblies, the behaviour of this coefficient is quite similar to that of the coefficient $\mathcal{C}_{\Phi,\kappa}$. Moreover, those two coefficients range similar magnitudes for comparable combination of the number $\varkappa_1$ and $\eta\Psi$, reinforcing the importance of the ratio $\Phi/\sin\theta_m$ in the determination of the drilling tendency.

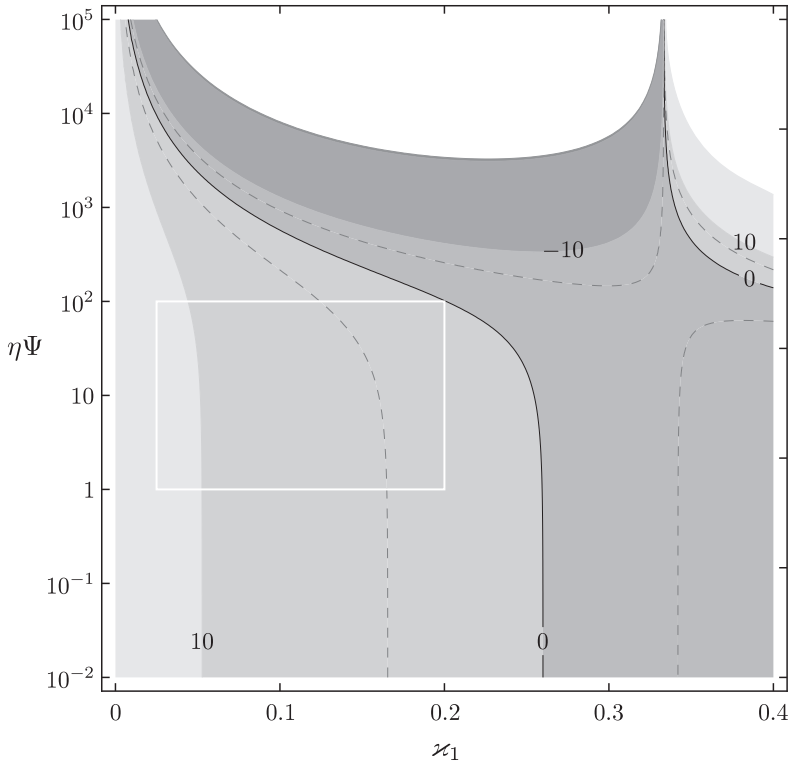

Figure 28: Magnitude of the coefficient $\mathcal{C}_{w,\kappa}$ in the space $(\varkappa_1, \eta\Psi)$ considering the upper stabilizer blocked in rotation

On the other hand, for values of the product $\eta\Psi$ superior to 10^3, the behaviour of this coefficient is highly sensitive to variation of the parameter $\varkappa_1$ and especially around 1/3 (0.382 if the upper stabilizer is free to rotate). While for low values of this product, the magnitude of $\mathcal{C}_{w,\kappa}$ has a weak reactivity to variation of $\varkappa_1$.

3.2.4 Coefficient $\mathcal{C}_{\Upsilon,\kappa}$

As it has already been pointed out, the coefficient $\mathcal{C}_{\Upsilon,\kappa}$ is always positive whatever the magnitude of the different parameters governing the solution. Moreover, unlike the coefficients $\mathcal{C}_{\Phi,\kappa}$ and $\mathcal{C}_{w,\kappa}$ appearing in the definition (115) of the borehole curvature, the coefficient $\mathcal{C}_{\Upsilon,\kappa}$ involves the angular steering resistance. Its expression (116) can advantageously be rewritten as

$$\begin{aligned}\mathcal{C}_{\Upsilon,\kappa} &= 24\left(2\eta\Psi^2\chi\varkappa_1^2 + 3\Psi\left(\eta\varkappa_1 + 2\chi(\varkappa_1+1)\right) + 6\right)\\ &= 24\left(2\left(\eta\Psi\right)^2\alpha\varkappa_1^2 + 3\left(\eta\Psi\varkappa_1 + 2\eta\Psi\alpha(\varkappa_1+1)\right) + 6\right)\end{aligned} \tag{131}$$

where α is defined as the ratio of the two steering resistances χ and η in order to highlight the influence of the bit gauge height. Indeed, considering the definition (71) of the angular steering resistance, the number α can be approximated by

$$\alpha \simeq \frac{2}{3}\left(\frac{b}{\ell}\right)^2 \tag{132}$$

and ranges from 0 to 1 for usual height of the bit gauge.

The magnitude of the coefficient $\mathcal{C}_{\Upsilon,\kappa}$ in the space $(\varkappa_1, \eta\Psi)$ is given in Figure 29 for two distinct values of the number α and considering the upper stabilizer blocked in rotation. The case corresponding to the second boundary condition is presented in Appendix G.3. For both configurations, the magnitude of the this coefficient is significantly higher than those appearing in the expression of the numerator. Indeed, for typical field assemblies, the two coefficients $\mathcal{C}_{\Phi,\kappa}$ and $\mathcal{C}_{w,\kappa}$ range both values from -5 to 50 while the coefficient $\mathcal{C}_{\Upsilon,\kappa}$, widely conditioned by the product $\eta\Psi$, can reach values up to 10^5.

Considering expression (131), we can affirm that an increase of the ratio b/ℓ involves an increase of the coefficient $\mathcal{C}_{\Upsilon,\kappa}$ magnitude, and thus, a decrease of the borehole curvature. Moreover, both extremely short ($\alpha \to 0$) and long ($\alpha \gg 1$) bit gauges do not modify significantly the behaviour of the coefficient $\mathcal{C}_{\Upsilon,\kappa}$.

Finally, the wide dependence of the coefficient $\mathcal{C}_{\Upsilon,\kappa}$ on the product $\eta\Psi$ combine to the fact that the two other coefficients $\mathcal{C}_{\Phi,\kappa}$ and $\mathcal{C}_{w,\kappa}$ fluctuate slightly for typical field assemblies suggests that the internal parameters of the *RSS* (bit-rock interactions and *BHA* parameters) act on the magnitude of the borehole curvature essentially through the coefficient $\mathcal{C}_{\Upsilon,\kappa}$.

3.2.5 Sum Up

Table 6 summarises tendencies of the coefficients $\mathcal{C}_\kappa$'s for typical field assemblies. Remembering the general expression (115) of the borehole curvature

$$\kappa_s = \frac{\mathcal{C}_{\Phi,\kappa}\Phi + \mathcal{C}_{w,\kappa}\sin\theta_m}{\mathcal{C}_{\Upsilon,\kappa}\Upsilon} \tag{133}$$

Upper arrows ($\nearrow$) denote positive correlations between the coefficient and the parameter, or in other words that the coefficient magnitude increases with the considered parameter.

We notice that high values of the product $\eta\Psi$ will generally lead to low values of the borehole curvature. Moreover, it appears that the coefficient $\mathcal{C}_{\Upsilon,\kappa}$ depends strongly on this number meaning that even weak variations of the weight-on-bit, the rock strength or the bluntness of the bit may lead to significant modification of the borehole curvature. On the other hand, an increase of the length between the bit and the first stabilizer may lead either to an increase of the borehole curvature or either to a decrease of this one depending on the other parameters.

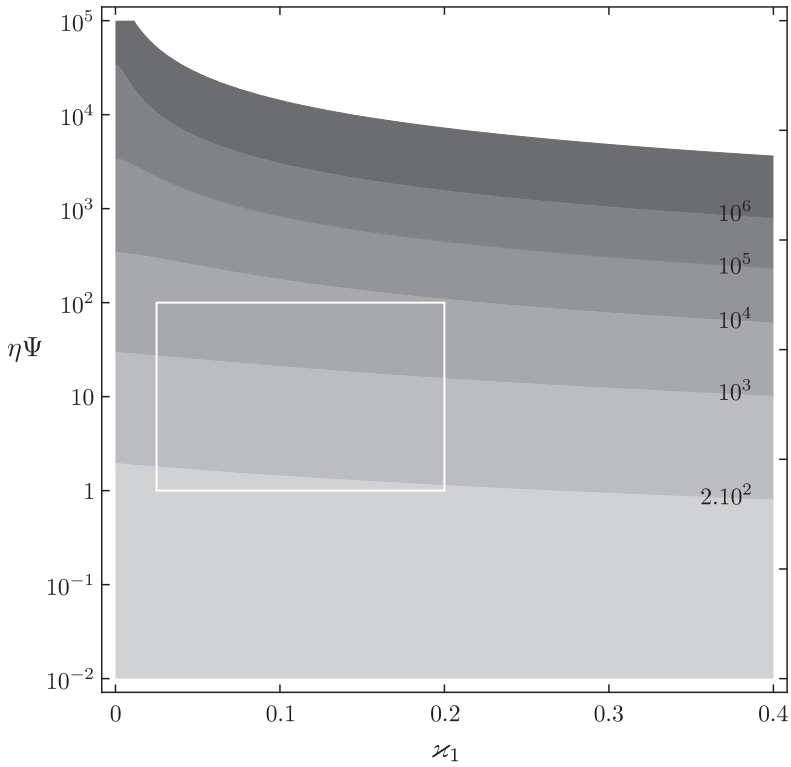

(a) The number α is equal to 0.2

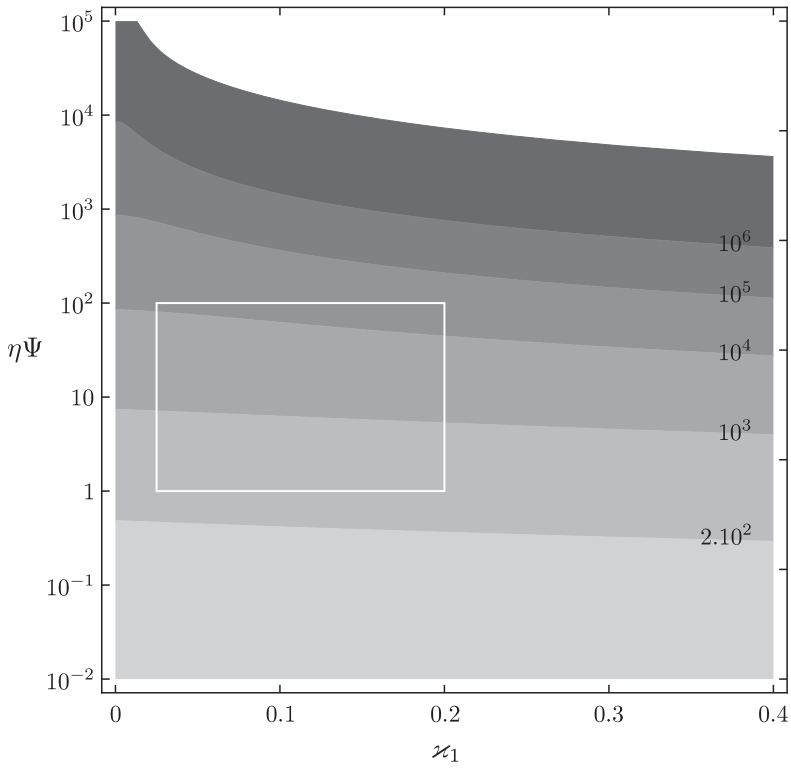

(b) The number α is equal to 0.8

Figure 29: Magnitude of the coefficient $\mathcal{C}_{\Upsilon,\kappa}$ in the space $(\varkappa_1, \eta\Psi)$ considering the upper stabilizer blocked in rotation

	$\varkappa_1$	$\varkappa_2$	$\eta\Psi$	α	Range	Range	
$\mathcal{C}_{\Phi,\kappa}$	$\searrow$	$\searrow$	$\searrow$	$-$	$-5 \sim 50$	$0 \sim 3$	$\lvert\Phi\rvert$
$\mathcal{C}_{w,\kappa}$	$\searrow$	$-$	$\searrow$	$-$	$0 \sim 15$	$0 \sim 1$	$\sin\theta_m$
$\mathcal{C}_{\Upsilon,\kappa}$	$\searrow$	$-$	$\nearrow$	$\nearrow$	$10^2 \sim 10^5$	$5 \sim 245$	Υ

Table 6: Tendencies and ranges of magnitude of the coefficients $\mathcal{C}_\kappa$'s for typical field assemblies

Part IV

Case Study

This section investigates the behaviour of a commercialised *RSS*. Dimensions and properties corresponding to this *real* assembly are introduce in the mathematical model in order to reproduce the performances predicted by the manufacturer, *i.e.,* the maximum dog leg severity.

Complete design characteristics of rotary steerable system are usually confidential and some of the dimensions involved in the mathematical model could not be defined accurately. However, gathering informations provided by main manufacturers of point-the-bit system and through personal communications, restricted ranges of those parameters have been defined to perform this study.

Others parameters, like the *WOB* and the *RSS* force, can be adjusted by the driller during drilling to control the geometry of the borehole. However, ranges of those control parameters are conditioned by assembly properties. While the hydraulic system embedded on the *RSS* defined the greatest force applied on the shaft by the actuator, the tension applied at the hook results from considerations about bit cleaning, vibrations, rate of penetration or buckling of the assembly.

The point-the-bit system investigated here is the *Wel-Guide* designed by Gyrodata and especially the 7-100 Series used to drill boreholes of diameter running from $8^{3/8}$ to $9^{7/8}$ inches. Similar studies and conclusions can be made for the 10-300 Series (borehole diameter form $12^{1/4}$ to $17^{1/2}$ inches) or for the *Geo-Pilot* developed by Halliburton.

Specifications of the assembly under considerations are summarized in Table 7. The length of the *RSS* is about 25 feet (see Figure 30) while the stiffness of the *RSS* specified by the manufacturer is given in terms of equivalent drill collar, *i.e.,* by the two diameters OD and ID. The drilling bit is a *PDC* bit with a diameter of $8^{1/2}$ inches.

Since a weak dependence of the solution on the boundary condition considered at the upper stabilizer has been highlighted, this brief analysis is only led for the solution obtained in the case of an upper stabilizer blocked in rotation. Finally, the number ξ characterizing the interactions

between the rock and the different part of the bit is chosen equal to 75.

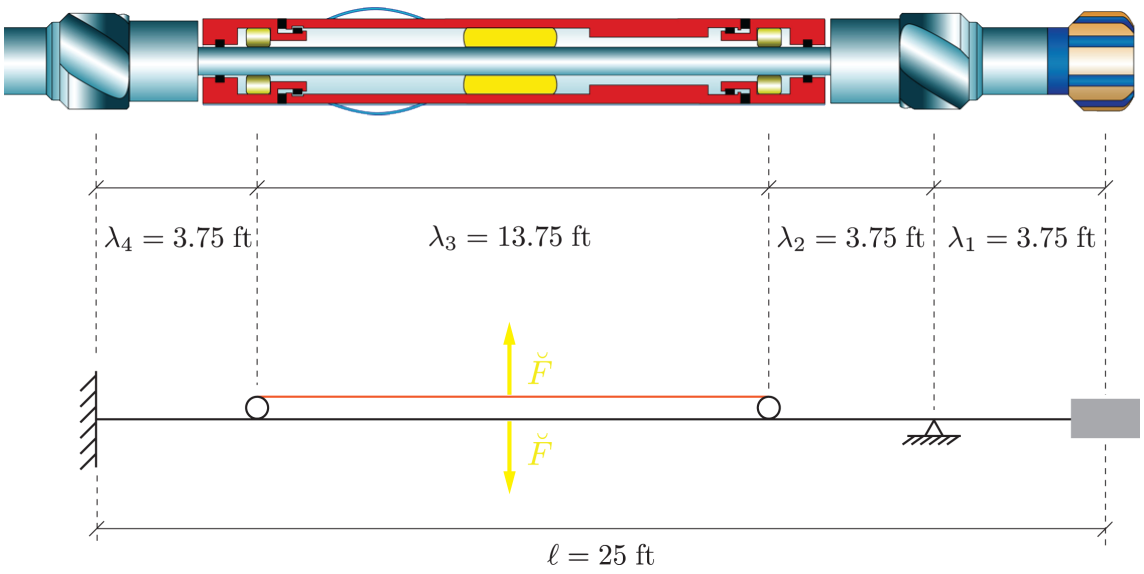

Figure 30: Dimensions of the *Well-Guide* 7-100 Series designed by Girodata and the free body diagram considered in the mathematical model

RSS	Model:	Well-Guide
	Constructor:	Gyrodata
Length		25 ft
OD		$7^{1/4}$ in
ID		$2^{1/4}$ in
$2a$		$8^{1/2}$ in
$2b$		$9^{1/2}$ in
Max. *WOB*		53,000 lb
Max. *RSS* force		7.5 kN

Table 7: Specifications of the assembly under consideration

1 Drilling Tendency

In Section 3.1 of the previous part, we conclude that the knowledge of the force orientation is not completely sufficient to establish the drilling tendency of an assembly. Considering now the particular configuration defined in Table 7, the influence of the ratio between the *RSS* force and the gravity (through the *BHA* mean inclination) can be highlighted. Figure 31 establishes the drilling tendency in the space $(\breve{F}, \theta_m)$ for various length between the bit and the first stabilizer, two distinct values of the length λ_2 (see Figure 16) are considered.

For mean inclinations closed to the horizontal, the borehole curvature is mainly positive meaning that the borehole angles builds up regardless the magnitude of the *RSS* force. This tendency is increased by a low value of the length λ_2 and by a long distance between the bit and the first

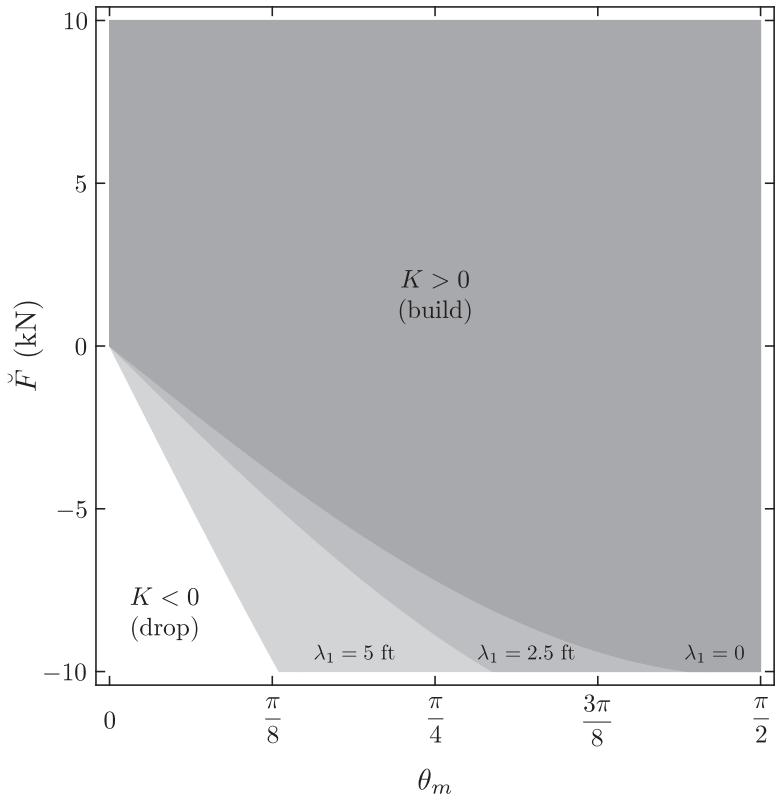

(a) The length λ_2 is equal to 1.25 ft ($\varkappa_2 = 0.05$)

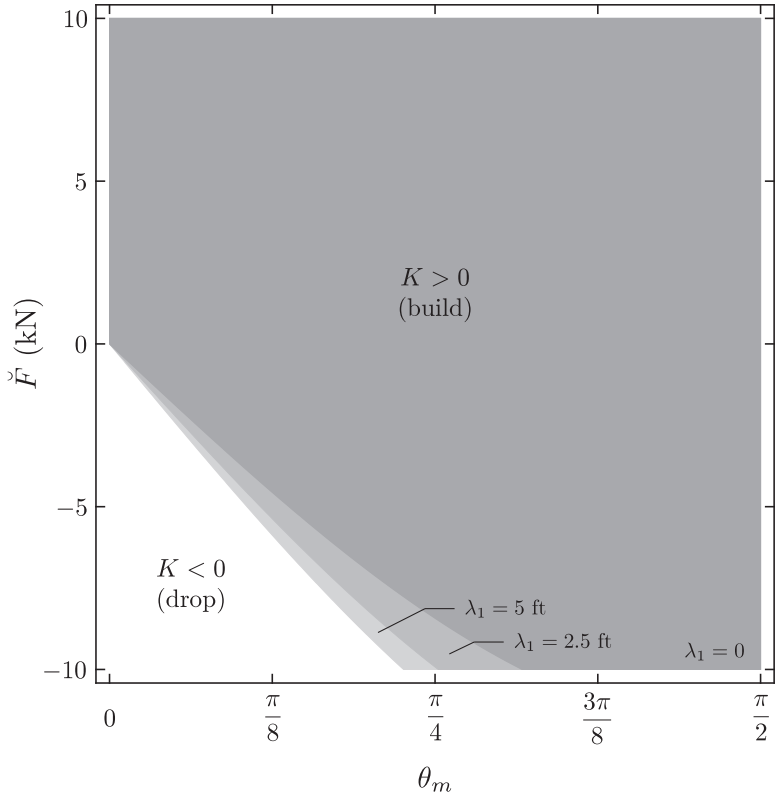

(b) The length λ_2 is equal to 3.75 ft ($\varkappa_2 = 0.15$)

Figure 31: Drilling tendency of the assembly under consideration for a *WOB* of 17.5 ton and considering the upper stabilizer blocked in rotation

stabilizer. Finally, results of simulations highlight a weak influence of the weight-on-bit and the bit height gauge on the drilling tendency.

2 Dog Leg Severity

The hook load and the *RSS* force are the only parameters that can be tuned during drilling. These two control parameters are then, from a driller point of view, of prime importance. Figure 32 relates the dog leg severity of the assembly under consideration to the force $\breve{F}$ exerted by the actuator of the *RSS* and to the *WOB* considering a mean inclination $\theta_m = \pi/8$ radian.

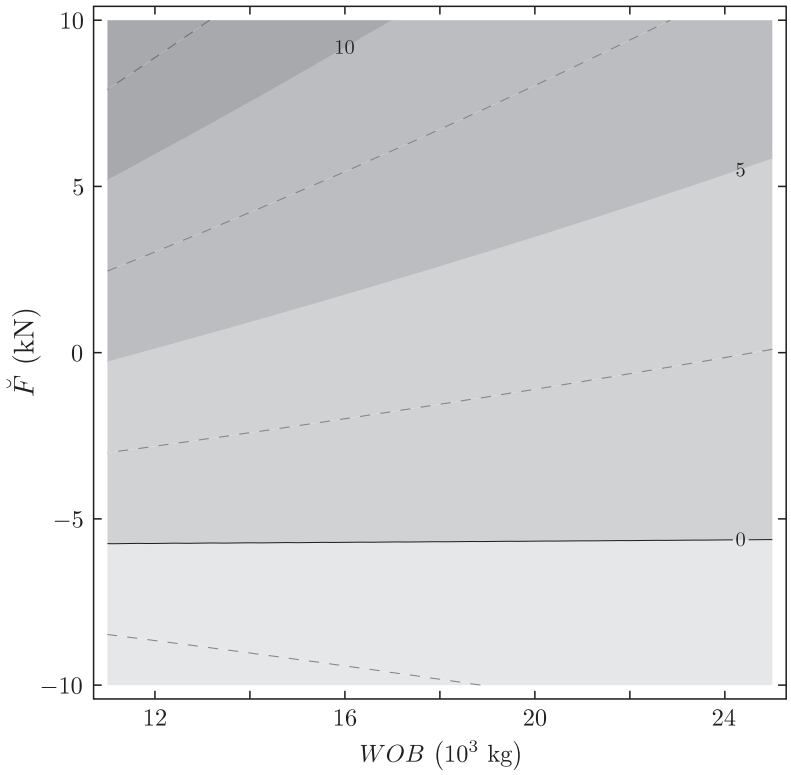

Figure 32: Dog leg severity in degrees per 100 feet for the assembly under consideration ($\lambda_1 = \lambda_2 = 3.75$ ft)

Usually, the weight applied on bits used to drill boreholes of diameter running from $8^{3/8}$ to $9^{7/8}$ inches ranges from 30 to 40 thousands pounds, *i.e.,* from 13.5 to 18 ton. For this window of the *WOB*, the mathematical model predicts dog leg severity around 7.5°/100 ft while the maximum dog leg severity predicts by Gyrodata for its *Well-Guide* 7-100 Series is about 7°/100 ft depending on drilling conditions, such as the formation characteristics, the bit properties or the *WOB*.

According to Gyrodata, a wide range of bit can be used with this *RSS* since the bit is supposed to drill only on its front face. Meaning that no side cutting action is required. However, the mathematical model highlights a relatively large dependence of the curvature (and thus of the dog leg severity) on the bit height gauge. Figure 33 illustrates the impact of this parameter, all other parameters being equal.

Figure 33(a) reveals that, for the same window of the *WOB*, halve the height of the bit gauge results in a substantial increase of the dog leg severity (approximately doubled). On the other side, double the height bit gauge decrease the magnitude of the borehole curvature, see Figure 33(b).

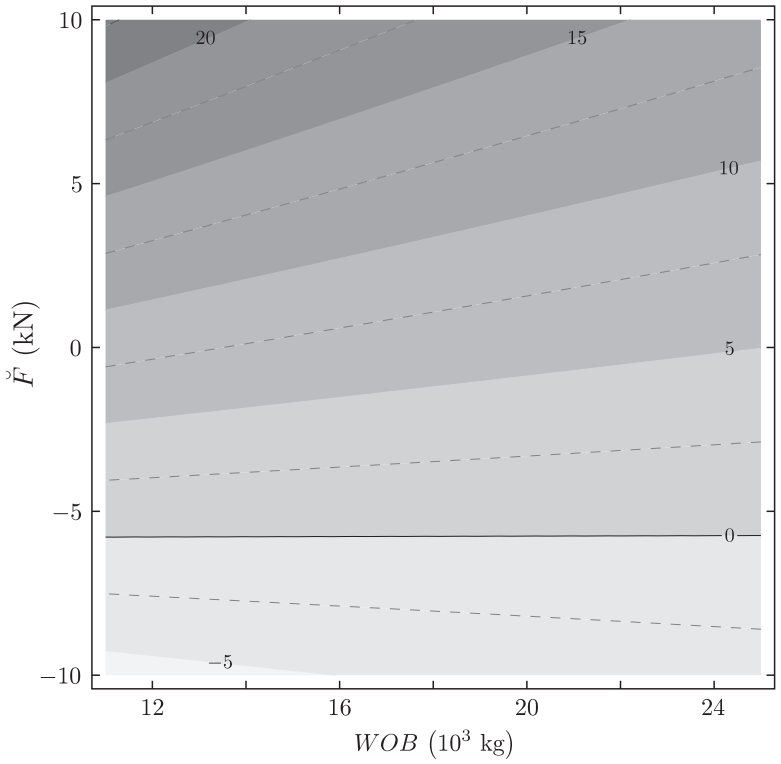

(a) The bit height gauge is equal to 4.25 in

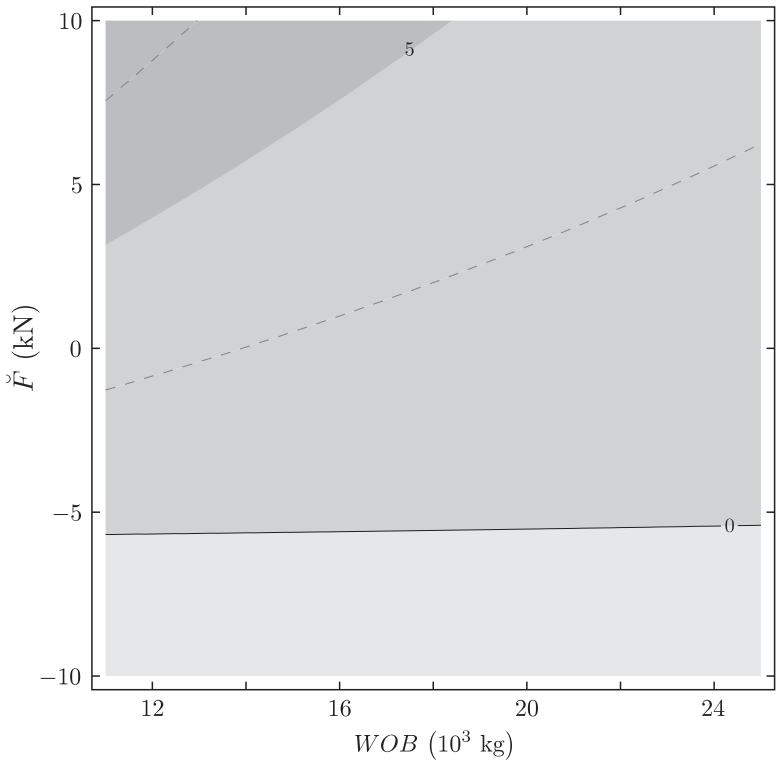

(b) The bit height gauge is equal to 17 in

Figure 33: Dog leg severity in degrees per 100 feet ($\lambda_1 = \lambda_2 = 3.75$ ft and $\theta_m = \pi/8$)

Those results are naturally in accordance with the conclusions issued in the parametric analysis presented in Part III. Indeed an increase of the bit gauge height results in an increase of both angular and lateral steering resistances and thus in the difficulty to steer the bit.

This disagreement in the behaviour of the assembly equipped with extremely short or long bit gauge is probably due to the modelling of the bit-rock interactions. Indeed, in this model, the bit is substituted by a point at the extremity of the *BHA*. Moreover the over-gauge effects between the bit and the borehole on the bit-rock interface laws is neglected.

3 Bit Tilt and Over-gauge

The impact of the bit gauge height is depicted in Figure 34 which presents the evolution of the bit tilt and of the over-gauge factor in function of this parameter and for different values of the *RSS* force.

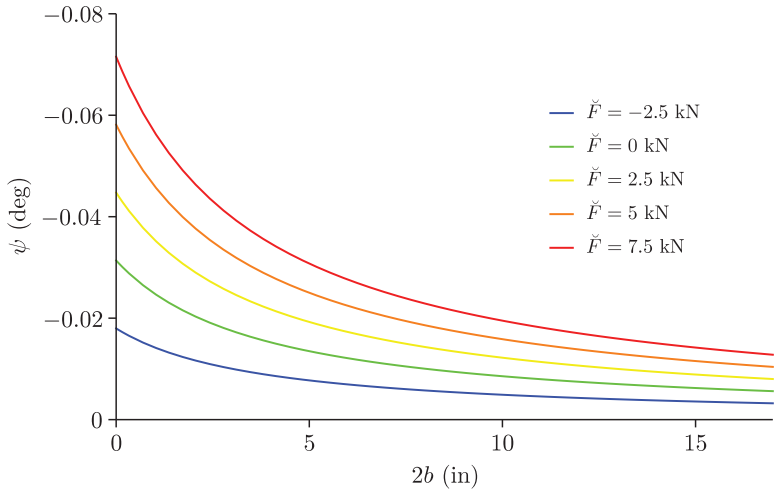

(a) Bit tilt

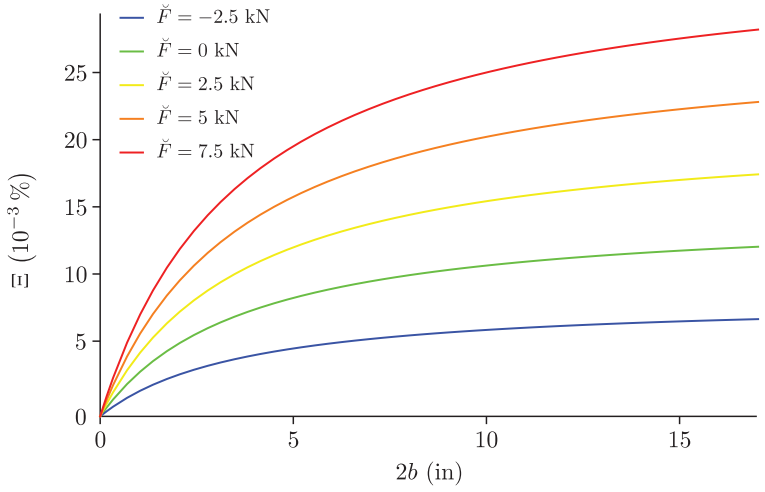

(b) Over-gauge factor

Figure 34: Influence of the *RSS* force for the assembly under consideration ($\lambda_1 = \lambda_2 = 3.75$ ft, $WOB = 17\,500$ kg and $\theta_m = \pi/8$)

First we notice that the assumption of small magnitude of the bit tilt required to write relation (51) is a posteriori fulfilled and that lateral penetration can thus be neglected compared to the axial penetration ($d \simeq d_1$).

As expected, bits with extended gauge are characterised by a greater angular restraint leading to a lower bit tilt. It appears also that the dependence of the bit tilt on the bit height gauge is mainly significant for low values of b. Moreover, for a given bit (b is constant) and constant rock properties (ξ is constant), the lateral force acting on the bit is proportional to the bit tilt, see equation (52). Meaning that the lateral force acting on the bit is proportional to the force developed by the *RSS*.

Considering now Figure 34(b), it appears that the over-gauge factor defined by

$$\Xi = \frac{2}{\pi}\nu|\psi| \tag{134}$$

reaches extremely small values, of the order of $10^{-3}\,\%$, while typical field over-gauge ranges values from 5 to 10 %. This observation highlights the significance of the over-gauge generated by vibrations (whirl) which are neglected in this model. Those results do not challenge the validity of the model which focus on the equilibrium points of the dynamical system while vibrations are non stationary phenomenon. However, they may justify complementary investigations in order to determine if directional response of the assembly is not affected by this over-gauge.

Part V

Conclusion

In this work, a mathematical model of a drilling assembly equipped with a point-the-bit system has been developed. This model of the near-bit region is based on the theory established by Detournay (2007) and is composed of three interacting components: *(i)* the equations governing the geometrical evolution of the borehole, *(ii)* the laws that link the kinematical bit-rock penetration variables to the forces on the bit, and *(iii)* the relationships between the forces on the bit and the loads on the drillstring.

The problem is reduced to the context of planar borehole trajectories and to the segment of the *BHA* between the bit and the second stabilizer. The outputs of the model are the borehole curvature and the bit tilt corresponding to the equilibrium points of the evolving system, *i.e.,* to segments of borehole characterized by a constant curvature and by a constant diameter.

It has been shown that the general solution of the problem can be written as the sum of two terms: the curvature (bit tilt) due to the gravity field and the curvature (bit tilt) due to the application of the *RSS* force on the shaft. Meaning that the knowledge of the force orientation is not sufficient to establish the drilling tendency of an assembly, which results from the balance between the gravity effects and the *RSS* load. Moreover some counter intuitive behaviour may appear, *e.g.*, the application of an upward force ($\breve{F} < 0$) may lead to a positive curvature.

The parametric analysis highlighted the weak dependence of the solution on the boundary condition considered at the upper stabilizer and suggests that taking into account the only two first stabilisers is probably sufficient to predict the borehole curvature.

The distance between the bit and the first stabilizer is of prime importance in this model. Both bit tilt and borehole curvature increase when the ratio λ_1/ℓ decreases. Moreover, low values of this ratio result in an amplification of the impact of the other parameters.

While the drilling tendency of an assembly is independent of the angular steering resistance χ, it appears that both angular and lateral steering resistances decrease the magnitude of the borehole

curvature. On the opposite, flexible assembly and low values of the weight-on-bit generate sinuous boreholes.

Through the study of a commercialised point-the-bit system, we showed that the mathematical model is able to reproduce the tendencies and the order of magnitudes for the quantities typically met on the field.

Issues and Possible Contributions

Besides the extension form plane trajectories to the complete 3D problem considering the whole drillstring and the contacts that may occur between the borehole and the drillstring, the mathematical model can be improved in different ways.

The main developments should concern the interaction laws. Since lateral forces acting on the bit and the first stabilizer reach similar order of magnitude, stabilizer/rock interaction laws should be added to the model in order to characterise the stabilizer penetration into the rock. Also, over-gauge effects, which alter the contact conditions between the borehole and the bit, should be considered with attention. This distinction between the bit and the borehole diameters may lead to non-linear bit/rock interaction laws complicating the model. A future step concerns an extension of the bit-rock interaction law to account for formation anisotropy and non-homogeneity.

Finally, the modelling of the evolving problem is a prerequisite step towards a better understanding of directional drilling and the prediction of borehole trajectories characterised by change in curvature (either sudden or progressive).

References

Well-Guide RSS: Rotary Steerable System, 2009.

M. Birades. ORPHEE 3D: Static and Dynamic Tridimensional BHA Computer Models. In *61st Annual Technical Conference and Exhibition of the Society of Petroleum Engineers*, number SPE 15466, page 12, New Orleans, LA, U.S.A., October 1986. Society of Petroleum Engineers,Richardson, TX; Elf Aquitaine.

M. Birades and R. Fenoul. ORPHEE 2D: A Microcomputer Program for Prediction of Bottomhole Assembly Trajectory. In *Symposlum on Petroleum Industry Application of Microcomputers of the Society of Petroleum Engineers*, number SPE 15285, pages 31–38, SilverCreek, CO, June 1986.

M. Birades and R. Fenoul. A Microcomputer Program for Prediction of Bottomhole Assembly Trajectory. *SPE Drilling Engineering*, 3(SPE 15285):167–172, June 1988. doi: 10.2118/15285-PA.

R. Boualleg, H. Sellami, S. Menand, and C. Simon. Effect of Formations Anisotropy on Directional Tendencies of Drilling Systems. In *IADC/SPE Drilling Conference*, number IADC/SPE 98865, pages 1–10, Miami, Florida, U.S.A., February 2006. doi: 10.2118/98865-MS.

BP. BP Statistical Review of World Energy, June 2010.

J. F. Brett, J. A. Gray, R. K. Bell, and M. E. Dunbar. A Method of Modeling the Directional Behavior of Bottomhole Assemblies Including Those With Bent Subs and Downhole Motors. In *IADC/SPE Drilling Conference*, number IADC/SPE 14767, pages 365–376, Dallas, Texas, U.S.A., February 1986. doi: 10.2118/14767-MS.

E. Detournay. Mathematical Model of the Near-Bit Region of an Advancing Drilling System. Technical Report SLB-BM-07-1, Schlumberger, April 2007.

G. Heisig, J. Oppelt, M. Neubert, and F. Donati. Closed-Loop Guided Directional Drilling Fundamentals, Concepts and Simulations, 1996.

H.-S. Ho. General Formulation of Drillstring Under Large Deformation and Its Use in BHA Analysis. In *61st Annual Technical Conference and Exhibition of the Society of Petroleum Engineers*, number SPE 15562, pages 1–12, New Orleans, LA, U.S.A., October 1986. doi: 10.2118/15562-MS.

H.-S. Ho. Prediction of Drilling Trajectory in Directional Wells Via a New Rock-Bit Interaction Model. In *62nd Annual Technology Conference and Exhibition of the Society of Petroleum Engineers*, number SPE 16658, pages 83–95, Dallas, Texas, U.S.A., September 1987. doi: 10.2118/16658-MS.

H.-S. Ho. Method of Predicting and Controlling the Drilling Trajectory in Directional Wells, February 1989.

H.-S. Ho. Method and system of trajectory prediction and control using PDC bits, October 1995.

International Energy Agency. Analysis of the Impact of High Oil Prices on the Global Economy. May 2004.

A. Lubinski and H. B. Woods. Factors Affecting the Angle of Inclination and Dog-Legging in Rotary Bore Holes. In *Mid-Continent District*, pages 222–250, Tulsa, U.S.A., 1953. American Petroleum Institute.

Z. Maouche. *Contribution à l'Amélioration de la Prédiction en Inclinaison des Systèmes de Forage Rotary Couplage Garniture-Outil de Forage*. Docteur de l'école nationale supérieure des mines de paris, École des Mines de Paris, Paris, France, December 1999.

S. Menand, H. Sellami, C. Simon, A. Besson, and N. da Silva. How the Bit Profile and Gages Affect the Well Trajectory. In *IADC/SPE Drilling Conference*, number SPE 74459, pages 1–13, Dallas, Texas, U.S.A., February 2002. doi: 10.2118/74459-MS.

S. Menand, H. Sellami, and C. Simon. Classification of PDC Bits According to Their Steerability. In *SPE/IADC Drilling Conference*, number SPE/IADC 79795, pages 1–13, Amsterdam, Netherlands, February 2003. doi: 10.2118/79795-MS.

S. Menand, H. Sellami, M. Tijani, O. Stab, and C. Simon. Advancements in 3D Drillstring Mechanics: From the Bit to the Topdrive. In *IADC/SPE Drilling Conference*, number IADC/SPE 98965, pages 1–12, Miami, Florida, U.S.A., February 2006. doi: 10.2118/98965-MS.

K. Millheim. The Effect of Hole Curvature on the Trajectory of a Borehole. In *52nd Annual Fall Technical Conference and Exhibition of the Society of Petroleum Engineers of AIME*, number SPE 6779, pages 1–8, Denver, Colorado, U.S.A., October 1977. doi: 10.2118/6779-MS.

K. Millheim, S. Jordan, and C. J. Ritter. Bottom-Hole Assembly Analysis Using Finite-Element Method. *Journal of Petroleum Technology*, 30(SPE 6057):265–274, February 1978. ISSN 0149-2136. doi: 10.2118/6057-PA.

K. K. Millheim and M. C. Apostal. The Effect of Bottomhole Assembly Dynamics on the Trajectory of a Bit. *Journal of Petroleum Technology*, 33(SPE 9222):2323–2338, December 1981. ISSN 0149-2136. doi: 10.2118/9222-PA.

K. K. Millheim and T. M. Warren. Side Cutting Characteristics of Rock Bits and Stabilizers While Drilling. In *53rd Annual Fall Technical Conference and Exhibition of the Society of Petroleum Engineers of AIME*, number SPE 7518, pages 1–8, Houston, Texas, U.S.A., October 1978. doi: 10.2118/7518-MS.

C. E. Murphey and J. B. Cheatham. Hole Deviation and Drill String Behavior. *Society of Petroleum Engineers Journal*, 6(SPE 1259):44–54, March 1965. doi: 10.2118/1259-PA.

M. Neubert. *Richtungsregelung beim Tiefbohren*. 1997. ISBN 3-920395-31-X.

M. Neubert and G. Heisig. Mathematical Description of the Directional Drilling Process and Simulation of Directional Control Algorithm. *Zeitschrift für angewandte Mathematik und Mechanik*, 76:361–362, 1996.

M. Neubert, G. Heisig, I. Forstner, and F. Mounzer. Verification of an Advanced Analysis Model With Downhole Bending Moment Measurements. In *Asia Pacific Oil and Gas Conference and Exhibition*, number SPE 93864, pages 1–10, Jakarta, Indonesia, April 2005. doi: 10.2118/93864-MS.

J. A. Norris, M. W. Dykstra, C. C. Beuershausen, and R. W. Fincher. Development and Successful Application of Unique Steerable PDC Bits. In *IADC/SPE Drilling Conference*, number IADC/SPE 39308, pages 153–166, Texas, U.S.A., March 1998. doi: 10.2118/39308-MS.

P. Pastusek, V. Brackin, and P. Lutes. A Fundamental Model for Prediction of Hole Curvature and Build Rates With Steerable Bottomhole Assemblies. In *SPE Annual Technical Conference and Exhibition*, number SPE 95546, pages 1–7, Dallas, Texas, U.S.A., October 2005. doi: 10.2118/95546-MS.

L. Perneder. Analytical and Experimental Investigations for Bit-Rock Interaction Laws in Directional Drilling. Master of science, Faculty of Civil Engineering of the University of Liège, Liege, Belgium, August 2008a.

L. Perneder. Simplified beam model of the bha and bit/bha interactions. Quarterly report, CSIRO, Perth, Australia, September-November 2008b.

T. Richard. Determination of rock strength from cutting tests. Master of science, University of Minnesota, Minneapolis, Minnesota, U.S.A., December 1999.

J. H. B. Sampaio. *Drilling Engineering*. Curtin University of Technology, Department of Petroleum Engineering, February 2008.

Schlumberger. Schlumberger Oilfield Glossary. URL http://www.glossary.oilfield.slb.com/.

C. Simon. *Modelisation du Comportement Directionnel des Outils de Forage Monoblocs en Formations Anisotropes*. Docteur de l'ecole nationale superieure des mines de paris, Ecole Nationale Superieure des Mines de Paris, April 1996.

Society of Petroleum Engineers, American Association of Petroleum Geologists, World Petroleum Council, and Society of Petroleum Evaluation Engineers. Petroleum resources management system. March 2007.

J. Sugiura. Optimal BHA Design for Steerability and Stability with Configurable Rotary-Steerable System. In *SPE Asia Pacific Oil and Gas Conference and Exhibition*, number SPE 114599, pages 126–138, Perth, Australia, October 2008. doi: 10.2118/114599-MS.

George E. Totten. A Timeline of Highlights from the Histories of ASTM Committee DO2 and the Petroleum Inudustry, June 2004. URL http://www.astm.org/COMMIT/D02/to1899_index.html.

T. M. Warren. Penetration-Rate Performance of Roller-Cone Bits. *SPE Drilling Engineering*, 2 (SPE 13259):9–18, March 1987. doi: 10.2118/13259-PA.

Wikipedia. The Free Encyclopedia, 2010. URL http://en.wikipedia.org.

Part VI

Appendix

A Cutter/Rock Interactions

Richard (1999) showed that the action of a rectangular cutter of width w which is steadily removing rock over a constant depth of cut d (see Figure A.1) can be dissociate in two independent processes:

- a pure cutting process taking place ahead of the cutting face;
- a frictional contact process mobilized along the interface between the wearflat and the rock.

The force $\boldsymbol{F}$ acting on the cutter can thus be dissociate in two components $\boldsymbol{F}_c$ and $\boldsymbol{F}_f$, acting on the cutting face and on the wearflat, respectively. Moreover, single cutter experiments in the ductile mode, *i.e.,* without chipping, indicate that the relationship between the forces applied on the cutter and the depth of cut d is bilinear.

Two regimes can thus be identified, according to Figure A.1(b) they will be denoted as I and! II. The first regime is characterized by a progressive increase of the contact forces with the depth of cut while, in the second regime, the contact forces are fully mobilized.

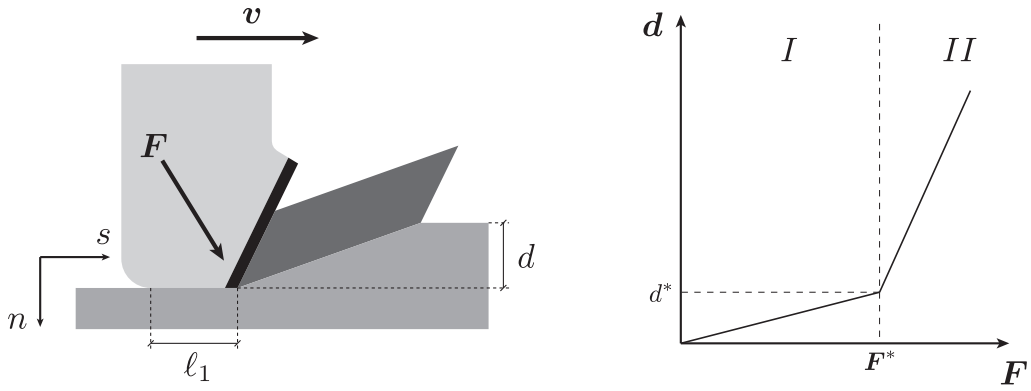

(a) Force acting on a rectangular cutter removing over a constant depth of cut d

(b) Relationship $(\boldsymbol{F} - \boldsymbol{d})$, identification of the two regimes I and II

Figure A.1: Cutter/rock interaction (Richard, 1999)

Defining by n the direction normal to the velocity of the cutter and by s the direction parallel to the velocity of the cutter, the two forces $\boldsymbol{F}_c$ and $\boldsymbol{F}_f$ can be uniquely decomposed in their n and s components. In regime I, the components of the force $\boldsymbol{F}$ are

$$F_n^I = \left(\varrho\frac{\sigma}{\varepsilon} + \zeta\right)\varepsilon w d = \zeta' \varepsilon w d \tag{A.1}$$

$$F_s^I = \left(\mu\varrho\frac{\sigma}{\varepsilon} + 1\right)\varepsilon w d = \zeta'' \varepsilon w d \tag{A.2}$$

and in regime II the same relations become

$$F_n^{II} = \sigma w \ell + \zeta \varepsilon w d \tag{A.3}$$

$$F_s^{II} = \mu\sigma w \ell + \varepsilon w d \tag{A.4}$$

where ϱ represents the rate of change of the contact length with d, σ is the contact strength (*i.e.,* the maximum contact pressure that can be transmitted at the wearflat/rock interface), ε is the intrinsic specific energy of the rock (*i.e.,* the energy required to remove a unit volume of rock in the absence of frictional contact), μ is a coefficient of friction and the ζ is a number of order $\mathcal{O}(0.1 \sim 1)$.

B The Force Method

As it has already been explained, the force method consists in making the beam isostatic by releasing appropriate boundary conditions and externalize those by forces. Amplitudes of those external forces are determined by imposing consistent deformations according to the released boundary conditions through a system of equations. For the problem under consideration, the boundary condition at the first stabilizer is realised and externalised by the force F_R. The amplitude of this reaction is computed so that the deflection in $\xi = 1 - \varkappa_1$ is null.

Deflections of the beam have multiple origins. If we denote[8] by

- u_{Φ_l} the transverse displacement at the stabilizer, *i.e.,* in $\xi = 1 - \varkappa_1$, due to the concentrated load Φ_l acting in $\xi = \varkappa_4$,

$$u_{\Phi_l} = -\frac{\Phi \varkappa_1^2 \varkappa_4^2 \left(2\left(\varkappa_4 - 1\right)\varkappa_4 + \varkappa_2\left(2\varkappa_4 - 3\right) + \varkappa_3\left(2\varkappa_4 - 3\right)\right)\left(\varkappa_3 + \varkappa_4 - \Lambda\right)}{6\varkappa_3} \tag{B.1}$$

- u_Φ the transverse displacement at the stabilizer, *i.e.,* $\xi = 1 - \varkappa_1$, due to the concentrated load Φ acting in $\xi = \Lambda$,

$$u_\Phi = -\frac{\Phi}{6}\Lambda^2 \varkappa_1^2 \left((2\Lambda - 3)\varkappa_1 - 3\Lambda + 3\right) \tag{B.2}$$

- u_{Φ_r} the transverse displacement at the stabilizer, *i.e.,* $\xi = 1 - \varkappa_1$, due to the concentrated load Φ_r acting in $\xi = \varkappa_4 + \varkappa_3$,

$$u_{\Phi_r} = -\frac{\Phi \varkappa_1^2 \left(2\varkappa_1^2 + 2\left(\varkappa_2 - 1\right)\varkappa_1 - 3\varkappa_2\right)\left(\varkappa_3 + \varkappa_4\right)^2 \left(\Lambda - \varkappa_4\right)}{6\varkappa_3} \tag{B.3}$$

- u_w the transverse displacement at the stabilizer, *i.e.,* $\xi = 1 - \varkappa_1$, due to the distributed load $\sin\theta_m$ and the boundary conditions at the bit and at the second stabilizer,

$$\begin{aligned} u_w \quad = \quad & -\frac{\varkappa_1\left(\varkappa_1 - 1\right)}{24}\left(\varkappa_1\left(24\Upsilon\left(\hat{\Theta} + \bar{\bar{\Theta}} + \psi - 2\theta_m\right) - \sin\theta_m\right)\right. \\ & \left. -24\left(\hat{\Theta} + \psi - \theta_m\right)\Upsilon + \varkappa_1^2 \sin\theta_m\right) \end{aligned} \tag{B.4}$$

- u_k the transverse displacement at the stabilizer, *i.e.,* $\xi = 1 - \varkappa_1$, due to the kink angle θ_k

$$u_k = 2\theta_k \Upsilon \left(\varkappa_2^2 + \left(2\varkappa_3 + 2\varkappa_4 - 1\right)\varkappa_2 + \varkappa_3^2 + \left(\varkappa_4 - 1\right)\varkappa_4 + \varkappa_3\left(2\varkappa_4 - 1\right)\right)^2 \tag{B.5}$$

- u_{F_R} the transverse displacement at the stabilizer, *i.e.,* $\xi = 1 - \varkappa_1$, due to the concentrated load F_R acting in $\xi = 1 - \varkappa_1$,

$$u_R = -\frac{F_R}{3}\left(\varkappa_2^2 + \left(2\varkappa_3 + 2\varkappa_4 - 1\right)\varkappa_2 + \varkappa_3^2 + \left(\varkappa_4 - 1\right)\varkappa_4 + \varkappa_3\left(2\varkappa_4 - 1\right)\right)^3 \tag{B.6}$$

we can determine the force F_R so that the transverse displacement at the stabilizer is null:

$$u_{\Phi_l} + u_\Phi + u_{\Phi_r} + u_w + u_k + u_{F_R} = 0 \tag{B.7}$$

This linear equation in F_R, which involves the superposition principle, can only be written under the assumptions of small rotations and small displacements by reference to an initial configuration.

[8] Displacements are only given for the case of a beam fixed at both end. The case of the beam fixed at one end and simply supported at the other one is treated equally.

Finally we obtain an expression of the reaction F_R, that is easier expressed as a sum of five terms like it is for the generalized efforts acting on the bit:

$$F_R = \mathcal{R}_b \Upsilon \left(\hat{\Theta} + \psi - \theta_m \right) + \mathcal{R}_s \Upsilon \left(\bar{\bar{\Theta}} - \theta_m \right) + \mathcal{R}_k \Upsilon \theta_k + \mathcal{R}_w \sin \theta_m + \mathcal{R}_\Phi \Phi \tag{B.8}$$

The $\mathcal{R}$'s coefficients are given in table B.1.

	Blocked rotation	Free rotation
$\mathcal{R}_b$	$-\dfrac{3}{\varkappa_1^2(1-\varkappa_1)}$	$-\dfrac{6\,(\varkappa_1-2)}{\varkappa_1^2\left(\varkappa_1^2-5\varkappa_1+4\right)}$
$\mathcal{R}_s$	$-\dfrac{3}{\varkappa_1(1-\varkappa_1)^2}$	0
$\mathcal{R}_k$	$\dfrac{6}{\varkappa_1(1-\varkappa_1)}$	$\dfrac{6\,(\varkappa_1-3)}{\varkappa_1\left(\varkappa_1^2-5\varkappa_1+4\right)}$
$\mathcal{R}_w$	$\dfrac{1}{8\varkappa_1(1-\varkappa_1)}$	$\dfrac{3-2\varkappa_1}{4\varkappa_1\left(\varkappa_1^2-5\varkappa_1+4\right)}$

$\mathcal{R}_\Phi$ for the blocked rotation
$-\dfrac{(\Lambda-\varkappa_4)\,(\Lambda-\varkappa_3-\varkappa_4)\left(2\varkappa_3\,(\Lambda+3\varkappa_4-1)+(2\Lambda-1)\varkappa_4+\varkappa_2\,(2\Lambda+2\varkappa_3+4\varkappa_4-3)+\Lambda+2\varkappa_3^2+4\varkappa_4^2\right)}{2\,(1-\varkappa_1)^3\,\varkappa_1}$

$\mathcal{R}_\Phi$ for the free rotation
$\dfrac{(3-\varkappa_1)\,(\Lambda-\varkappa_4)\left(\Lambda^2+\Lambda\varkappa_4-\varkappa_3^2-2\varkappa_4^2-3\varkappa_3\varkappa_4\right)}{(1-\varkappa_1)^2\,(4-\varkappa_1)\,\varkappa_1}$

Table B.1: Coefficients $\mathcal{R}$'s of the reaction F_R

C Coefficients $\mathcal{F}$'s and $\mathcal{M}$'s when the First Stabilizer is Suppressed

The mechanical problem of the drillsting can also be solved when the central stabilizer is suppressed, meaning that the point of abscissa $\xi = 1 - \varkappa_1$ is not constrained to sit on the borehole axis. In this case, the solution is immediate and the coefficients $\mathcal{F}$'s and $\mathcal{M}$'s are numbers except $\mathcal{F}_\Phi$ and $\mathcal{M}_\Phi$ which are still functions of $\varkappa_3$, $\varkappa_4$ and Λ. Those coefficients are given in Table C.1.

D Simplifications for Stationary Solutions

Stationary solutions are the equilibrium points of the dynamical system corresponding to the borehole evolution problem

$$\frac{\mathrm{d}^2\Theta}{\mathrm{d}S^2} = F(S) \qquad \text{and} \qquad \frac{\mathrm{d}\Xi}{\mathrm{d}S} = G(S) \tag{D.1}$$

they correspond to segments of borehole characterized by a constant curvature K_s and by a constant diameter A_s. In this context of steady state, several equations governing the general problem can

	Blocked rotation	Free rotation
$\mathcal{F}_b$	-6	-3
$\mathcal{F}_s$	-6	0
$\mathcal{F}_k$	0	0
$\mathcal{F}_w$	$\frac{1}{2}$	$\frac{5}{8}$
$\mathcal{F}_r$	$-(\Lambda-\varkappa_4)(\Lambda-\varkappa_3-\varkappa_4)(2\Lambda+2\varkappa_3+4\varkappa_4-3)$	$-\frac{1}{2}(\Lambda-\varkappa_4)(\Lambda-\varkappa_3-\varkappa_4)(\Lambda+\varkappa_3+2\varkappa_4)$
$\mathcal{M}_b$	4	3
$\mathcal{M}_s$	2	0
$\mathcal{M}_k$	0	0
$\mathcal{M}_w$	$-\frac{1}{12}$	$-\frac{1}{8}$
$\mathcal{M}_r$	$(\Lambda-\varkappa_4)(\Lambda-\varkappa_3-\varkappa_4)(\Lambda+\varkappa_3+2\varkappa_4-1)$	$\frac{1}{2}(\Lambda-\varkappa_4)(\Lambda-\varkappa_3-\varkappa_4)(\Lambda+\varkappa_3+2\varkappa_4)$

Table C.1: Coefficients $\mathcal{F}$'s and $\mathcal{M}$'s when the first stabilizer is suppressed

be simplified using the knowledge that the borehole segment between the second stabilizer and the bit is a circular arc.

D.1 Relations Between Angles and Curvature

Figure D.1 depicts a borehole segment of constant curvature κ, the bit is at the point B while the second stabilizer is at the point A. The amplitude of the angles α_1 and α_2 can be deduced from the chord inclination θ_m, the inclinations of the borehole at the bit $\hat{\Theta}$ and at the second stabilizer $\bar{\bar{\Theta}}$

$$\alpha_1 = \frac{\pi}{2} - \hat{\Theta} + \theta_m \tag{D.2}$$

$$\alpha_2 = \frac{\pi}{2} + \bar{\bar{\Theta}} - \theta_m \tag{D.3}$$

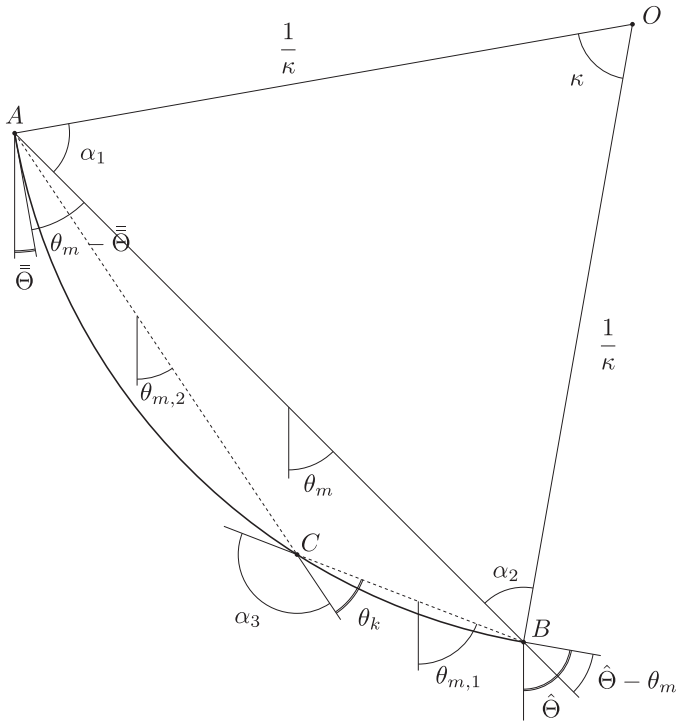

Figure D.1: Relations between angles and curvature in the context of the stationary solution

Moreover, considering that the two sides AO and BO of the triangle AOB have the same length κ^{-1}, those two angles have the same amplitude. We can thus write the relationship

$$\alpha_1 = \alpha_2 \tag{D.4}$$

$$\iff \hat{\Theta} + \theta_m = \bar{\bar{\Theta}} - \theta_m \tag{D.5}$$

to obtain the expression of the chord inclination

$$\theta_m = \frac{\hat{\Theta} + \bar{\bar{\Theta}}}{2} \tag{D.6}$$

On top of that, in a triangle, the sum of the amplitudes angles is equal to π

$$\alpha_1 + \alpha_2 + \kappa = \pi \tag{D.7}$$

$$\iff \hat{\Theta} - \bar{\bar{\Theta}} = \kappa \tag{D.8}$$

Combining this relation with the relation (D.6) we finally get

$$\hat{\Theta} - \theta_m = \frac{\kappa}{2} \tag{D.9}$$

$$\bar{\bar{\Theta}} - \theta_m = -\frac{\kappa}{2} \tag{D.10}$$

Considering the *Central Angle Theorem* which states that an angle inscribed into a circle measures half the central angle subtending the same arc, we can write that the inscribed angle α_3 measures half the central angle $2\pi - \kappa$ and determine the expression of the kink angle

$$\theta_k = \frac{\kappa}{2} \tag{D.11}$$

D.2 Transverse Displacement of the First Stabilizer

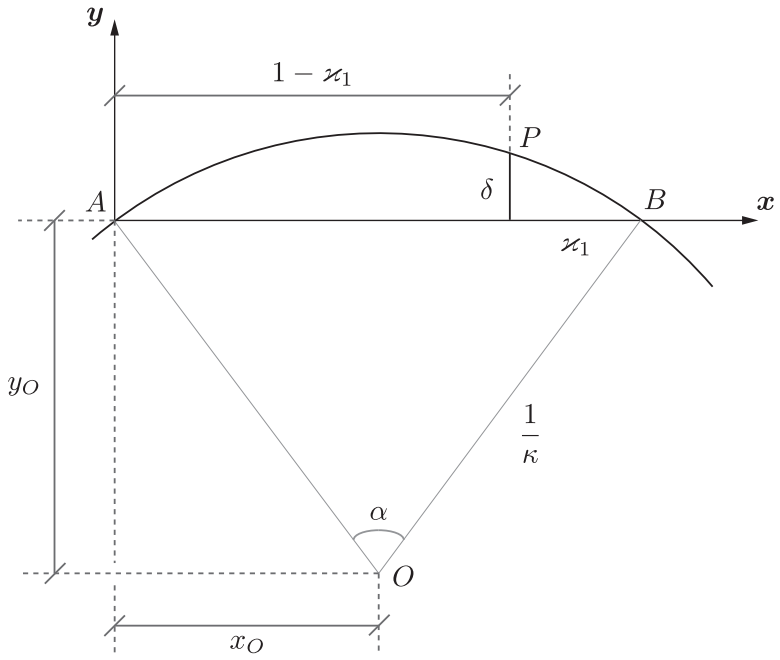

Figure D.2: Determination of the lateral displacement δ

The transverse displacement of the first stabilizer can be easily determined considering the general equation of the circle

$$(x - x_O)^2 + (y - y_O)^2 = \frac{1}{\kappa^2} \tag{D.12}$$

represented in Figure D.2 which is scaled by the length of the *BHA* segment. The length of the arc $\widehat{AB}$ is then equal to 1 and we can write

$$\frac{\alpha}{2} = \arcsin \frac{\kappa}{2}$$

The coordinates of the circle center are given by

$$x_O = 0,5 \tag{D.13}$$

$$y_O = -\frac{1}{\kappa}\cos\frac{\alpha}{2} = -\frac{\sqrt{1-\frac{\kappa^2}{4}}}{\kappa} \tag{D.14}$$

and the equation (D.12) becomes

$$(x-0,5)^2 + \left(y + \frac{\sqrt{1-\frac{\kappa^2}{4}}}{\kappa}\right)^2 = \frac{1}{\kappa^2} \tag{D.15}$$

The transversal displacement δ corresponds to the ordinate y at the abscissa $x = 1 - \varkappa 1$, the equation of the circle can be written as

$$\kappa = \frac{2\delta}{\sqrt{\left((1-\varkappa 1)^2 + \delta^2\right)(\varkappa 1^2 + \delta^2)}} \tag{D.16}$$

Considering that the curvature of the borehole is extremely small, we can affirm that

$$\delta^2 \ll (1-\varkappa 1)^2 \tag{D.17a}$$

$$\delta^2 \ll \varkappa 1^2 \tag{D.17b}$$

Equation (D.16) can be expressed as

$$\kappa = \frac{2\delta}{\varkappa 1\,(1-\varkappa 1)} \tag{D.18}$$

Finally the settlement δ can be approximated by

$$\delta = \frac{\kappa}{2}\varkappa 1\,(1-\varkappa 1) \tag{D.19}$$

as $\kappa \ll$, we may see that the former assumptions (D.17a) and (D.17b) are precisely met.

E Limiting Behaviour of a Three Supports Beam

The behaviour of the *RSS* when the length λ_1, between the bit and the first stabilizer, decreases is of primary importance. The goal of this short section is to improve the understanding of this limiting behaviour of the *RSS* through the study of a simple beam lying on three supports. Deflections and support reactions of the beam are approached in the general context of the beam theory before being transposed to the more specific context of limiting behaviour of the *RSS*.

E.1 Formulation

The beam presented in Figure E.1(a) is loaded by the weight per unit length, w, while its rigidity, EI, is constant along the beam. The coordinate system (x, y) is defined with its origin on the left support and with the x-axis coinciding with the beam. Any deformation of the beam is reflected by a transverse deflection $U(x)$, taken positive in the direction of the y-axis.

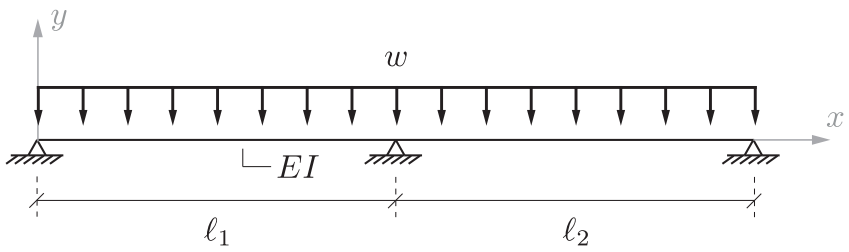

(a) Beam on three supports uniformly loaded

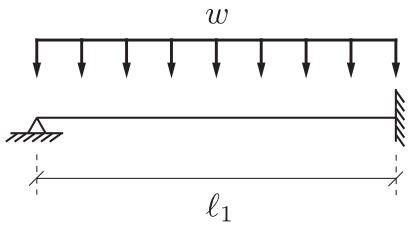

(b) Cantilever beam with one supports uniformly loaded

Figure E.1: Limiting behaviour of a three supports beam when $\ell_2 \to 0$

Considering that shear deformations can be neglected compare to bending deformations, as it is usual with circular or tubular cross sections, transverse deflections of the beam are expressed in the framework of the Euler-Bernoulli theory. According to the assumptions of small rotations and small displacement by reference to its initial configuration, the elastic response of the beam is given by the governing equation

$$EI \frac{\mathrm{d}^4 U}{\mathrm{d}x^4} + w = 0 \tag{E.1}$$

which can be integrated in order to obtain the expression of the deflection of the beam

$$U(x) = -\frac{wx^4}{24EI} + C_4 x^3 + C_3 x^2 + C_2 x + C_1 \tag{E.2}$$

This expression involves four integration constants determined based on four boundary conditions. The slope $\theta(x)$, the bending moment $M_3(x)$ and the shear force $F_2(x)$ of the beam are of prime importance in the computation of the those integration constants. They are obtained by derivation of the transverse deflection

$$\theta(x) = \frac{\mathrm{d}U}{\mathrm{d}dx} \tag{E.3}$$

$$M_3(x) = EI \frac{\mathrm{d}^2 U}{\mathrm{d}x^2} \tag{E.4}$$

$$F_2(x) = -EI \frac{\mathrm{d}^3 U}{\mathrm{d}x^3} \tag{E.5}$$

The beam presented in Figure E.1(a) involves five boundary conditions

- Two at the left support: the deflection and the moment are both equal to zero;
- Two at the right support: the deflection and the moment are both equal to zero;
- One at the central support: the deflection is equal to zero.

The beam is overdetermined and we cannot impose the five boundary conditions using only four integration constants. An alternative is to consider two *sub-beams* and restore the continuity by imposing, in addition to the usual boundary conditions, the same rotations and moments at the junction. Finally we obtain a system of eight equations and eight unknowns, which are the integration constants of the governing equation. If we denote by $U_1(x)$ the deflection of the left beam of length ℓ_1 and by $U_2(x)$ the deflection of the right beam of length ℓ_2, the eight equations corresponding to the configuration presented in Figure E.1(a) are

$$U_1(0) = 0 \quad \text{(E.6)} \qquad U_2(\ell_1+\ell_2) = 0 \quad \text{(E.10)}$$

$$\left.\frac{\mathrm{d}^2U_1}{\mathrm{d}x^2}\right|_{x=0} = 0 \quad \text{(E.7)} \qquad \left.\frac{\mathrm{d}^2U_2}{\mathrm{d}x^2}\right|_{x=\ell_1+\ell_2} = 0 \quad \text{(E.11)}$$

$$U_1(\ell_1) = 0 \quad \text{(E.8)} \qquad U_2(\ell_1) = 0 \quad \text{(E.12)}$$

$$\left.\frac{\mathrm{d}U_1}{\mathrm{d}x}\right|_{x=\ell_1} = \left.\frac{\mathrm{d}U_2}{\mathrm{d}x}\right|_{x=\ell_1} \quad \text{(E.9)} \qquad \left.\frac{\mathrm{d}^2U_1}{\mathrm{d}x^2}\right|_{x=\ell_1} = \left.\frac{\mathrm{d}^2U_2}{\mathrm{d}x^2}\right|_{x=\ell_1} \quad \text{(E.13)}$$

Transverse deflections of those *sub-beams* are then given by

$$U_1(x) = -\frac{wx(\ell_1-x)\left(\ell_1^3+\ell_1^2(\ell_2+x)-\ell_1\left(\ell_2^2-\ell_2x+2x^2\right)-\ell_2^2x\right)}{48EI\ell_1} \quad \text{(E.14)}$$

$$U_2(x) = -\frac{w(\ell_1-x)(\ell_1+\ell_2-x)\left(\ell_1^3+\ell_1^2(3\ell_2-x)+\ell_1\ell_2(\ell_2-3x)+\ell_2x(2x-3\ell_2)\right)}{48EI\ell_2} \quad \text{(E.15)}$$

The transverse deflection of the total beam is the combination of the deflection $U_1(x)$ for $x \in [0, \ell_1]$ and the deflection $U_2(x)$ for $x \in [\ell_1, \ell_2]$. This can be written as

$$U_{tot}(x) = U_1(x)\left(H_0 - H_{\ell_1}\right) + U_2(x)\left(H_{\ell_1} - H_{\ell_1+\ell_2}\right) \quad \text{(E.16)}$$

where H_ℓ denotes the Heaviside step function in $x = \ell$. Deflections of the beam are presented in Figure E.2 for different values of the ratio ℓ_2/ℓ_1 and for two different configuration of the beam. Figure E.2(a) depicts the behaviour of the three supports beam uniformly loaded shown in Figure E.1(a). While Figure E.2(b) pictures the behaviour of the beam when a fixed end substitutes the right support, *i.e.,* if Equation (E.11) is replaced by

$$\left.\frac{\mathrm{d}U_2}{\mathrm{d}x}\right|_{x=\ell_1+\ell_2} = 0 \quad \text{(E.17)}$$

E.2 Limiting Behaviour of the Beam

The goal of this section is to analyse the behaviour of the beam when the length ℓ_2 becomes small compare to the length ℓ_1, *i.e.,* when the ratio ℓ_2/ℓ_1 become smaller than 1 and specifically when this ratio tends to zero. For both configurations, the rigidity of the right beam segment increases gradually when the ratio ℓ_2/ℓ_1 decreases. The influence of the right beam segment on the left beam segment can be replaced by a torsional spring whose rigidity is proportional to the rigidity of the right beam segment:

$$\frac{EI}{\ell_2^3} \quad \text{(E.18)}$$

Therefore when the ratio ℓ_2/ℓ_1 decreases the rigidity of the torsional spring increases gradually compare to the rigidity of the left beam segment. If we take the limit for $\ell_2 \to 0$, the rigidity of

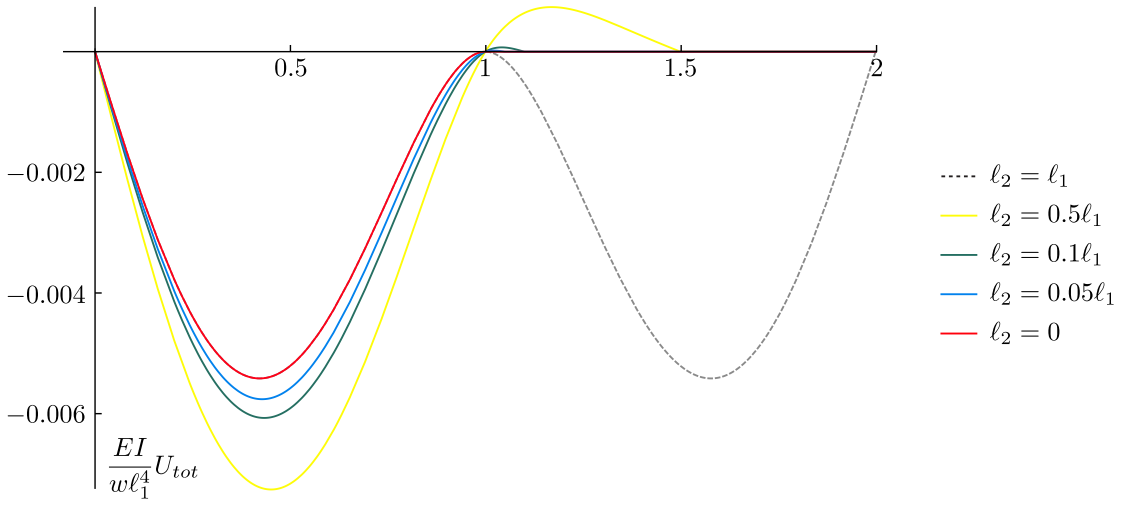

(a) Three supports

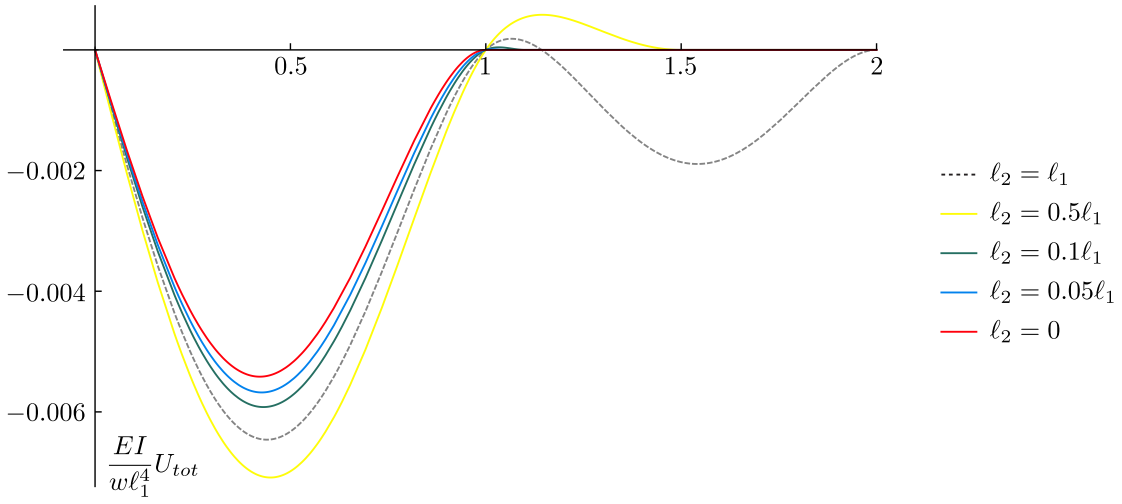

(b) Three supports and one blocked rotation

Figure E.2: Deflection of the beam for different values of the ratio ℓ_2/ℓ_1

the torsional spring tends thus to the infinity and the right beam segment can be finally viewed as a fixed support.

The limiting behaviour can be obtained taking the limit

$$U_{\text{lim}}(x) = \lim_{\ell_2 \to 0} U_{tot}(x) = -\frac{wx(\ell_1 - x)^2(\ell_1 + 2x)}{48EI}\left(H_0 - H_{\ell_1}\right) \tag{E.19}$$

Which corresponds exactly to the deflection of the beam presented in Figure 1(b). The central and right supports degenerate thus to a unique fixed support.

The convergence of the total deflection $U_{tot}(x)$ to $U_{\text{lim}}(x)$ when the length ℓ_2 tends to 0 is presented in Figure E.3. This graph depicts how the error between those two deflections evolves with the ratio ℓ_2/ℓ_1. The error is determined by

$$\max_{0 \leqslant x \leqslant \ell_1} \left| \frac{U_{\text{lim}} - U_{tot}}{U_{\text{lim}}} \right|$$

For both configurations, the error committed by considering the limit solution instead of the general solution when $\ell_1 \geqslant 25\ell_2$ is already lower than 5%.

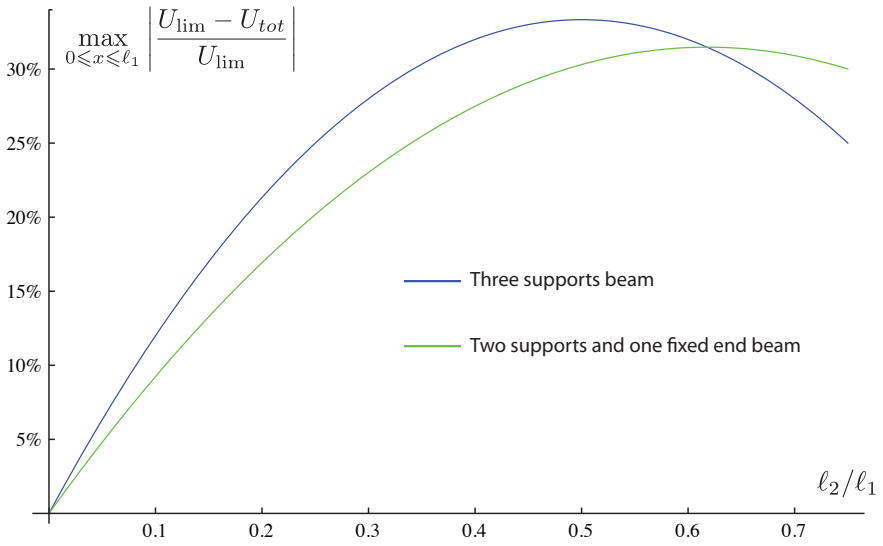

Figure E.3: Convergence of the total deflection $U_{tot}(x)$ to $U_{\text{lim}}(x)$ when ℓ_2 tends to 0

Considering now the three reactions acting on beam, they are given by the variation of the shear force $F_2(x)$ at supports:

$$R_1 = -EI \left.\frac{\mathrm{d}^3 U_1}{\mathrm{d}x^3}\right|_{x=0} \tag{E.20}$$

$$R_2 = -EI \left(\left.\frac{\mathrm{d}^3 U_2}{\mathrm{d}x^3}\right|_{x=\ell_1} - \left.\frac{\mathrm{d}^3 U_1}{\mathrm{d}x^3}\right|_{x=\ell_2} \right) \tag{E.21}$$

$$R_3 = EI \left.\frac{\mathrm{d}^3 U_2}{\mathrm{d}x^3}\right|_{x=\ell_1+\ell_2} \tag{E.22}$$

$$R_{\text{lim}} = EI \left.\frac{\mathrm{d}^3 U_{\text{lim}}}{\mathrm{d}x^3}\right|_{x=\ell_1} \tag{E.23}$$

Reactions for the configuration presented in Figure E.1(a) are shown in Figure E.4 for different values of the ratio ℓ_2/ℓ_1, behaviours of the reactions when a fixed end substitutes the right support are similar.

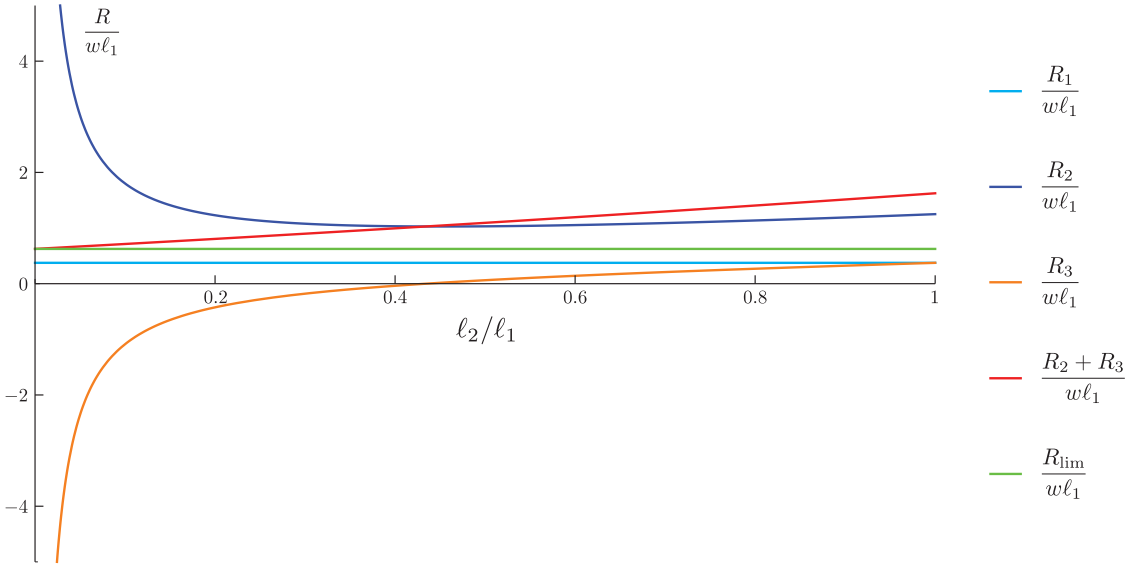

Figure E.4: Reactions acting on the three supports beam in terms of the ratio ℓ_2/ℓ_1

Reaction R_1 remains relatively constant which means that the left reaction is weakly dependant on the configuration of the right beam segment. While the central reaction R_2 remains positive, the right reaction R_3 changes sign. Both magnitudes of these reactions increase quickly when $\ell_1 \geqslant 5\ell_2$ and tends to infinity for $\ell_2 \to 0$. On the other side, the sum of these two reactions tends linearly to the reaction R_{lim}, *i.e.,* the right reaction of the beam presented in Figure E.1(b). This observation allows to state that the moment created by the couple of reactions

$$M_{R_2R_3} = -\ell_2 R_2 = \ell_2 R_3 \tag{E.24}$$

has a finite value (regardless to the value of the ratio ℓ_2/ℓ_1) and tends to the moment M_{lim} taken by the fixed end of the beam presented in Figure E.1(b).

F *BHA* without Rotary Steerable System

F.1 Evolution of the Bit Tilt with the Dimensionless Borehole Curvature, Upper Stabilizer Free to Rotate

In the context of a *BHA* without *RSS* and considering that the upper stabilizer is free to rotate, the relation between the bit tilt and the dimensionless curvature of the borehole is depicted in Figure F.1.

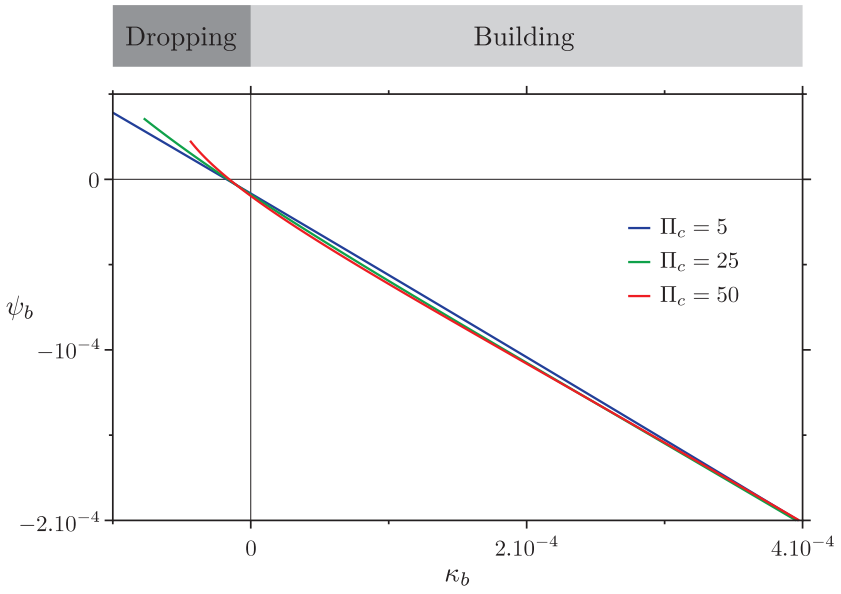

(a) For different values of the parameter Π_c

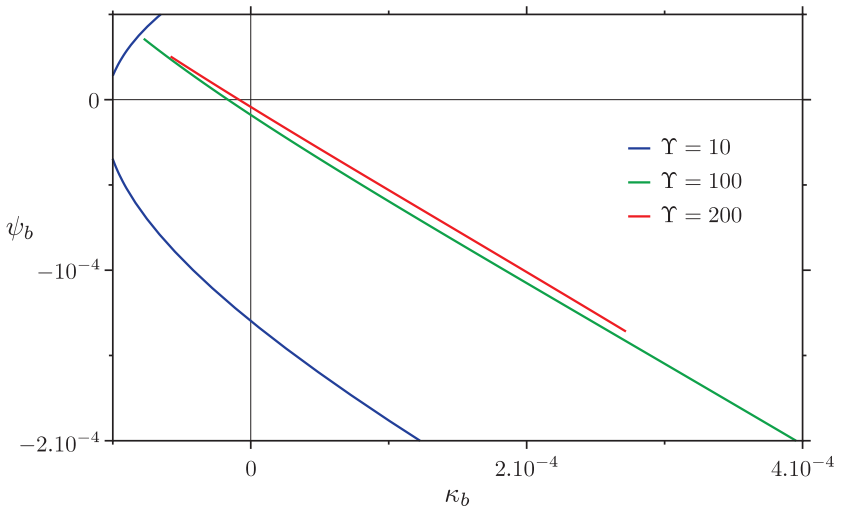

(b) For different values of the dimensionless stiffness Υ

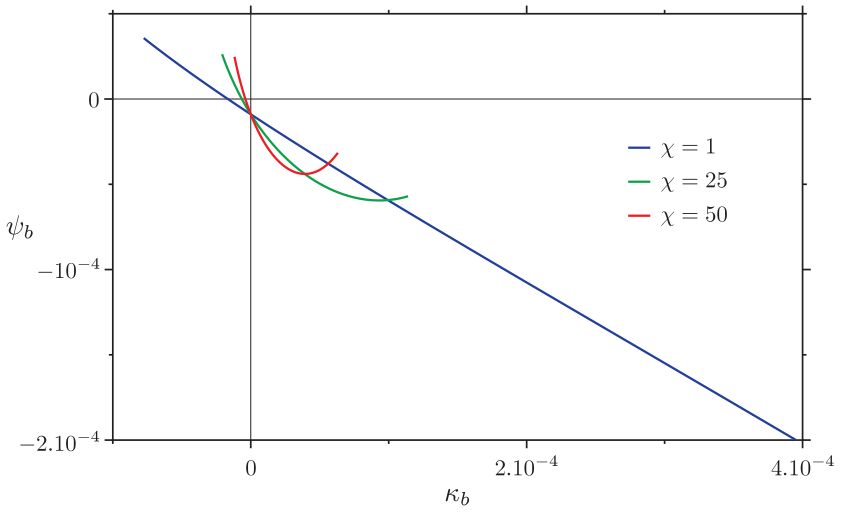

(c) For different values of the lateral steering resistance η

Figure F.1: Evolution of the bit tilt with the dimensionless borehole curvature for varying $\varkappa_1$ and considering the upper stabilizer free to rotate ($\chi = 1$, $\eta = 50$, $\Pi_c = 25$, $\Upsilon = 100$ and $\theta_m = \pi/4$)

G *BHA* Equipped with a Rotary Steerable System

G.1 Expression of the Borehole Curvature and the Penetration Inclination, Upper Stabilizer Free to Rotate

Considering that the upper stabilizer is free to rotate, the borehole curvature can also be written as

$$\kappa_f = \frac{\mathcal{C}_{\Phi,\kappa}\Phi + \mathcal{C}_{w,\kappa}\sin\theta_m}{\mathcal{C}_{\Upsilon,\kappa}\Upsilon} \tag{G.1}$$

with the coefficients

$$\begin{aligned}
\mathcal{C}_{\Phi,\kappa} &= 3(1-\varkappa_1-2\varkappa_2)^2\left(6-\eta\Psi\varkappa_1^2\right)\\
\mathcal{C}_{w,\kappa} &= -2\left(\eta\Psi\left(\varkappa_1^2-3\varkappa_1+1\right)\varkappa_1^2+6\left(\varkappa_1^2+3\varkappa_1-1\right)\right)\\
\mathcal{C}_{\Upsilon,\kappa} &= 8\left(\eta\Psi^2\chi(4-\varkappa_1)\varkappa_1^2+3\Psi\left(\eta(2-\varkappa_1)\varkappa_1+2\chi(\varkappa_1+2)\right)+18\right)
\end{aligned} \tag{G.2}$$

Similarly, the penetration inclination read

$$\beta_f = \frac{\mathcal{C}_{\Phi,\beta}\Phi + \mathcal{C}_{w,\beta}\sin\theta_m}{\mathcal{C}_{\Upsilon,\beta}\Upsilon} \tag{G.3}$$

with the coefficients

$$\begin{aligned}
\mathcal{C}_{\Phi,\beta} &= 9(1-\varkappa_1-2\varkappa_2)^2(\chi\Psi\varkappa_1+1)\\
\mathcal{C}_{w,\beta} &= 2\left(\chi\Psi\varkappa_1\left(\varkappa_1^3-\varkappa_1^2-9\varkappa_1+3\right)+3\left(\varkappa_1^3-\varkappa_1^2-3\varkappa_1+1\right)\right)\\
\mathcal{C}_{\Upsilon,\beta} &= 8\left(\eta\Psi^2\chi(4-\varkappa_1)\varkappa_1^2+3\Psi\left(\eta(2-\varkappa_1)\varkappa_1+2\chi(\varkappa_1+2)\right)+18\right)
\end{aligned} \tag{G.4}$$

Analogously to the solution considering the upper stabilizer blocked in rotation, the general expressions of the solution (G.1) and (G.3) can be expand for small values of the parameter $\varkappa_1$

$$\kappa_f = \kappa_f^0 + \frac{\mathcal{C}'_{\Phi,\kappa}\Phi + \mathcal{C}'_{w,\kappa}\sin\theta_m}{\mathcal{C}'_{\Upsilon,\kappa}\Upsilon}\varkappa_1 + \mathcal{O}\left(\varkappa_1^2\right) \tag{G.5}$$

while the penetration inclination is expressed as

$$\beta_f = \beta_f^0 + \frac{\mathcal{C}'_{\Phi,\beta}\Phi + \mathcal{C}'_{w,\beta}\sin\theta_m}{\mathcal{C}'_{\Upsilon,\beta}\Upsilon}\varkappa_1 + \mathcal{O}\left(\varkappa_1^2\right) \tag{G.6}$$

Where κ_f^0 and β_f^0 are the limit borehole curvature and penetration inclination, respectively, for $\varkappa_1$ tending to zero

$$\begin{aligned}
\kappa_f^0 &= \lim_{\varkappa_1\to 0}\kappa_f\\
&= \frac{3\left(1-2\varkappa_2\right)^2\Phi+2\sin\theta_m}{8\Upsilon(2\chi\Psi+3)}
\end{aligned} \tag{G.7}$$

$$\begin{aligned}
\beta_f^0 &= \lim_{\varkappa_1\to 0}\beta_f\\
&= \frac{3\left(1-2\varkappa_2\right)^2\Phi+2\sin\theta_m}{16\Upsilon(2\chi\Psi+3)}
\end{aligned} \tag{G.8}$$

G.2 Coefficients $\mathcal{C}'_\kappa$'s and $\mathcal{C}'_\beta$'s

Coefficients $\mathcal{C}'_\kappa$'s and $\mathcal{C}'_\beta$'s involved in the expressions (123), (124), (G.5) and (G.6) of the asymptotic behaviour of the solution for small values of the parameter $\varkappa_1$ are given by

$$\begin{aligned}
\mathcal{C}'_{\Phi,\kappa} &= 3\left(\eta\Psi\left(2\varkappa_2^2+\varkappa_2-1\right)+2\left(3\chi\Psi(3\varkappa_2-2)-2\varkappa_2^2+8\varkappa_2-5\right)\right)\\
\mathcal{C}'_{w,\kappa} &= -2\left(\eta\Psi+8\Psi\chi+6\right)\\
\mathcal{C}'_{\Upsilon,\kappa} &= 48\left(\Psi\chi+1\right)^2
\end{aligned} \tag{G.9}$$

and

$$\begin{aligned}
\mathcal{C}'_{\Phi,\beta} &= 3\left(\eta\Psi\left(2\varkappa_2^2+\varkappa_2-1\right)+2\left(\chi^2\Psi^2(1-2\varkappa_2)+\left(2\varkappa_2^2+6\varkappa_2-5\right)\chi\Psi+7\varkappa_2-5\right)\right)\\
\mathcal{C}'_{w,\beta} &= -2\left(\eta\Psi-2\chi^2\Psi^2+6\chi\Psi+6\right)\\
\mathcal{C}'_{\Upsilon,\beta} &= 96\left(\chi\Psi+1\right)^2
\end{aligned} \tag{G.10}$$

if the upper stabilizer is blocked in rotation or by

$$\begin{aligned}
\mathcal{C}'_{\Phi,\kappa} &= 3(1-2\varkappa_2)\left(\eta\Psi(1-2\varkappa_2)+\chi\Psi(5-2\varkappa_2)+6\right)\\
\mathcal{C}'_{w,\kappa} &= 2(\eta\Psi+7\chi\Psi+9)\\
\mathcal{C}'_{\Upsilon,\kappa} &= 8(2\chi\Psi+3)^2
\end{aligned} \tag{G.11}$$

and

$$\begin{aligned}
\mathcal{C}'_{\Phi,\beta} &= 3(1-2\varkappa_2)\left(\eta\Psi(1-2\varkappa_2)+2\left(\chi^2\Psi^2(1-2\varkappa_2)-\chi\Psi(2\varkappa_2+1)+3\right)\right)\\
\mathcal{C}'_{w,\beta} &= 2(\eta\Psi+7\chi\Psi+9)\\
\mathcal{C}'_{\Upsilon,\beta} &= 8(2\chi\Psi+3)^2
\end{aligned} \tag{G.12}$$

if it is free to rotate.

G.3 Coefficients $\mathcal{C}_{\Phi,\kappa}$, $\mathcal{C}_{w,\kappa}$ and $\mathcal{C}_{\Upsilon,\kappa}$, Upper Stabilizer Free to Rotate

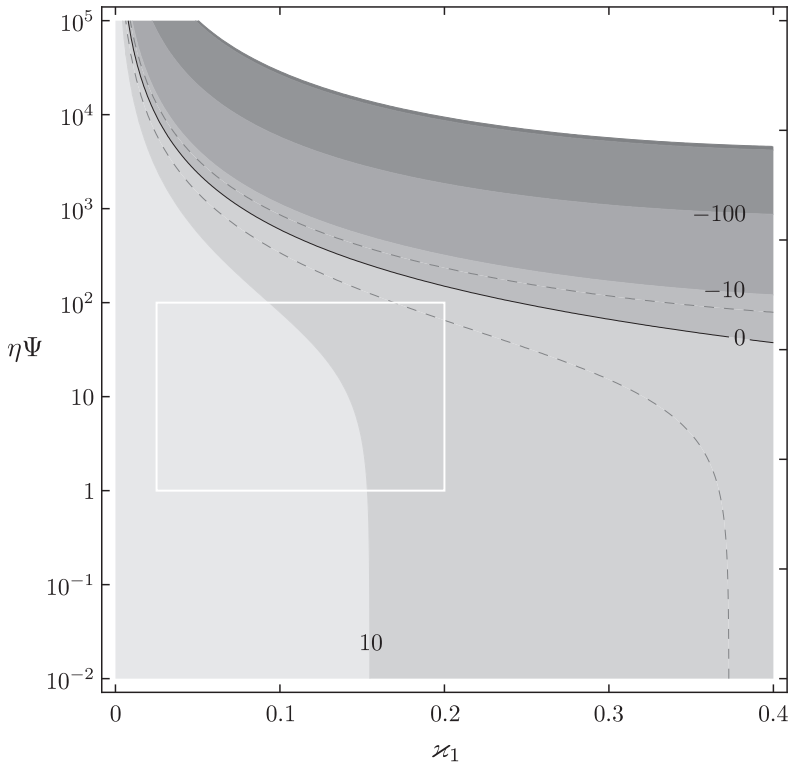

(a) The parameter $\varkappa_2$ is equal to 0.05

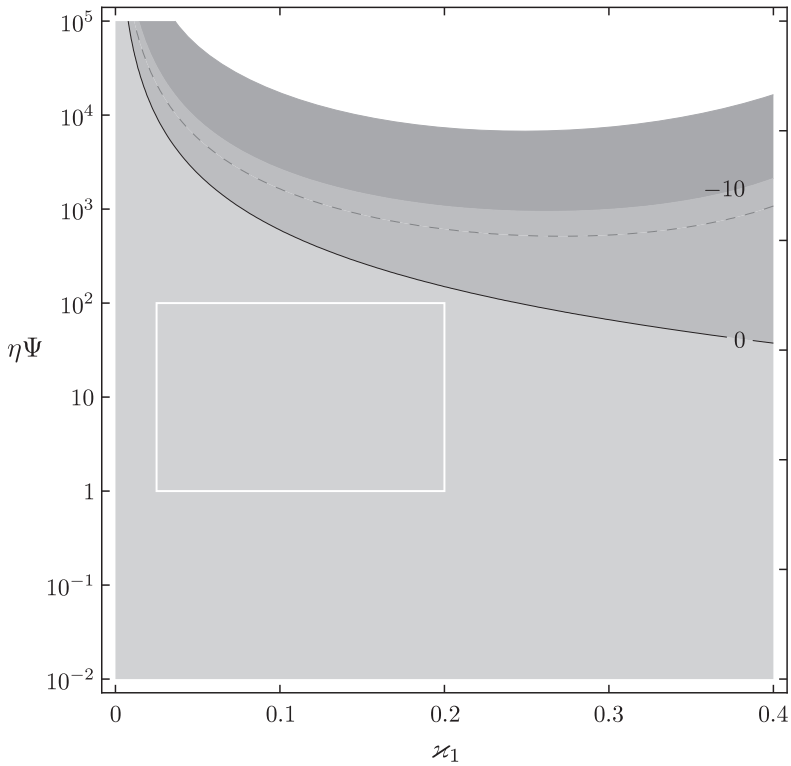

(b) The parameter $\varkappa_2$ is equal to 0.25

Figure G.1: Magnitude of the coefficient $\mathcal{C}_{\Phi,\kappa}$ in the space $(\varkappa_1, \eta\Psi)$ considering the upper stabilizer free to rotate

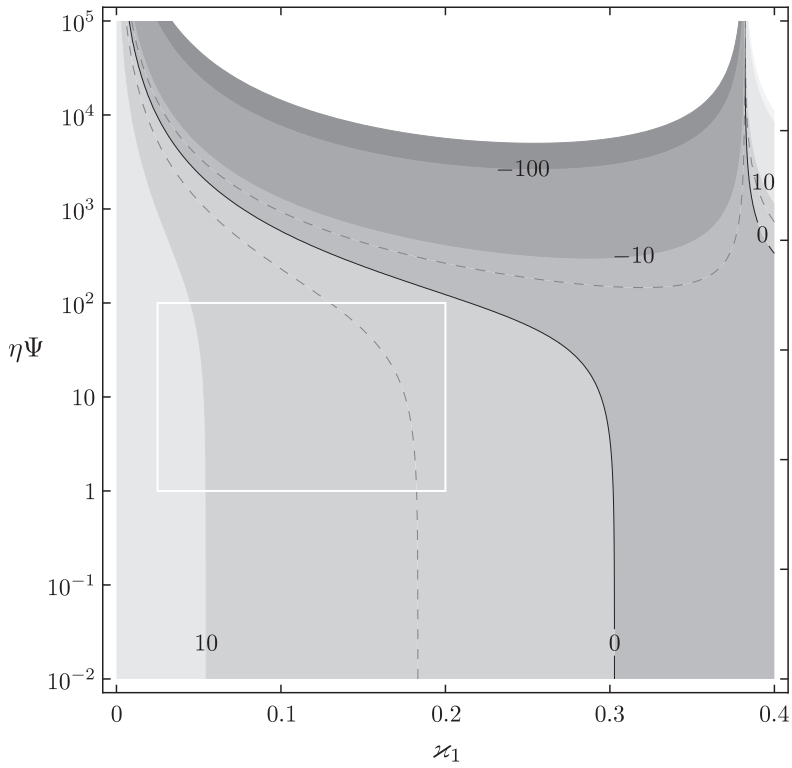

Figure G.2: Magnitude of the coefficient $\mathcal{C}_{w,\kappa}$ in the space $(\varkappa_1, \eta\Psi)$ considering the upper stabilizer free to rotate

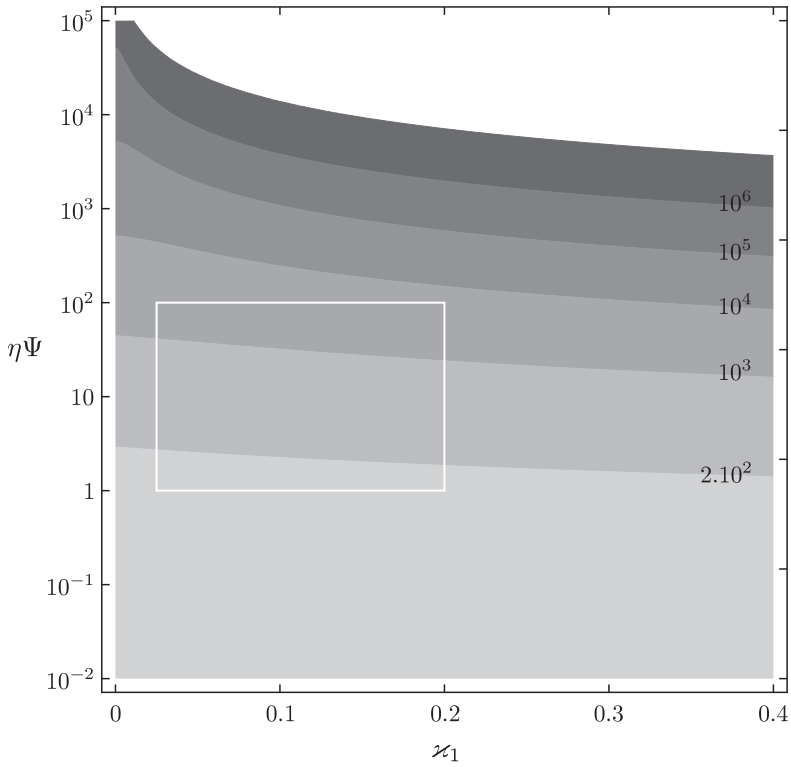

(a) The number α is equal to 0.2

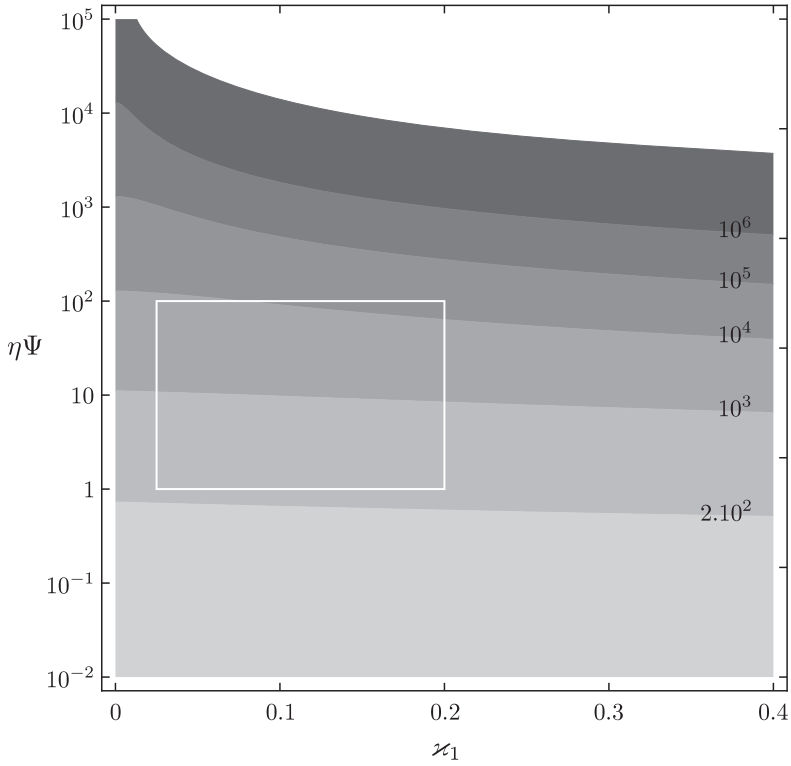

(b) The number α is equal to 0.8

Figure G.3: Magnitude of the coefficient $\mathcal{C}_{\Upsilon,\kappa}$ in the space $(\varkappa_1, \eta\Psi)$ considering the upper stabilizer free to rotate